


5-2016

# Investigation of climate variability and climate change impacts on corn yield in the Eastern Corn Belt, USA

Ruoyu Wang  
*Purdue University*

Follow this and additional works at: [https://docs.lib.purdue.edu/open\\_access\\_dissertations](https://docs.lib.purdue.edu/open_access_dissertations)

 Part of the [Bioresource and Agricultural Engineering Commons](#), [Hydrology Commons](#), and the [Water Resource Management Commons](#)

---

## Recommended Citation

Wang, Ruoyu, "Investigation of climate variability and climate change impacts on corn yield in the Eastern Corn Belt, USA" (2016). *Open Access Dissertations*. 726.  
[https://docs.lib.purdue.edu/open\\_access\\_dissertations/726](https://docs.lib.purdue.edu/open_access_dissertations/726)

This document has been made available through Purdue e-Pubs, a service of the Purdue University Libraries. Please contact [epubs@purdue.edu](mailto:epubs@purdue.edu) for additional information.

**PURDUE UNIVERSITY  
GRADUATE SCHOOL  
Thesis/Dissertation Acceptance**

This is to certify that the thesis/dissertation prepared

By Ruoyu Wang

Entitled

INVESTIGATION OF CLIMATE VARIABILITY AND CLIMATE CHANGE IMPACTS ON CORN YIELD IN THE EASTERN CORN BELT, USA

For the degree of Doctor of Philosophy

Is approved by the final examining committee:

Dr. Keith A. Cherkauer

Co-chair

Dr. Laura C. Bowling

Co-chair

Dr. Indrajeet Chaubey

Dr. Jeffery J. Volenec

To the best of my knowledge and as understood by the student in the Thesis/Dissertation Agreement, Publication Delay, and Certification Disclaimer (Graduate School Form 32), this thesis/dissertation adheres to the provisions of Purdue University's "Policy of Integrity in Research" and the use of copyright material.

Approved by Major Professor(s): Dr. Keith A. Cherkauer

Approved by: Dr. Bernard A. Engel

Head of the Departmental Graduate Program

3/2/2016

Date



INVESTIGATION OF CLIMATE VARIABILITY AND CLIMATE CHANGE  
IMPACTS ON CORN YIELD IN THE EASTERN CORN BELT, USA

A Dissertation

Submitted to the Faculty

of

Purdue University

by

Ruoyu Wang

In Partial Fulfillment of the

Requirements for the Degree

of

Doctor of Philosophy

May 2016

Purdue University

West Lafayette, Indiana

For my dreams I hold my life. For wishes I behold my nights.

## ACKNOWLEDGEMENTS

I owe my deepest sense of gratitude to my major advisors Dr. Keith Cherkauer and Dr. Laura Bowling, without their enthusiasm, inspiration and encouragement, this work would not have been possible. I really enjoy the brainstorms we three made at each weekly meeting. It helps me to think differently and think out of the box, which is really important for this research. I also appreciate their help for pulling me back to the right track when I got lost or stuck in some step. I express my sincere thanks and regards to Dr. Indrajeet Chaubey and Dr. Jeff Volenec for serving on my committee. Dr. Chaubey's group is very strong at SWAT modeling, and I always get valuable suggestions from him and his group members. Dr. Volenec broadened my understanding of this subject from physiological view and I am grateful to it.

I express my special thanks to Dr. Cibin Raj, who is a good friend and also a good teacher in my Ph.D study. His direct or indirect help is beneficial to all SWAT modelers in this department. I really appreciate his patience and kindness. Thanks are due to Dr. Younggu Her for setting up model in the St. Joseph River watershed. Thanks are due to Dr. Yaoze Liu for his help in teaching survey for ABE 325. I also would like to thank all my PHIG members. It is my pleasure to work with you guys. Special thanks to Anthony and Jing for teaching me remote sensing technology. And special thanks to Natalie and Andi for their

encouragement and countless help. I am thankful to all my Purdue colleagues and friends Feng, Wonsoek, Garret, Shaoping, Wei-Zhen, Yan, Yi, Baodan, Tian, Shule, Jingqiu, and Xiaoyu.

I would like to express my most heartfelt appreciation to my Master Professor Dr. Latif Kalin, who introduced me to research and always provides valuable suggestions and encouragement. Most importantly, I would like to express my best regards to my family, especially my parents, who have supported me tirelessly. Without your endless love I would have not been capable of completing this work.

## TABLE OF CONTENTS

	Page
LIST OF TABLES .....	ix
LIST OF FIGURES .....	xi
ABSTRACT .....	xvii
CHAPTER 1. INTRODUCTION .....	1
1.1 Research Background .....	1
1.2 Research Hypothesis and Objectives.....	6
1.3 Dissertation Organization .....	9
1.4 References .....	11
CHAPTER 2. ESTIMATION OF THE EFFECTS OF CLIMATE VARIABILITY ON CROP YIELD IN THE MIDWEST USA .....	15
2.1 Abstract.....	15
2.2 Introduction .....	16
2.3 Methods .....	20
2.3.1 SWAT model overview and modification .....	20
2.3.2 Study area and data .....	25
2.4 Model implementation.....	27
2.4.1 Crop yield calibration steps .....	27
2.4.2 Simulated crop yield upscaling.....	28
2.4.3 Model performance evaluation .....	30
2.4.4 Soil moisture content calibration .....	31
2.4.5 Management timing parameterization .....	33
2.4.5.1 Planting.....	34
2.4.5.2 Maturity.....	34



	Page
2.4.5.3 Harvest .....	35
2.4.5.4 Senescence .....	35
2.4.6 Annual yield amount/variation calibration .....	37
2.4.7 Weekly biomass accumulation validation .....	42
2.4.8 The relationship between crop yield and climate variability .....	42
2.5 Results .....	45
2.5.1 Model performance in soil moisture prediction.....	45
2.5.2 Model performance in crop yield/biomass prediction .....	46
2.5.3 Role of climate variability on crop yield .....	50
2.5.4 Long term crop yield reduction due to climate stress .....	54
2.6 Discussion.....	55
2.7 Summary and conclusions .....	59
2.8 References .....	62
<b>CHAPTER 3. CORN RESPONSES TO CLIMATE STRESS DETECTED WITH SATELLITE-BASED NDVI TIME SERIES.....</b>	<b>67</b>
3.1 Abstract.....	67
3.2 Introduction .....	68
3.3 Method.....	71
3.3.1 Study Area .....	71
3.3.2 Data.....	73
3.3.2.1 Land cover and crop progress data.....	73
3.3.2.2 Remote Sensing observations .....	74
3.3.3 Data Processing.....	74
3.3.3.1 NDVI calculation for corn pixels .....	77
3.3.3.2 Normal curve generalization and NDVI residual calculation .....	82
3.3.3.3 Growth stress metrics .....	83
3.4 Results .....	86
3.4.1 Normalized Difference Vegetative Index with Time.....	86

	Page
3.4.2 Normal growth condition.....	89
3.4.3 Yield-NDVI residual relationship.....	93
3.4.4 Stress-NDVI residual relationship.....	96
3.4.5 Risky pixel rate – stress relationship.....	100
3.5 Discussion.....	104
3.6 Conclusion.....	107
3.7 References.....	110
<b>CHAPTER 4. IMPROVED SIMULATION OF ANNUAL CROP SENSITIVITY TO CLIMATE VARIABILITY IN THE EASTERN CORN BELT.....</b>	<b>115</b>
4.1 Abstract.....	115
4.2 Introduction.....	116
4.3 Method.....	121
4.3.1 Study area.....	121
4.3.2 Data Processing.....	123
4.3.2.1 Soil moisture data preprocessing.....	123
4.3.2.2 Regional Leaf Area development curve.....	125
4.3.3 Multi-variable calibration.....	127
4.3.4 Yield adjustment.....	128
4.4 Results and Discussions.....	131
4.4.1 Model performance in calibration/validation.....	131
4.4.2 Parameter sensitivity to streamflow, LAI and interannual yield.....	134
4.4.3 Evaluation of soil moisture.....	135
4.4.4 Spatial distribution of corn yield.....	139
4.5 Conclusions.....	145
4.6 References.....	149
<b>CHAPTER 5. BIOPHYSICAL AND HYDROLOGICAL EFFECTS OF FUTURE CLIMATE CHANGE INCLUDING TRENDS IN CO<sub>2</sub>, IN THE ST. JOSEPH RIVER WATERSHED, EASTERN CORN BELT.....</b>	<b>153</b>
5.1 Abstract.....	153

	Page
5.2 Introduction .....	154
5.3 Method.....	159
5.3.1 Study area.....	159
5.3.2 SWAT model overview .....	160
5.3.3 The representation of CO <sub>2</sub> effects in the SWAT model .....	162
5.3.4 Input Data.....	164
5.3.4.1 Historical climate input .....	164
5.3.4.2 GCM climate input.....	164
5.3.4.3 CO <sub>2</sub> input.....	165
5.3.5 Model implementation .....	165
5.4 Results and Discussions .....	166
5.4.1 Future climate change and CO <sub>2</sub> enhancement .....	166
5.4.2 Crop biophysical responses to future climate and CO <sub>2</sub> change .....	170
5.4.3 Streamflow response to future climate change and enhanced CO <sub>2</sub> .....	179
5.5 Conclusions .....	181
5.6 References .....	184
CHAPTER 6. CONCLUSIONS AND RECOMMEDATIONS FOR FUTURE WORK	
.....	189
6.1 Conclusions .....	190
6.2 Limitations and Future Work .....	194
VITA.....	196

## LIST OF TABLES

Table	Page
Table 2.1 Data used in this study .....	26
Table 2.2 Soil water content parameterization .....	32
Table 2.3 Hydrologic parameter calibration .....	33
Table 2.4 Parameters adjusted for management time and potential growth curve .....	34
Table 2.5 Parameters used for yield calibration for the four sites .....	40
Table 2.6 Growing degree day requirements for different phenological stages of 2700 GDD corn.....	43
Table 2.7 Model performance in predicting soil moisture at the four SCAN sites .....	47
Table 2.8 Model performance in predicting corn yield in the four SCAN counties.....	48
Table 2.9 Correlation coefficient (Pearson's r) between corn yield and drought stress intensity for different growth stages .....	51
Table 2.10 Correlation coefficient (Pearson's r) between corn yield and aeration stress intensity for different growth stages .....	51
Table 3.1 Selected Landsat TM5 images during the growing season, path 21, row 31 ...	76
Table 3.2 NASS corn progress dates for the St. Joseph River Basin.....	81
Table 3.3 Date of maximum NDVI variation (range of the 95% prediction interval) for each year .....	88

Table	Page
Table 3.4 Rank of NDVI residual for each set of annual images. Rank 1 = best NDVIs, while Rank 11 = worst NDVIs. ....	93
Table 3.5 Pearson correlation coefficient, $r$ , between grain yield and average NDVI residuals for different growth stages.....	95
Table 3.6 Pearson correlation coefficient, $r$ , between stress indices and NDVI residuals for different growth stages .....	100
Table 4.1 Regional vs. default LAI development parameters .....	126
Table 4.2 Parameter calibration values for streamflow, seasonal LAI and annual corn yield for parameters that differed from those used by Her and Chaubey (2015) .....	133
Table 4.3 Bias of simulated soil moisture versus observed data during corn growing season for different sites. ....	137
Table 4.4 Range of uncertainty in soil moisture prediction during corn growing season for different sites based on the final set of parameters for each calibration.....	138
Table 4.5 Watershed area with a non-zero probability of failing to meet the low yield threshold (6.43 ton/ha) in any given year. ....	145
Table 5.1 Statistics for stresses and corn yield based on all modeling experiments. ....	173
Table 5.2 Mean discharge from the five modeling experiments. ....	180

## LIST OF FIGURES

Figure	Page
Figure 2.1 Aeration stress algorithm modifications.....	23
Figure 2.2 Geographic location of the four NRCS-SCAN plots across the Midwest USA .....	27
Figure 2.3 Crop yield calibration strategy .....	28
Figure 2.4 Typical arable soil types and their weight factors in the four study counties .	30
Figure 2.5 Management timing for the four study counties. The gray shaded zone reflects the date range for each management practice recorded by NASS State Crop Progress Data, with top and bottom defined by the begin and end dates. Blue squares indicate the 50% date of NASS data. Black circles indicate the default management date from SWAT. White circles indicate the calibrated date. 1a) to 1d) reflect the corn planting date for four counties; 2a) to 2d) reflect maturity date; 3a) to 3d) reflect harvest date. ....	37
Figure 2.6 Suggested calibration range for aeration/drought stress scaling function .....	39
Figure 2.7 Calibrated vs. observed volumetric soil moisture content (average daily value for 6 years) in Boone, IA. (a) 0-20 cm, (b) 46-58 cm, (c) 94-119 cm .....	41
Figure 2.8 Observed potential yield calculation .....	44
Figure 2.9 Model performance in yield a) calibration and b) validation for: 1) Boone, IA, 2) Woodbury, IA, 3) Mason, IL 4) Madison, OH.....	48
Figure 2.10 Model performance in daily biomass accumulation in 2005 at Boone, IA. ..	50

Figure	Page
Figure 2.11 Relationship of corn yields with drought stress intensity in silking-blister period at a) Boone, IA; b) Woodbury, IA; c) Madison, OH; d) Mason, IL.....	52
Figure 2.12 Relationship of corn yields with aeration stress intensity in reproductive period at a) Boone, IA; b) Woodbury, IA; c) Madison, OH; d) Mason, IL.....	53
Figure 2.13 Relative crop yield reduction due to drought stress or aeration stress. Relative yield reduction is calculated by eq. (2.9), which is shown on the y-axis. Recurrence probability which is represented as “return period” associated with the amount of yield reduction is shown in the x-axis. Red diamonds and blue dots represent the relative yield reduction caused by drought and aeration stress. Black triangles are relative yield reduction of observed data.....	54
Figure 3.1 Subset from the July 6th, 2008 Landsat TM5 image showing the St. Joseph River Watershed.....	72
Figure 3.2 Boxplot for corn NDVI values in 2003: (a) original data for all corn pixels within the region, (b) after applying the first filter: edge-of-field pixels are removed, (c) after applying filter 2: pixels without sufficient seasonal variation are removed, and (d) after applying filter 3: between images from May-22 and Jun-23. Pixels with decreasing NDVI values between the two dates were removed. The third filter was also applied between images from Jul-25 and Sep-11. Pixels with increasing NDVI values between two dates were removed.....	80
Figure 3.3 Cumulative rainfall comparison between long term average (1991-2010) and specific years.....	86

Figure	Page
Figure 3.4 (a) Median Normalized Difference Vegetative Index (NDVI) and (b) Coefficient of Variation (CV) from NDVI values in St. Joseph River watershed for 11 years. ....	87
Figure 3.5 Spatial distribution of NDVI as observed from Landsat 5 TM imagery for De Kalb County, IN on the following dates in 2003: (a) May 22nd, NDVI mean=0.19, CV=0.16; (b) Jul 25th, NDVI mean=0.83, CV=0.02; (c) Sep 27th, NDVI mean=0.54, CV=0.20.....	89
Figure 3.6 Generation of normal NDVI curve based on 11 years data versus: (a) days after planting, (b) PHU, and (c) GDD. The normal curve is generated by smoothing NDVI using robust loess method, with a span of 40%.....	91
Figure 3.7 Eleven year median NDVI values minus normal NDVI for the same: (a) number of days after planting, (b) PHU, and (c) GDD.....	92
Figure 3.8 The relationship between basin level corn yield and (a) mean NDVI residual for pre-silking period images; (b) mean NDVI residual for pre-maturity period images; (c) mean NDVI residual for all images in the growing period; (d) residual of the highest NDVI image for each year. Residuals are calculated based on GDD. ....	96
Figure 3.9 Relationship between ws value and median image NDVI residuals at (a) Pre-silking period; (b) Pre-maturity period; (c) whole growing period. ....	99
Figure 3.10 Relationship between water stress and risky pixel rate based on a) days, b) PHU, c) GDD. Red cross indicates the outlier at the very end of the growing season (Oct. 13th) in wet year 2003. ....	101



Figure	Page
Figure 3.11 Spatial distribution of corn pixels identified as being under stress and experiencing no stress (using the GDD based normal curve) in De Kalb county: (a) 2002 dry year, and (b) 2003 wet year. ....	102
Figure 3.12 Relationship between ws value and NDVI residual based on (a) number of days after planting, (b) PHU, (c) GDD for risky cells when risky pixel rate is below 0.2. ....	104
Figure 4.1. Geographic location of St. Joseph River watershed and the distribution of observational stations used for the model simulation. ....	122
Figure 4.2 NSERL soil moisture sensor position (denoted by ‘x’) and soil layer depth information from SSURGO database (each identified layer is given a unique color)....	124
Figure 4.3 The default SWAT potential LAI development curve and NDVI derived LAI from Landsat images (see Chapter 3 for details). The default curve is adjusted to better represent NDVI derived LAI. ....	126
Figure 4.4 Soil properties of corn HRUs in St. Joseph River watershed. a) soil saturated conductivity; b) bulk density; c) porosity; d) clay content; e) silt content; and f) sand content. All experience significant differences across county boundaries. ....	129
Figure 4.5 Model performance in daily streamflow for the St. Joseph River near Fort Wayne,IN (USGS 04180500) during the a) calibration period with log scale, b) validation period with log scale, c) calibration period with linear scale; d) validation period with linear scale. ....	132
Figure 4.6 Model performance in simulation of watershed average annual yield a) 2000-2010; b) 1995-1999; and c) corn leaf area index (LAI), 2000-2010. ....	133

Figure	Page
Figure 4.7 Sensitivity of parameters to streamflow, seasonal LAI and interannual yield .....	135
Figure 4.8 Evaluation of soil moisture in site BLG at (a) First layer (0-230 mm); (b) Second layer (230-430 mm); (c) Third layer (430-760 mm).....	139
Figure 4.9 The spatial distribution of annual mean yield by a) streamflow only calibration; b) multi-variable calibration; and the spatial distribution of interannual yield variation by c) only flow calibration. d) multi-variable calibration in the St. Joseph River watershed. ....	140
Figure 4.10 The spatial distribution of adjusted annual mean yield after removing the effect of soil inconsistencies, for a) streamflow only calibration; b) multi-variable calibration; and the spatial distribution of interannual yield variation by c) streamflow only calibration. d) multi-variable calibration .....	141
Figure 4.11 The probability distribution of HRU with yield lower than threshold (6.43 ton/ha) based on a) streamflow calibration. b) multi-variable calibration.....	143
Figure 4.12 Mean annual yield and interannual yield variability for all corn HRUs in St. Joseph River watershed, based on different calibration strategy after bias-correction...	144
Figure 5.1 Location and land cover of the St. Joseph River watershed. Land cover is from the USDA NASS Cropland Data Layer for 2010. The location of three USGS gauging stations and seven weather stations are also shown.....	161

Figure	Page
Figure 5.2 Annual mean temperature and precipitation change from the baseline period (1981-2010) to a) the near future period (2021-2050) and b) the far future period (2061-2090) according to three GCMs under three GHG scenarios .....	167
Figure 5.3 Monthly mean: (a) temperature and (b) precipitation variation between the baseline period (1981-2010) and the near future period (2021-2050); Monthly mean: (c) temperature and (d) precipitation variation between the baseline period (1981-2010) and the far future period (2061-2090) .....	169
Figure 5.4 Future changes to CO <sub>2</sub> and radiation use efficiency as estimated by the modified SWAT model.....	170
Figure 5.5 Boxplots for annual basin level stress and corn yield for the different modeling experiments: a) Aeration stress, b) Drought stress, c) Temperature stress, and d) corn yield. Box plots for each experiment based on annual average results for the 30 year period as projected by three GCMs and three climate change scenarios. BL: Baseline, NF: Near future, FF: Far future.....	172
Figure 5.6 SWAT estimated corn yield vs. aeration stress for all model experiments...	177
Figure 5.7 SWAT estimated corn yield vs. drought stress for all model experiments ...	177
Figure 5.8 SWAT estimated corn yield vs. temperature stress for all model experiments .....	178
Figure 5.9 The SWAT modeled relationship between corn temperature stress and mean daily air temperature .....	178
Figure 5.10 Flow duration curves for all modeling experiments.....	180

## ABSTRACT

Ruoyu, Wang. Ph.D., Purdue University, May 2016. Investigation of Climate Variability and Climate Change Impacts on Corn Yield in the Eastern Corn Belt, USA.  
Major Professors: Keith Cherkauer, Laura Bowling.

The increasing demand for both food and biofuels requires more corn production at global scale. However, current corn yield is not able to meet bio-ethanol demand without jeopardizing food security or intensifying and expanding corn cultivation. An alternative solution is to utilize cellulose and hemi-cellulose from perennial grasses to fulfill the increasing demand for biofuel energy. A watershed level scenario analysis is often applied to figure out a sustainable way to strike the balance between food and fuel demands, and maintain environment integrity. However, a solid modeling application requires a clear understanding of crop responses under various climate stresses. This is especially important for evaluating future climate impacts. Therefore, correct representation of corn growth and yield projection under various climate conditions (limited or oversupplied water) is essential for quantifying the relative benefits of alternative biofuel crops.

The main objective of this study is to improve the evaluation of climate variability and climate change effects on corn growth based on plant-water interaction in the Midwestern US via a modeling approach. Traditional crop modeling methods with the Soil and Water Assessment Tool (SWAT) are improved from many points, including introducing stress

parameters under limited or oversupplied water conditions, improving seasonal crop growth simulation from imagery-based LAI information, and integrating CO<sub>2</sub> effects on crop growth and crop-water relations. The SWAT model's ability to represent crop responses under various climate conditions are evaluated at both plot scale, where observed soil moisture data is available and watershed scale, where direct soil moisture evaluation is not feasible.

My results indicate that soil moisture evaluation is important in constraining crop water availability and thus better simulates crop responses to climate variability. Over a long term period, drought stress (limited moisture) explains the majority of yield reduction across all return periods at regional scale. Aeration stress (oversupplied water) results in higher yield decline over smaller spatial areas. Future climate change introduces more variability in drought and aeration stress, resulting in yield reduction, which cannot be compensated by positive effects brought by CO<sub>2</sub> enhancement on crop growth.

Information conveyed from this study can also provide valuable suggestions to local stakeholders for developing better watershed management plans. It helps to accurately identify climate sensitive cropland inside a watershed, which could be potential places for more climate resilient plants, like biofuel crops. This is a sustainable strategy to maintain both food/fuel provision, and mitigate the negative impact of future climate change on cash crops

## CHAPTER 1. INTRODUCTION

### 1.1 Research Background

The global population reached seven billion in 2011, and is projected to increase to nine billion by 2050 (Cohen, 2003). Global agriculture is faced with challenges due to the growing population: more food is needed to feed people and livestock (Sinha et al., 1988), and more fuel is needed to meet the potential ethanol demand from bio-energy markets (William and Kucharik, 2011). Corn is traditionally considered as a food or animal feed crop, but ethanol is also obtained by fermenting maize grain in first-generation biofuel production (Hill *et al.*, 2006). At the global scale, the major portion of agricultural products, like corn is provided by a few high-yield cropping systems from a relatively small area of arable land (Cassman and Wood, 2005). The Midwestern Region of the United States is one of the world's largest and most productive cropping systems. Also known as the U.S. Corn Belt, this region occupies around 12% of the US continental area, and supplies around 40% of the world's corn (Connor et al., 2011). Therefore, any yield reduction in the US Corn Belt would seriously affect both national and global corn supplies.

In 2014, 38.8% of the US corn crop was used to feed livestock, 30.5% was used for ethanol, 12.9% was exported, and the remaining 17.8% was used for food and beverage production (Capehart et al., 2014). However, current corn yield is still not able to meet ethanol demand targets without jeopardizing food security (Davis *et al.*, 2012) or intensifying and

expanding corn cultivation (Zhuang *et al.*, 2013). Since both of them will likely have significant agricultural and environmental implications, utilizing the cellulose and hemicellulose from perennial grasses as an alternative biofuel feedstock has been recommended by the Advance Energy Initiative (AEI) of the US Government.

Compared to corn, biofuel crops, like switchgrass and *Miscanthus* may require less management and financial inputs, such as tillage, fertilization, and herbicide/ pesticide application, which has the potential to reduce non-point source pollution from cropland. Secondly, some biofuel crops have higher land and water use efficiencies than traditional crops (VanLoocke *et al.*, 2012; Heaton, *et al.*, 2008). If perennial grasses can be processed efficiently, there is the potential that less land and water will be needed for perennial grasses to match ethanol demands than corn. Lastly, biofuel crops have higher biomass productivity due to their high adaptability to different soils and climates than grain crops, following the initial establishment period (Heaton, *et al.*, 2004; Dohleman and Long, 2009). Therefore, replacing grain crops with biofuel crops in areas where grain yield is relatively low or has strong yield variability might be a sustainable strategy to maintain both food/fuel provision and environmental integrity, especially to mitigate the negative impact of future climate change on grain yield. To realize this sustainable strategy, it is essential to understand the responses of corn crops under various climate conditions, and apply this information to the watershed scale scenario analysis to quantify the trade-offs in food and fuel production, and provide scientific based suggestions to watershed managers.

Agriculture is a climate-sensitive system. Although the climate in the US Corn Belt is generally suitable for crop growth, variation in temperature, precipitation and extreme

events such as flooding or drought can seriously affect production, often negatively. Climate variability affects soil moisture dynamics, which are directly related to crop growth. Soil moisture has a complicated relationship with crop development. Over shorter spatial and temporal scales, either limited or oversupplied soil moisture is harmful for crop growth. Based on historical records, cooler and wetter conditions are favorable for corn production in the grain fill period, while warmer and drier conditions in spring months are beneficial for early season crop growth (Lobell and Asner, 2003; Mishra and Cherkauer, 2010).

Due to the increasing trend in greenhouse gas (GHG) emissions, the world is faced with the challenge of climate change, especially in the agricultural sector. Average US temperatures are expected to increase by 2°C to 6°C by 2100, depending on the level of future GHG emissions, and the projections from various climate models (USGCRP, 2009). Projections show that future patterns of precipitation and storm events will vary temporally and spatially (Meehl et al, 2007). The Midwest USA is projected to face an increase in temperature of 3°C to 6°C, by the end of 21 century, accompanied by a shift in seasonal rainfall distribution towards wetter springs (Christensen, 2007) and lower summertime soil moisture (Cherkauer and Sinha, 2010).

Projected seasonal changes in precipitation and temperature in the Midwest are likely to lead to sub-optimal conditions for crop growth (Pryor, 2013). Increased annual temperature is generally considered to benefit crop production in the Midwest, due to the longer growing season (Wuebbles and Hayhoe, 2004). However, the increased summer temperature and decreased moisture during the grain fill period may seriously affect final



yield (Lobell and Asner, 2003). If soil is too wet in the spring, planting date is adversely affected. Later planting affects final yield by reducing grain filling time (Arjal et al., 1978), and increasing the risk of exposure of cold temperatures late in the season before grain maturation (Nielsen et al., 2002). Planting crops in cold and wet soil will reduce oxygen transport rates, adversely affect root metabolism and retard root development, causing plant wilting after soil submersion (Glinski and Stepniewski, 1983).

To quantify the impact of climate variability and future climate change on crop growth, modeling is widely employed in many studies (Semenov and Porter, 1995; Srticevic et al., 2011; Matthew et al., 2015). As a mathematical representation and simplification of natural processes, properly validated crop simulation models consider the environmental impacts of climate on crop growth processes (Southworth et al., 2000). However, many current modeling studies either lack the algorithms to represent crop responses under adverse climate conditions, for example, crop responses to excess water conditions (Ines et al., 2001; Rosenzweig et al., 2002), or neglect to evaluate simulated soil moisture conditions at all (Liu et al., 2015; Niyogi et al., 2015; Ummenhofer et al., 2015). Further, it is not simple to accurately estimate the impact of water stress on seasonal growth at the regional scale. The best currently available datasets, for example, the National Agricultural Statistics Service (NASS) Crop Progress and Condition data, are too coarse in spatial resolution (state or sub-state level for crop progress, county level for yield) to detect events that are infrequent at large spatial scale, but that may be frequent at small scales (i.e. the low spot in the field), so it is difficult to isolate the biophysical effect of water stress in a way that can be quantified. Therefore, correct representation of crop growth and yield

projection under various climate conditions (limited or oversupplied water) is essential for crop modeling for analysis of future climate impacts (Rotter et al., 2011) and the relative benefits of alternative crops.

The future increases in CO<sub>2</sub> should be considered in crop modeling studies as well. This is because CO<sub>2</sub> stimulates photosynthetic rates directly as the substrate of photosynthesis (Oliver et al., 2009), and reduces the stomatal conductance, which improves the drought tolerance of some plants by delaying a response to water limitation stresses (Long et al., 2004). Therefore, the negative effect of precipitation and temperature change could be mitigated by increasing concentrations of CO<sub>2</sub> in the atmosphere.

Considering current deficiencies in model representations of physical processes and analysis of biophysical impacts, it is essential to improve the evaluation of climate variability and climate change effects on corn growth based on plant-water interaction in the Midwestern US. The research in this dissertation will investigate the important role of moisture related indices (oversupplied or limited water) in seasonal crop growth and annual yield, and evaluate their effects at plot and regional scales. The modeling process will be improved to better reflect crop responses to climate variability via moisture related bioclimatic indices, with extension to future periods with more adverse climate conditions and an increasing trend of CO<sub>2</sub>.

## 1.2 Research Hypothesis and Objectives

The main goal of this study is to assess the impact of climate variability and climate change on maize growth, yield and hydrologic response in the Eastern Corn Belt via a modeling approach. The current practice of applying crop growth models to explore climate impacts on crop yield without evaluation of regional hydrology is problematic. Without water balance constraints at the regional to watershed scale, neither soil moisture nor crop responses to deficit/excess water may be well reproduced by the model. Therefore, in this research, the projections of crop yield response to climate variability are enhanced through improvements in ecohydrologic modeling to constrain simultaneous prediction of seasonal crop growth, annual yield and streamflow. Further, the hydrological and biophysical effects of future climate change also consider the impact of CO<sub>2</sub> enhancement combined with precipitation and temperature change, which has rarely been considered in previous modeling studies.

Four main hypotheses will be tested in this research:

Hypothesis 1: Annual crop yield variability is regulated by moisture-related (oversupplied or limited water) bioclimatic stresses. Those stresses have significant effects on crop yield at specific growing periods.

Hypothesis 2: Crop response to oversupplied or limited water varies with spatial scale. Drought stress results in regional yield declines, while aeration stress results in higher yield decline over smaller spatial areas, but is not detectable at large special scales. Drought stress explains the majority of yield reduction across all return periods.

Hypothesis 3: Multi-variable calibration of streamflow, the seasonal crop growth curve (LAI development), and annual yield within an ecohydrologic model can improve simulation performance in the face of climate variability, and reduce uncertainty in moisture prediction.

Hypothesis 4: Future climate change will have negative impacts on rainfed corn yield, and introduce more interannual variability in the Eastern Corn Belt because of increased spring wetness and decreased summer rainfall. CO<sub>2</sub> enhancement cannot compensate for yield reduction due to changes in rainfall and temperature.

Hypothesis 1, 3, and 4 were addressed using an ecohydrologic model, the Soil-Water-Assessment Tool (SWAT) (Arnold et al., 1998) at both plot scale across Midwest, USA (Hypothesis 1) and watershed scale (Hypothesis 3 and 4). Hypothesis 2 was addressed using both remote sensing technology and modeling with the help of multiple years' Landsat TM5 images in St. Joseph River watershed, Eastern Corn Belt. The specific objectives of this research were to:

1. Conduct multi-step calibration at the plot scale where observed soil moisture data is available. Calibrate crop yield based on biophysical parameters and the simulated soil moisture via the modeled crop stress functions (bioclimatic variables).
  - Improve model to include aeration stress computation algorithm and drought stress parameters
  - Use a multi-step calibration including management timing, soil moisture, biophysical and stress parameters.

2. Examine the relationship between crop yield and climate variability in the historical period.
  - Identify relationships between observed crop yields and simulated climate stress variability at different crop physiological stages via regression analysis.
  - Investigate yield reduction due to individual stresses over a longer historical period via frequency analysis.
3. Evaluate variability in corn growth conditions and phenology both spatially and temporally.
  - Evaluate bioclimatic stress effect on seasonal corn leaf growth via comparison of individual measurements of NDVI with long term “normal curve”.
  - Identify the spatial pattern of risky pixels in both dry year and wet years.
4. Conduct a multi-variable calibration at the watershed scale to constrain streamflow, seasonal leaf area development and annual yield simultaneously.
  - Identify areas with climate sensitivity, defined as areas that always have lower crop yield and higher interannual variability.
  - Examine the possible spatial differences when different calibration strategies are applied.
5. Explore the biophysical and hydrological effects of future climate change including trends in CO<sub>2</sub> at watershed scale.

- Improve model to take dynamic CO<sub>2</sub> concentration as input.
- Evaluate future corn yield and bioclimate stress variation considering both CO<sub>2</sub> and precipitation and temperature change.
- Investigate streamflow response to future climate change and enhanced CO<sub>2</sub> via flow frequency analysis.

### 1.3 Dissertation Organization

This dissertation is organized into six chapters. First is the introduction (this chapter) which includes general background information, research needs, research objectives and the hypotheses tested in this dissertation. Chapters 2-5 are presented in the format of journal manuscripts, which provide detailed information related to the main objectives. Chapter 2 tests hypothesis 1 and 2 to parameterize and improve SWAT model in corn responses at various climate conditions at plot scale in Midwest USA, and explore historical variability (moisture related) on crop yield via modeling method. Chapter 3 tests hypothesis 2 to detect corn response to climate stress using remote sensing technology, and analyze spatial and temporal variability of corn NDVI in the St. Joseph River watershed. Chapter 4 tests hypothesis 1 and 3 to use multi-objective calibration strategy to regulate model performance in surface water, seasonal LAI development and annual yield simultaneously, where moisture calibration is not feasible at basin scale. Chapter 5 tests hypothesis 2 and 4 to investigate biophysical and hydrological effects of future climate change including trends in CO<sub>2</sub>. Chapter 6 provides a summary and conclusion for the whole dissertation,

including main findings for this study and recommendations for future research. This research work has generated four research papers:

Wang, R, Bowling LC, Cherkauer KA. 2016. Estimation of the Effects of climate variability on Crop yield in the Midwest USA. *Agricultural and Forest Meteorology*, **216**: 141–156.

Wang R, Cherkauer KA, Bowling LC. 2016. Corn response to climate stress detected with satellite-based NDVI time series (Submitted to *Remote Sensing*)

Wang R, Bowling LC and Cherkauer KA. 20XX. Improved simulation of annual crop sensitivity to climate variability in the Eastern Corn Belt. (In internal revision)

Wang R, Bowling LC, Cherkauer KA, Raj C, Her Y, Chaubey I. 2016. Biophysical and hydrological effects of future climate change including trends in CO<sub>2</sub>, in the St. Joseph River watershed, Eastern Corn Belt. (Submitted to *Agricultural Water Management*).

## 1.4 References

- Arjal RD, Prato JD, Peterson ML. 1978. Response of corn to fertilizer, plant population, and planting date. *California Agriculture* **32(3)**: 14-15.
- Arnold JG, Srinivasan R, Muttiah RS, Williams JR. 1998. Large area hydrologic modeling and assessment part I: Model Development. *Journal of the American Water Resources Association* **34(1)**: 73-89
- Capehart T, Allen E, Bond J. 2014. USDA, ERS Feed Outlook, FDS-13c, <http://www.ers.usda.gov/media/1056601/fds13c.pdf>  
<http://www.worldofcorn.com/#corn-usage-by-segment>
- Cassman KG, Wood S. 2005. Cultivated system. In Millennium Ecosystem Assessment: Global Ecosystem Assessment Report on Conditions and Trends. Washington D.C.: Island Press, pp. 745-94.
- Cherkauer KA, Sinha T. 2010. Hydrologic impacts of projected future climate change in the Lake Michigan region. *Journal of Great Lakes Research* **36**: 33-50.
- Christensen JH, Hewitson B, Busuioc A, Chen A, Gao X, Held I, Jones R, Kolli RK, Kwon WT, Laprise R, Magana RV, Mearns L, Menendez CG, Raisanen J, Rinke A, Sarr A, Whetton P. 2007. Regional Climate Projections. In: *Climate Change 2007: The Physical Science Basis. Contribution of Working Group I to the Fourth Assessment Report of the Intergovernmental Panel on Climate Change* [Solomon S, Qin D, Manning M, Chen Z, Marquis M, Averyt KB, Tignor M, Miller HL (eds.)]. Cambridge University Press, Cambridge, United Kingdom and New York, NY, USA.
- Cohen JE. 2003. Human population: the next half century. *Science* **302**:1172-1175.
- Connor DJ, Loomis RS, Cassman KG (Ed.). 2001. Crop Ecology: productivity and management in agricultural systems. Cambridge University Press.
- Davis SC, Parton WJ, Grosso SJD, Keough C, Marx E, Adler PR, Delucia EH. 2012. Impact of second-generation biofuel agriculture on greenhouse-gas emissions in the corn-growing regions of the US. *Frontiers in Ecology and the Environment* **10**:69-74.
- Dohleman FG, Long SP. 2009. More productive than maize in the Midwest: how does Miscanthus do it? *Plant Physiology* **150**: 2104-2115.
- Glinski J, Stepniowski W. 1983. Soil aeration and its role for plants. Boca Raton, Florida.
- Heaton E, Voigt T, Long SP. 2004. A quantitative review comparing the yields of two candidate C4 perennial biomass crops in relation to nitrogen, temperature and water. *Biomass and Bioenergy* **27**:21-30.



- Heaton EA, Dohleman FG, Long SP. 2008. Meeting US biofuel goals with less land: the potential of Miscanthus. *Global Change Biology* **14**: 2000-2014.
- Hill J, Nelson E, Tilman D, Polasky S, Tiffany D. 2006. Environmental, economic, and energetic costs and benefits of biodiesel and ethanol biofuels. *PNAS, Proceedings of the National Academy of Sciences* **103**: 11206-11210.
- Ines AVM, Droogers P, Makin IW, Gupta AD. 2001. Crop growth and soil water balance modelling to explore water management options, Working Paper 22, International Water Management Institute (IWMI), Colombo, Sri Lanka, p. 26.
- Liu X, Andresen J, Yang H, Niyogi D. 2015: Calibration and Validation of the Hybrid-Maize Crop Model for Regional Analysis and Application over the U.S. Corn Belt. *Earth Interaction*.**19**: 1–16.
- Lobell DB, Asner GP. 2003. Climate and management contributions to recent trends in U.S. agricultural yields. *Science* **299** (5609).
- Long ST, Ainsworth EA, Rogers A, Ort DR. 2004. Rising atmospheric carbon dioxide: plants FACE the future. *Annual Review of Plant Biology* **55**:591-628.
- Matthew OJ, Abiodun BJ, Salami AT. 2015. Modelling the impacts of climate variability on crop yields in Nigeria: performance evaluation of RegCM3-GLAM system. *Meteorological Applications* 22:198–212.
- Meehl GA, Stocker TF, Collins WD, Friedlingstein P, Gaye AT, Gregory JM, Kitoh A, Knutti R, Murphy JM, Noda A, Raper SCB, Watterson IG, Weaver AJ, Zhao ZC (2007). Global Climate Projections. In: *Climate Change 2007: The Physical Science Basis. Contribution of Working Group I to the Fourth Assessment Report of the Intergovernmental Panel on Climate Change* [Solomon S, Qin D, Manning M, Chen Z, Marquis M, Averyt KB, Tignor M, Miller HL (eds.)]. Cambridge University Press, Cambridge, United Kingdom and New York, NY, USA.
- Mishra V, Cherkauer KA. 2010. Retrospective droughts in the crop growing season: implications to corn and soybean yield in the Midwestern United States. *Agricultural and Forest meteorology*. **150**: 1030-1045.
- Nielsen RL, Thomison PR, Brown GA, Halter AL, Wells J, Wuethrich KL. 2002. Delayed planting effects on flowering and grain maturation of dent corn. *Agronomy Journal* **94**:549-558.
- Niyogi D, Liu X, Andresen J, Song Y, Jain AK, Kellner O, Takle ES, Doering OC. 2015. Crop models capture the impacts of climate variability on corn yield. *Geophysical Research Letters* **42**: 3356-3363.

- Oliver RJ, Finch JW, Taylor G. 2009. Second generation bioenergy crops and climate change: a review of the effects of elevated atmospheric CO<sub>2</sub> and drought on water use and the implications for yield. *GCB Bioenergy* **1**:97-114.
- Pryor SC. (Ed.). 2013. Climate change in the Midwest: impacts, risks, vulnerability, and adaptation. Indiana University Press.
- Rosenzweig C, Tubiello FN, Goldberg R, Mills E, Bollmield J. 2002. Increased crop damage in the US from excess precipitation under climate change. *Global Environmental Change* **12**: 197-202.
- Rotter RP, Carter TR, Olesen JE, Porter JR. 2011. Crop-climate models need an overhaul. *Nature Climate Change* **1**: 175-177.
- Semenov MA, Porter JR. 1995. Climatic variability and the modelling of crop yields. *Agricultural and Forest Meteorology* **73**: 265–283.
- Sinha SK, Rao NH, Swaminathan MS. 1988. Food security in the changing global climate. In the conference proceedings for The Changing Atmosphere: Implications for Global Security, 27-30 June 1988, in Toronto, Canada, 167-192. WMO-No. 170. Geneva: World Meteorological Organization.
- Southworth J, Randolph JC, Habeck M, Doering OC, Pfeifer RA, Rao DG, Johnston, JJ. 2000. Consequences of future climate change and changing climate variability on maize yields in the Midwestern United States. *Agriculture, Ecosystems & Environment* **82**: 139-158.
- Srticevic R, Cosic M, Djurovic N, Pejic B, Maksimovic L. 2011. Assessment of FAO AquaCrop model in the simulation of rainfed and supplementally irrigated maize, sugar beet and sunflower. *Agricultural Water Management* **98**:1615-1621.
- Ummenhofer CC, Xu H, Twine TE, Girvetz EH, McCarthy HR, Chhetri N, Nicholas KA. 2015: How Climate Change Affects Extremes in Maize and Wheat Yield in Two Cropping Regions. *Journal of Climate* **28**: 4653–4687.
- USGCRP 2009. *Global Climate Change Impacts in the United States*. Thomas R. Karl, Jerry M. Melillo, and Thomas C. Peterson (eds.). United States Global Change Research Program. Cambridge University Press, New York, NY, USA.
- VanLoocke A, Twine TE, Zeri M, Bernacchi CJ. 2012. A regional comparison of water use efficiency for Miscanthus, switchgrass and maize. *Agricultural and Forest Meteorology* **164**:82-95.
- William JS, Kucharik CJ. 2011. Crop management and phenology trends in the U.S. Corn Belt: Impacts on yields, evapotranspiration and energy balance. *Agricultural and Forest Meteorology* **151**: 882-894.

- Wuebbles DJ, Hayhoe K. 2004. Climate change projections for the United States Midwest. *Mitigation and Adaptation Strategies for Global Change* **9**: 335–363.
- Zhuang Q, Qin Z, Chen M. 2013. Biofuel, land and water: maize, switchgrass or Miscanthus? *Environment Research Letter* **8**:015020.

## CHAPTER 2. ESTIMATION OF THE EFFECTS OF CLIMATE VARIABILITY ON CROP YIELD IN THE MIDWEST USA

### 2.1 Abstract

Crop yield is strongly affected by climate variability. When applying ecohydrologic models to study climate impacts on crop yield, especially interannual yield responses to climate stresses, the model simulation of plant available soil moisture must be constrained in order to reproduce plant production variation via moisture related bio-climate variables. In this study, the Soil and Water Assessment Tool (SWAT) is used to investigate the relationship between climate variability and crop yield at four sites (Boone, Woodbury, Madison, and Mason) in the Midwestern USA. The model was first calibrated for soil moisture at the plot scale. The calibrated model was then used to extend the observational records between 1991 and 2010 to better capture the effect of climate variability on crop yield over a longer period (1941-2010). We also explored the relative yield reduction due to individual stresses. Our results indicated that annual observed yield from 1991 to 2010 is correlated with drought stress intensity in the early and middle reproductive stage at most sites. The early and middle reproductive periods were thought more critical than other stages, because severe drought stress in those periods is substantially correlated with low observed yields. No significant relationship between crop yield and aeration stress was

found at any of the four sites, due to their different impacts under different spatial scales, as well as low frequency of events in the historical record. Long-term simulation of yield reduction indicates that drought stress was the dominant factor affecting yield in the historical period when compared with aeration stress both at short and long return periods (high/low probability of exceedance). For a 70 year period, the total yield reduction due to drought stress is 8.1%, 17.5%, 15.2% and 9.7% respectively for Boone, Woodbury, Madison and Mason.

## 2.2 Introduction

Crop yield is of great concern all over the world. The Food and Agriculture Organization of the United Nations (FAO) has predicted that “although the growth of food demands are expected to slow to 1.2 percent a year over the period 2015 to 2030, by 2030, an extra billion tons of cereals will still be needed each year” (FAO, 2002). The increasing food demands have to be matched by a corresponding increase of food supply. An unbalanced supply-demand relation can lead to tight food markets and rising food prices. To release the pressure in food supply, increased exploitation of arable land, crop productivity growth and increases in cropping intensity are often employed (Rosegrant et al., 2012). Productivity growth is the most critical component of agricultural supply increases. However, there are many factors that can affect crop yields negatively. Annual crop yields are strongly controlled by specific hybrids and specific growing conditions, including weather and nutrient availability. Further, at different growth stages, the magnitude of influence could be different for each factor.

Among all of the factors, soil moisture could have the most complicated relationship with crop development. We can subcategorize the impact of this factor into two parts. One is water deficiency, and the other is excess water stress. Both of them will negatively affect plant growth and threaten crop yields. Limited soil moisture results in a decrease of plant water uptake. Drought will also cause plant tissue dehydration and in turn reduce shoot and root growth, membrane integrity and decrease crop production. Drought-induced crop yield reduction is well documented by many researchers. In the 1930s in the southern Great Plains of the US, drought caused as much as a 50% reduction in corn and wheat yields (Warrick, 1984). The 1988 Midwest US drought led to a 30% reduction in US corn production and cost three billion dollars in direct relief payments to farmers (Rosenzweig and Hillel, 1988). The recent 2012 drought affected at least 60% of farms in the US, and caused the lowest national yield value since 1995, 123.4 bu/acre (Crutchfield, 2012)

Limited water supply (drought) is not the only factor affecting crop growth. If soil water is oversupplied, oxygen transport rates in the soil are reduced, adversely affecting root metabolism and retarding root development. In such cases, a paradoxical phenomenon may occur where the plant wilts not due to lack of water but due to a lack of oxygen. The relative proportion of water to air plays an important role in plant health. The optimum moisture content for healthy growth recommended by Kirkham and Powers (1972) is 25% of total soil pore space for both water and air content. Boyer (1982) found that 41% of crop losses in the United States are caused by drought, while excess water causes crop losses of 16% on average. In the United States, 25% of the soils are threatened by drought, and 16% are too wet, both resulting in a limit to crop production (Boyer, 1982).

Historically, much of the Midwestern U.S. has been faced with excess water. Due to previous glacial activities, dense till restricts water infiltration, which means much of this area maintains a high water table and is very poorly drained (Thompson and Bell, 1998; Muenich, 2011). Under such conditions, organic matter is easily accumulated, resulting in some of the most fertile lands in the world (Blann et al., 2009), but also requiring drainage to make the region workable. Without drainage improvements, this region is subject to delayed planting, denitrification, manganese toxicity, poor root development, depressed nodule activity in legumes, and serious root diseases (Ohio Agronomy Guide, 14th Edition). These soils can be the most or least productive ones, depending on how they are managed. Therefore, in the Midwestern U.S., croplands in poorly drained condition are likely to be drained using subsurface tile lines to release excess water problems and guarantee the healthy growth of crops (Naz et al., 2009).

Understanding the role of soil moisture in crop yield variation will bring great benefits to a range of users in the Midwestern U.S., including farmers and crop marketing agencies. Many studies have investigated the close relationship between soil moisture or moisture related bioclimatic indices and plant yields (Torell et al., 2011; Singh et al., 1998). Bioclimatic or agro-meteorological indices are preferred over meteorological metrics by land managers, because of their clearer association with crop phenology and management practices (Matthews et al., 2008). Bioclimatic indices used in previous research to explore drought effects include annual maximum soil moisture deficit (Brown, 2013), Soil Moisture Percentile (SMP) (Mishra and Cherkauer, 2010), and the Evapotranspiration Deficit Index (ETDI) (Narasimham and Srinivasan, 2005). When soil water is oversupplied,

the soil aeration capacity (SAC) (Viesser, 1977) and the Least Limiting Water Range (LLWR) (Benjamin et al., 2003) metrics are often employed to evaluate crop yield response. All of these indices have been found to be good indicators of crop yield under dry or wet conditions, respectively.

To explore the response of crop growth to climate variability and estimate crop yield under various climate conditions, crop growth modeling is often employed. A good model should be able to capture soil moisture dynamics under various climate conditions. The response of crops to both oversupplied and limited moisture conditions must also be clearly reflected. Thus the close relationship between crop production and moisture related bioclimatic variables (Physical-Physiological index) should be addressed by the model for serious analysis of future climate impacts. Although there are many crop modeling studies and most of the models used have water balance modules, only a few of them evaluate model performance for both soil moisture and yield prediction (Saseendran et al., 2004; Mkhabela and Bullock, 2012). Furthermore, not all models consider crop response under excess water conditions. For example, Hybrid-Maize (Yang et al., 2004), AquaCrop (Steduto et al., 2009) and Cropsyst (Stockle, et al., 1994) only consider yield reduction under drought stress, which limits use in areas that suffer from excess water problems, such as fields with limited drainage in the Midwest U.S.

The main objective of this paper is to study the role of climate variability on crop yield at four sites across the Midwestern U.S. with extended data sets of climate observation and crop yield. The Soil and Water Assessment Tool (SWAT) is used in this study because of its robustness in water quantity simulation and the availability of modules to represent plant



response in both dry and wet soil conditions. SWAT's ability to capture daily soil moisture was first tested at four Natural Resources Conservation Service (NRCS) - Soil Climate Analysis Network (SCAN) sites. The model's ability to represent historical corn production using observed climate (1991-2010) was then evaluated at the same sites. The response of simulated crop yields to the timing and duration of different bio-climate extremes (related to drought and aeration stress) was explored. Finally, yield reduction due to individual stresses for a longer historical period (1941-2010) was investigated through frequency analysis.

## 2.3 Methods

### 2.3.1 SWAT model overview and modification

The Soil and Water Assessment Tool (SWAT) was developed by USDA-ARS and is widely used to assess the impact of climate variability on hydrologic process and crop production. The Hydrologic Response Unit (HRU) is the basic spatial unit required for simulation. It is a lumped land area, possessing unique combinations of land use, soil and slope within a subbasin. The hydrologic cycle is simulated based on a water balance equation of soil water content, including evapotranspiration, surface runoff, infiltration, percolation, shallow and deep aquifer flow (Arnold et al., 1998). A detailed description of SWAT hydrological simulation can be found in Neithsch et al., (2009).

Plant growth is also simulated at the HRU level. The growth cycle of each plant is regulated by specific attributes in the SWAT plant database, as well as the timing of operations in

the management files. Growing Degree Days are often used to define crop growth period and schedule management operations, but SWAT makes use of a variant, the heat unit or *PHU*. Crop planting date is decided by the fraction ( $fr_{PHU0}$ ) of annual total  $PHU_0$  (heat unit accumulation above 0 °C). The plant begins to accumulate *PHU* (heat unit accumulation above the plant specific base temperature  $T_{base}$ ) after planting until it reaches  $PHU_{mat}$  (heat unit accumulation to maturity), which is also defined by crop type and cultivar. The value of  $fr_{PHU}$  is the ratio of current *PHU* to  $PHU_{mat}$  and is used to decide the timing of other management operations, such as fertilizer/pesticide application ( $< 1.00$ ), and harvest ( $>1.00$ ). The crop has reached maturity when  $fr_{PHU}=1.00$ .

Under optimal conditions (no growth stress), daily biomass accumulation ( $\Delta bio$ ; kg/ha) is regulated by leaf area index (*LAI*) development, light interception ( $k_l$ ), photosynthetically active radiation ( $H_{day}$ ; MJ m<sup>-2</sup>), and radiation-use efficiency (*RUE*; 10<sup>-1</sup> g/MJ).

$$\Delta bio = 0.5H_{day} \cdot (1 - \exp(-k_l \cdot LAI)) \cdot RUE \quad (2.1)$$

For annual crops, *LAI* accumulates each day following an optimal leaf area development curve, with similar shape, but different parameters for different plants. *LAI* increases from the planting date until it reaches the maximum *LAI* value and is then stable until the senescence point (*DLAI*) is attained. *LAI* drops from this point until the crop reaches maturity.

Actual daily growth varies from the optimal growth rate due to an accumulation of stresses, which include water deficit or excess, nutrient limitation, extreme temperature, pests, and diseases. The total actual biomass accumulation over the growing season is calculated as:

$$bio = \sum_{i=1}^d \Delta bio_i \cdot [1 - \max(wstrs, astrs, tstrs, nstrs, pstrs)] \quad (2.2)$$

where  $bio$  is the total plant biomass on a given day ( $\text{kg ha}^{-1}$ ), and  $\Delta bio_i$  is the increase in total plant biomass on day  $i$  ( $\text{kg/ha}$ ). The terms  $wstrs$ ,  $astrs$ ,  $tstrs$ ,  $nstrs$  and  $pstrs$  represent drought, aeration, temperature, nitrogen and phosphorus stress, respectively and are the five growth constraints considered by SWAT.  $d$  is the number of days from planting to the simulation day. In our case, auto fertilization is applied to avoid any nutrient limitation. Therefore, stress from nutrient limitation is not considered in this research.

SWAT considers daily water stresses either under oversupplied or limited conditions (aeration and drought stress). Aeration stress ( $astrs$ ) is related to a function ( $satco$ ) of porosity, field capacity and soil water content in the soil profile.

$$satco = \frac{\theta - \theta_{fc}}{\eta - \theta_{fc}} \quad (2.3)$$

where  $\theta$  is the soil water content in the soil profile (mm water),  $\theta_{fc}$  is field capacity for the entire soil profile (mm water), and  $\eta$  is the soil water content at saturation (mm water). The variable  $satco$  is the fraction of saturation over field capacity in the soil profile and is used to define aeration (excess water) stress based on a function from the APEX model (Steglich and Williams, 2008):

$$astrs = \frac{satco}{satco + \exp(b1 - b2 * satco)} \quad (2.4)$$

Plotting  $astrs$  versus  $satco$ , an S-shaped curve can be attained. The S-shaped curve is used to describe the behavior of many processes (aeration stress, potential harvest index, P plant use-soil P concentration) in the APEX model. The variables  $b1$  and  $b2$  control the shape of the S-curve and therefore the degree to which the plant experiences stress due to an increasing excess of soil water.

The original SWAT aeration algorithm calculates  $astrs$  based on the water content for the entire soil profile. This could be suitable if the plants' root system is in or close to maturity status, but will not reflect conditions leading to aeration stress earlier in the growing season when plant roots are shallow. We modified the original aeration stress calculation algorithm so that it considers root depth. The modified algorithm only considers aeration stress in the root related soil layers instead of the whole soil profile (Figure 2.1).

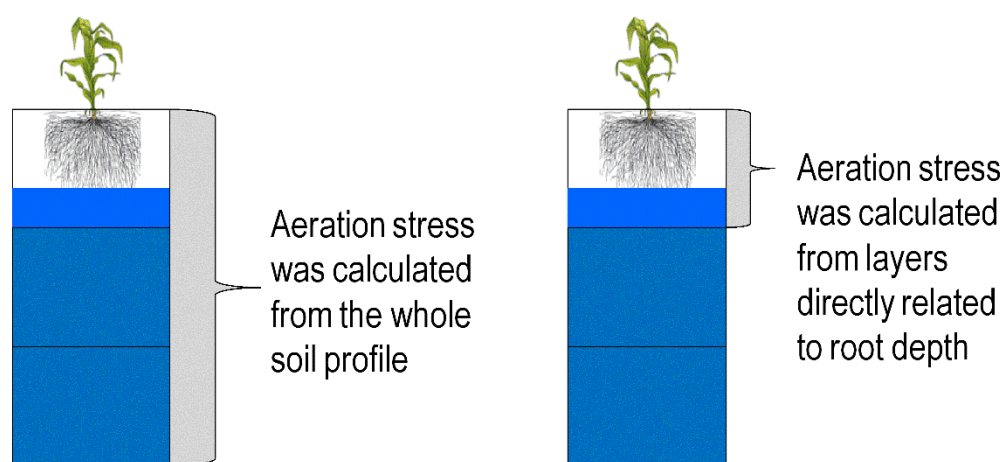


**Figure 2.1 Aeration stress algorithm modifications**

Drought stress is defined as a comparison between actual and potential plant transpiration:

$$wstrs = 1 - \frac{W_{actualup}}{E_t} = 1 - strsw \quad (2.5)$$

where  $wstrs$  is the drought stress for a given day,  $E_t$  is the maximum plant transpiration on a given day (mm water),  $W_{actualup}$  is the actual amount of transpiration on a given day or total plant water uptake for the day (mm water),  $strsw$  is the ratio of actual to maximum transpiration.

Compared with eq. (2.3),  $strsw$  has a similar pattern with  $satco$ , which are both physical parameters, showing the ratio of an actual to a potential condition. Aeration and drought stresses are physiological parameters, which are transformed from physical parameters, like  $satco$  and  $strsw$ . The transformation method is quite subjective and mostly based on expertise and experience (Kozak et al., 2006). Therefore, like aeration stress, a new equation to calculate drought stress is introduced, which is shown in eq. (2.6). The S-curve method is used to adjust yield which is over/under sensitive in some places to the original drought stress.

$$wstrs' = 1 - \frac{strsw}{strsw + \exp(c1 - c2 * strsw)} \quad (2.6)$$

Daily biomass is controlled by stresses and keeps accumulating until the accumulated heat units reach  $PHU_{mat.}$ , then biomass keeps constant until harvest. Annual yield is then separated from total above-ground biomass ( $bio_{ag}$ ) via multiplying the harvest index ( $HI$ ).  $HI$  is a function of the optimal harvest index ( $HI_{opt}$ ) and  $fr_{PHU}$ . If heat units do not accumulate to  $PHU_{mat.}$ ,  $HI$  is less than  $HI_{opt}$ . Therefore, early harvesting results in less yield

from accumulated aboveground biomass. Otherwise,  $HI$  is close to  $HI_{opt}$ , which means that above ground biomass transfers to crop yield at an optimal rate. Water deficiency also affects the value of  $HI$  during the active growing season ( $0.5 < fr_{PHU} < DLAI$ ), with the actual harvest index for each crop,  $HI_{act}$ , calculated as

$$HI_{act} = (HI - HI_{min}) \bullet \frac{\gamma_{wu}}{\gamma_{wu} + \exp[6.13 - 0.883 \times \gamma_{wu}]} + HI_{min} \quad (2.7)$$

where  $HI_{min}$  is the harvest index for the plant in drought condition and represents the minimum harvest index allowed for the plant, and  $\gamma_{wu}$  is the ratio of actual to potential evapotranspiration for the active growing season.

In sum, the complicated process of crop growth is mathematically simplified by SWAT considering potential accumulation (heat unit based) of biomass and growth stresses. Annual crop yield is then calculated from the total biomass and harvest index.

### 2.3.2 Study area and data

Four soil moisture monitoring sites established by the NRCS-SCAN across the Midwest USA (Figure 2.2) were used in this study: Boone, IA (42°1'N, 93°44'W), Woodbury, IA (42°26'N, 95°46'W), Madison, OH (39°57'N, 83°26'W) and Mason, IL (40°19'N, 89°54'W). All provide 5-6 years of continuous daily soil moisture data at multiple depths. This offers a valuable chance to evaluate model performance in soil moisture prediction. Current land use/cover information is based on site pictures on the NRCS website, which

resulted in all sites being classified as range grass using default SWAT parameters. Soil, crop and weather data used in this study are summarized in Table 2.1.

**Table 2.1 Data used in this study**

<b>Data</b>	<b>Source</b>	<b>Unit</b>	<b>Description</b>	<b>Data Process</b>
Soil moisture content	NRCS-SCAN	Percentage	Layer specific daily data (5, 10, 20, 50, 100 cm)	Bias-correction to avoid observed data over porosity
Site specific soil physical properties	NRCS-SCAN, pedon report.	g/cm <sup>3</sup> , percentage	Number of layers, bulk density, field capacity, permanent wilting point, porosity	NA
County level crop yield	NASS quick stats 2.0	Bu/acre	Annual corn yield	Best-fit least square regression method to remove trend
State level crop progress	NASS quick stats 2.0	weeks	Weekly update of farmer activities and crop phenological stages, like emergence, silking, dough, dented, and physiologic maturation at state level	NA
Weather	NRCS-SCAN, NOAA	mm, °C	Daily precipitation and temperature	NOAA stations within 30km used to generate precipitation when SCAN has missing data using inverse distance weighting method

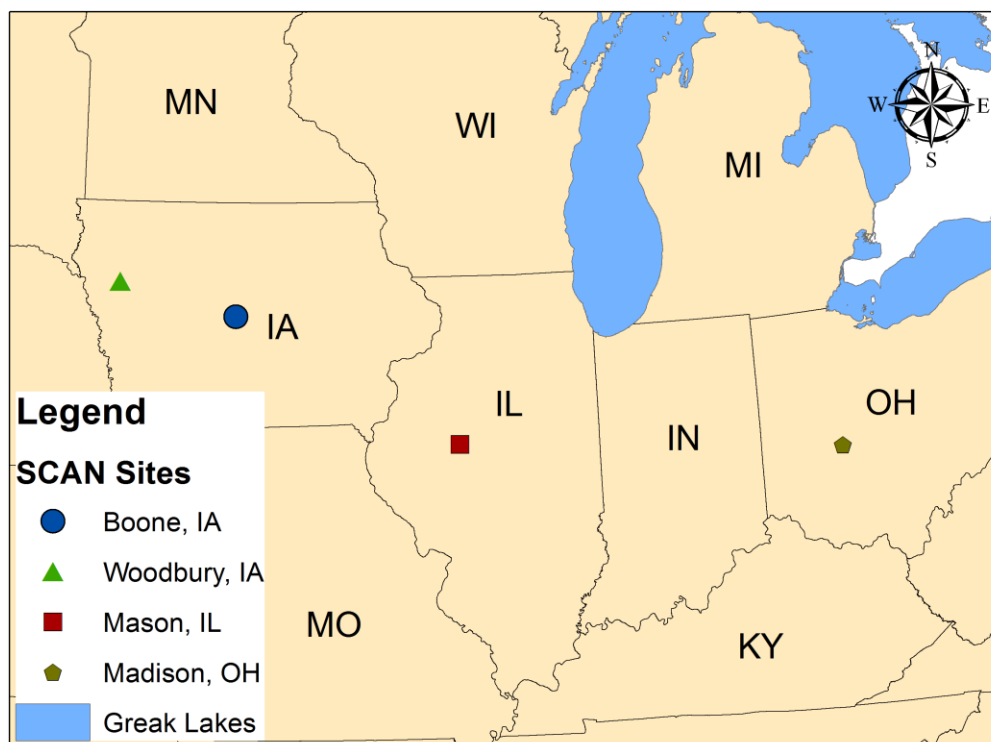


**Figure 2.2 Geographic location of the four NRCS-SCAN plots across the Midwest USA**

## 2.4 Model implementation

### 2.4.1 Crop yield calibration steps

Simulation of crop yield is dependent on both biophysical processes and the simulated soil moisture via the stress functions (bioclimatic variables). Model implementation therefore followed a multistep procedure as illustrated in Figure 2.3. The statistical metrics mentioned in Figure 2.3 will be addressed in section 2.4.3.



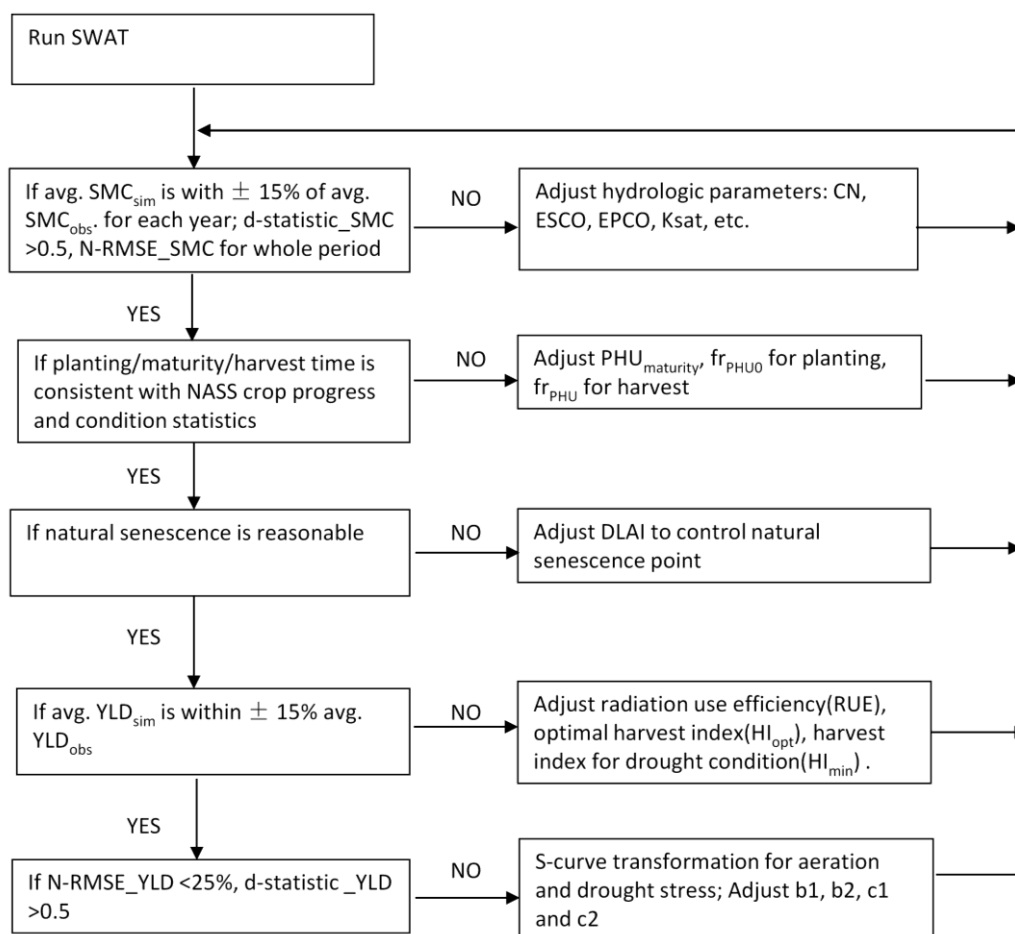


**Figure 2.3 Crop yield calibration strategy**

#### 2.4.2 Simulated crop yield upscaling

Due to the spatial scale difference of observed (detrended county level yield from the National Agriculture Statistic Service (NASS)) and simulated yields (SWAT single HRU scale), these two datasets cannot be compared directly. The scale discrepancy will affect inter-annual variations, because data averaged to coarse scales are less variable than data for small plots, which introduces a bias in the yield calibration (Maltais-Landry and Lobell,

2012). Therefore, in this study, an approach to upscale simulated yield from HRU to county was developed, considering the effect of arable soil varieties on yield across the county.

First, arable soils from the NRCS SSURGO (Soil Survey Geographic Database) in each county were classified into different groups based on the two properties (NRCS curve number and saturated hydraulic conductivity) that most influence SWAT simulated hydrology (Figure 2.4). Secondly, the model was run for various soil groups without calibration to provide yield values based on the default parameter set. Then, the model was run at the SCAN site in each county using the default and calibrated parameter sets. The yield difference between the SCAN site simulations with the two parameter sets was treated as bias. This bias was employed to adjust the simulated yield values for the other arable soil groups based on the assumption that calibration would have similar influence on all soil groups. The proportion of each arable soil (Figure 2.4) in each county is also considered when upscaling the crop yield simulated for the individual HRUs representing SCAN sites to the whole county, as follows:

$$Y_{county}^{cali} = \sum_{n=1}^N (Y_{plot}^{cali} - Y_{plot}^{def} + Y_n^{def}) \times \frac{A_n}{A_{arable}} \quad (2.8)$$

where  $Y_{county}^{cali}$  is the county level crop yield after upscaling;  $N$  is the number of arable soil groups simulated in the county;  $Y_n^{def}$  is the annual simulated crop yield for soil  $n$ , using the default parameter set;  $Y_{plot}^{cali}$  is the simulated yield at plot scale using calibrated parameters;  $Y_{plot}^{def}$  is the simulated yield at plot scale using default parameters;  $A_n$  is area of soil  $n$  in each county; and  $A_{arable}$  is the total area of arable soil in each county.

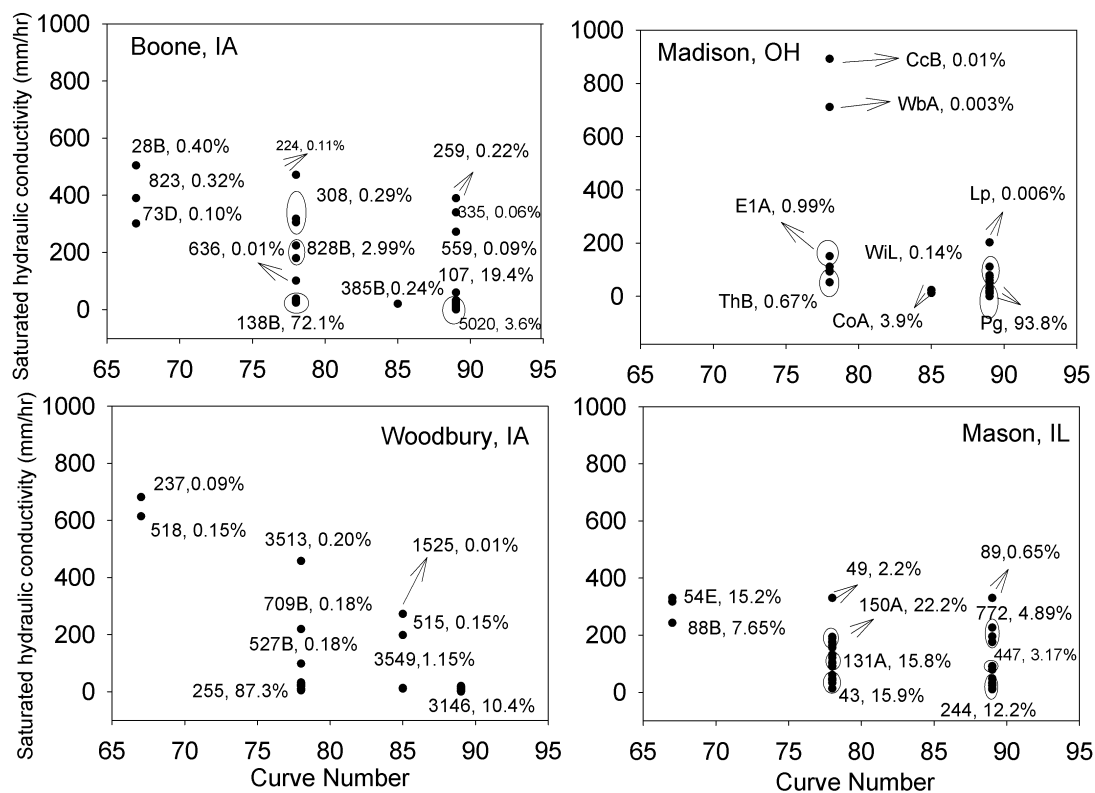


**Figure 2.4 Typical arable soil types and their weight factors in the four study counties**

### 2.4.3 Model performance evaluation

To evaluate the deviation of the soil moisture content and crop yield simulations, statistics of mean bias error (MBE), Willmott's index of agreement ( $d$ ), and the normalized root mean square error (N-RMSE) were calculated. MBE measures the average tendency of the simulated data to differ from their observed counterparts (Gupta et al., 1999). The  $d$ -statistic (Willmott, 1982) reflects the degree to which the simulated variation estimates the measured variation (Han et al., 2010), which has a value between 0 and 1, where higher values of  $d$  indicate better model performance. Since it overcomes the insensitivity to

additive and proportional differences between observed and simulated data, the d-statistic is more appropriate to evaluate soil water content when compared with the correlation coefficient (Legates and McCage, 1999). As recommended by Legates and McCage (1999), a complete assessment of model performance should also include at least one error index for diagnostic purposes. Therefore, N-RMSE (Loague and Green, 1991) is employed in this study, which is the root mean square error (RMSE) divided by the average observed soil moisture or crop yield. RMSE indicates error in the units of the constituent of interest, while N-RMSE includes a normalization factor, making the resulting statistic comparable across constituents. A value of N-RMSE smaller than 10% indicates that the model is an excellent predictor, between 10 and 20% is a good predictor and between 20 and 30% is a fair predictor (Bannayan and Hoogenboom, 2009). These three metrics were used to evaluate model performance both in soil moisture and annual crop yield.

#### 2.4.4 Soil moisture content calibration

Observed soil water content during the winter period (Nov to Feb) is often missing from SCAN datasets, presumably due to soil freezing. Moisture data in the winter period is less related to crop yield in the Midwestern US, since corn has either been harvested or has not been planted. Therefore, our soil moisture calibration is just based on observed data from March 1<sup>st</sup> to Oct. 31<sup>th</sup> for each year. This captures soil moisture prior to planting, which is more important to crop growth than variations in soil moisture through the winter.

Measured soil moisture contents were compared with daily simulated values for different layers. A 10-year spin-up period was used to minimize the impact of uncertain initial moisture conditions. Site-specific soil physical properties used to parameterize moisture are summarized in Table 2.2. Hydrologic parameters that were manually adjusted to calibrate soil moisture are listed in Table 2.3.

**Table 2.2 Soil water content parameterization**

<b>Parameters</b>	<b>Physical Meaning</b>	<b>Boone, IA</b>	<b>Woodbury, IA</b>	<b>Madison, OH</b>	<b>Mason, IL</b>
Por <sub>i</sub>	Porosity of soil layer i**	0.365- 0.529	0.453- 0.478	0.284- 0.479	0.310- 0.374
FC <sub>i</sub>	Field capacity of soil layer i**	0.290- 0.470	0.320- 0.350	0.220- 0.380	0.090- 0.310
PWP <sub>i</sub>	Permanent wilting point of soil layer i**	0.130- 0.270	0.150- 0.210	0.100- 0.200	0.040- 0.170
DEPIMP_B SN (mm)	Depth to impervious layer for modeling perched water table	1200	NA	NA	NA
sol_zmx (m)	Maximum rooting depth	0.46	2	2	2

\*\*i indicates different soil layers. For Boone, IA, i=1, 2...6; For Woodbury, IA, i=1, 2...5; For Madison, OH, i=1, 2...7; For Mason, IL, i=1, 2...6.

**Table 2.3 Hydrologic parameter calibration**

<b>Parameters</b>	<b>Physical Meaning</b>	<b>Boone, IA</b>	<b>Woodbury, IA</b>	<b>Madison, OH</b>	<b>Mason, IL</b>
ESCO:	Soil evaporation compensation coefficient	0.979	0.97	0.5	0.966
EPCO	Plant transpiration compensation coefficient	0.02	0.2	0.6	0.99
CN2	Runoff curve number	59	59	81	58
Ksat_i(mm/hr)	Saturated hydraulic conductivity of soil layer i**	0.09-0.19	0.10-0.19	0.01-0.20	0.11-4.64
GW_REVAP	Groundwater re-evaporation coefficient	0.02	0.2	0.02	0.02
$\beta_w$	Water use distribution parameter	10	10	9	10

\*\*i indicates different soil layers. For Boone, IA, i=1, 2...6; For Woodbury, IA, i=1, 2...5; For Madison, OH, i=1, 2...7; For Mason, IL, i=1, 2...6.

#### 2.4.5 Management timing parameterization

SWAT calculates heat unit accumulation at a daily scale, and uses those values to control when important management decisions are made. Frequently, an exact date for planting and harvest is assigned in SWAT, but heat unit accumulation can also be used to vary planting time from year to year. This method is more consistent with actual practice and was used for these simulations. The accumulation of heat units also helps to define different phenology stages, or at least the approximate timing of their occurrence. We used this relationship to compare simulated plant growth stages to those provided in the USDA-NASS database, and to calibrate the crop growth model within SWAT to improve the

simulation of corn yields. Default and calibrated parameters are shown in Table 2.4, while the calibration process is described below.

**Table 2.4 Parameters adjusted for management time and potential growth curve**

	Original Values				Adjusted Values			
	$fr_{PHU0}$	$PHU_{mat}$	$fr_{PHUhar}$	DLAI	$fr_{PHU0}$	$PHU_{mat}$	$fr_{PHUhar}$	DLAI
Iowa	0.15	1451	1.2	0.7	0.11	1652	1.1	0.75
Ohio	0.15	1512	1.2	0.7	0.15	1712	1.1	0.75
Illinois	0.15	1536	1.2	0.7	0.15	1700	1.15	0.75

#### 2.4.5.1 Planting

Planting time determines when the simulated crop begins to accumulate biomass. Incorrect planting time will directly affect the timing of other management stages, and finally cause incorrect simulation of annual total biomass and yield. For the two sites in Iowa, Boone and Woodbury, the default crop model settings resulted in planting dates consistently later than the mean planting date from 20 years of NASS data (Figure 2.5). This was adjusted by changing the value of  $fr_{PHU0}$  to start crop growth more in line with USDA NASS observations. The simulations reflect corn planting time very well after proper parameterization for all 20 years. For Mason and Madison, the default settings are good enough, so there is no change of  $fr_{PHU0}$  in these two counties.

#### 2.4.5.2 Maturity

In SWAT, maturity date is controlled by total heat unit accumulation from the date of planting. Compared with the NASS data, the default maturity date was too early (Figure

2.5(2a-2d)). Therefore,  $PHU_{mat}$  was adjusted. In the Midwestern U.S., the average mid-season commercial corn hybrid requires 130 days or 2700 growing degree days (GDD) from planting to maturity (Neild and Newman, 1990). GDD is another daily heat unit calculation method similar to PHU, and conversion between them is straight-forward. To do this, GDD and PHU were accumulated from the observed planting date for each year, and the PHU for the day that GDD reaches 2700 is obtained. Figure 2.5(2a-2d) reflects the simulated maturity date before and after parameterization, indicating that 2700 GDD (around 1652 to 1712 PHU in all sites) accumulation from the planting date results in a simulated maturity time that compares well to observed data.

#### 2.4.5.3 Harvest

Similar to planting date, PHU fraction is adjusted for harvest ( $fr_{PHU_{har}}$ ) to better reflect observed harvest date. For some cold years, heat units do not accumulate to the required harvest amount and the crop is terminated on the 352<sup>nd</sup> day of the year. Harvest date before and after parameterization is also shown in Figure 2.5(3a-3d).

#### 2.4.5.4 Senescence

Senescence is not a management timing, however, like other management practices it relates to crop biomass accumulation. When corn reaches some fraction of  $PHU_{mat}$ , LAI begins to decrease. This fraction is used as an adjustable parameter (DLAI) to control the



beginning of senescence. Usually, senescence happens at around the end of the grain filling period (Nielsen, 1998), but no clear criteria for the timing of natural senescence is defined. Current literature provides the timing of senescence in some specific years. For example, Dohleman et al. (2009) recorded the corn planting, senescence and maturity timing (Day of year) in Champaign, IL (40.033N, 88.233W). With this information and the recorded daily temperature data from the nearest NOAA station, the heat unit between planting and senescence were calculated. The senescence point relative to the PHU for maturity was 0.786 and 0.759 in 2007 and 2008, respectively. Similarly, Yang et al., (2003) recorded the planting, emergence and maturity date of corn in Manchester, IA (42.47N, 91.45W). They found that LAI decreases 85-90 days after emergence. Thus, DLAI in this area was calculated as 0.751 for 2002. Since our study plots are close to these sites, DLAI was set to 0.75 (around the end of denting stage for a 2700 GDD corn).

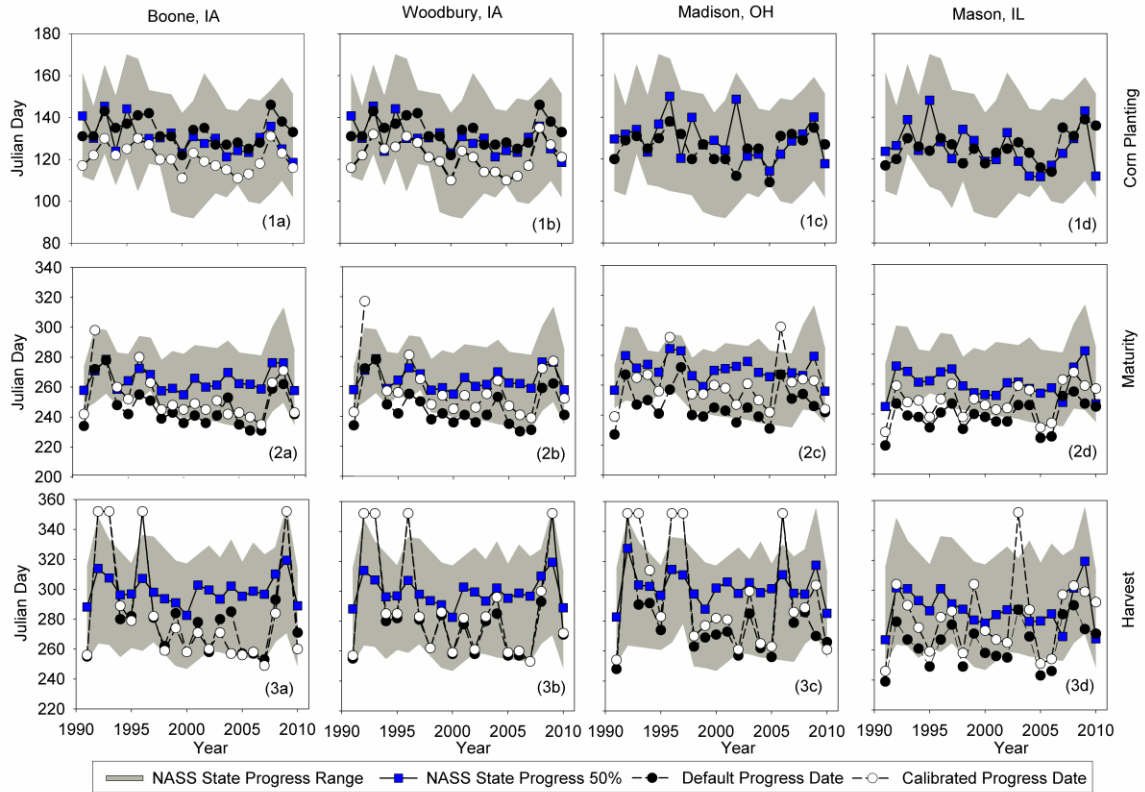


**Figure 2.5** Management timing for the four study counties. The gray shaded zone reflects the date range for each management practice recorded by NASS State Crop Progress Data, with top and bottom defined by the begin and end dates. Blue squares indicate the 50% date of NASS data. Black circles indicate the default management date from SWAT. White circles indicate the calibrated date. 1a) to 1d) reflect the corn planting date for four counties; 2a) to 2d) reflect maturity date; 3a) to 3d) reflect harvest date.

#### 2.4.6 Annual yield amount/variation calibration

For crop yield calibration,  $HI_{opt}$ ,  $HI_{min}$ ,  $RUE$ ,  $b1$ ,  $b2$ ,  $c1$  and  $c2$  were chosen to adjust the annual yield.  $RUE$ ,  $HI_{opt}$  and  $HI_{min}$  are often considered the most sensitive parameters affecting mean annual crop yield in SWAT crop growth studies (Anderson et al., 2009; Nair et al., 2011; Sun and Ren, 2012). The S-curve transformation parameters for aeration

stress ( $b_1$ ,  $b_2$ ), and drought stress ( $c_1$ ,  $c_2$ ) were used to modify the yield sensitivity to environmental stresses in this study. Thus, variation of yield is regulated by four S-curve transformation parameters. The parameters  $b_1$  and  $c_1$  control the position of the curve, with smaller  $b_1$  or  $c_1$  values increasing the initial slope of the S-curve which in turn increases the sensitivity of crops to small levels of aeration or drought stress. Large values of  $b_1$  or  $c_1$  decrease the initial slope so that yields are not substantially affected until higher levels of aeration or drought stress. The difference ( $b_1 - b_2$ ) or ( $c_1 - c_2$ ) controls how closely the S-curve passes through the 1-1 point on both relationships. For use of the equation, we calculate  $b_2$  or  $c_2$  from the value of  $b_1$  or  $c_1$  to keep the tail of the curve within 0-3% of a final value of aeration or drought stress of 1.

For aeration stress, S-curves used by three previous models (Steglich and Williams, 2008; Neitsch et al., 2009; Du et al., 2005) are shown in Figure 2.6, which are all above the 1:1 line, indicating that aeration stress grows rapidly for relatively low fraction of saturation, but stays stable in a high stress status, when relative saturation (*satco*) keeps increasing. For drought stress, a 1:1 line is shown as the SWAT default setting, which means no s-curve transformation; drought stress equals  $1 - AET/PET$ , and stress responds to AET/PET linearly. Suggested calibration ranges for the aeration and drought stress scaling functions are displayed as gray shaded zones. Any curve in the shaded zone could be chosen by end users as a possible one to transform the physical parameter (*satco* or  $1 - AET/PET$ ) to physiological parameter (aeration or drought stress).

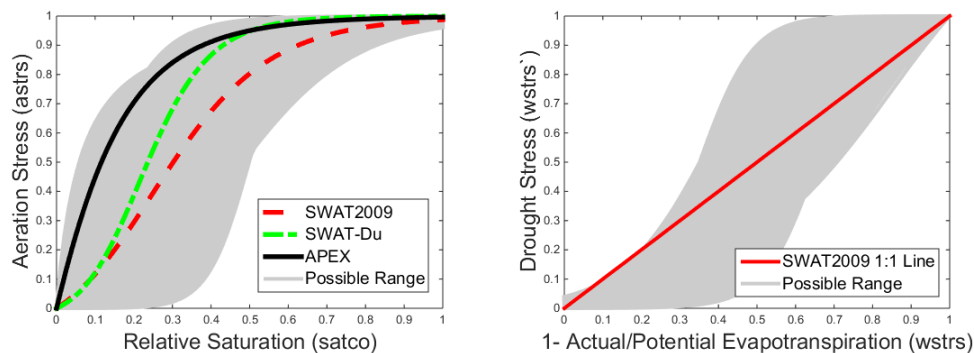


**Figure 2.6 Suggested calibration range for aeration/drought stress scaling function**

The calibration range was selected based on the area under any possible s-curve. Actually, this area also reflects the mean stress value, supposing *satco* or  $1-AET/PET$  is evenly distributed between 0 and 1. Take drought stress for example, the area under the 1:1 line is 0.5, indicating that the mean stress value is 0.5. The suggested calibration range constrains the mean stress between 0.35 and 0.65 (15% deviation from the 1:1 line). Similar to drought stress, considering the response of aeration stress to different percent saturation, any curve with mean aeration stress between 0.5 and 0.85 is suggested for calibration, which covers all three previous models and stays above the 1:1 line.

A 20-year period (1991-2010) is used for crop yield calibration and validation. Crop yield calibration is executed in years (6-7 years) which have observed soil moisture data at the SCAN sites and moisture calibration is described in Section 2.4.4. The remaining years (13-14 years) in this period are used for crop yield validation. Parameters employed for crop yield calibration are summarized in Table 2.5.

**Table 2.5 Parameters used for yield calibration for the four sites**

	HI <sub>opt</sub>	RUE	HI <sub>min</sub>	b1	b1-b2	c1	c1-c2
Boone, IA	0.504	36.18	0.262	0.485	-9.098	0.8858	-3.6977
Woodbury, IA	0.493	33.07	0.328	3.916	-3.326	-1.879	-4.201
Mason, IL	0.473	34.91	0.171	3.093	-3.402	-0.024	-8.925
Madision , OH	0.508	33.94	0.306	-1.365	-7.416	-2.188	-8.626

All sites were assumed to be undrained when calibrating crop yield with the exception of Boone, IA. Figure 2.7 shows that the bottom layers (below 46 cm) of the edge-of-field SCAN site in Boone, IA are almost saturated, indicating a very serious continuous aeration stress for crops. Tile drainage is widely applied in Midwest when soil is poorly drained (Singh et al., 2006; Schilling and Helmers, 2008). Therefore, when modeling crop yield in Boone, IA, it was assumed that all fields are tile drained.

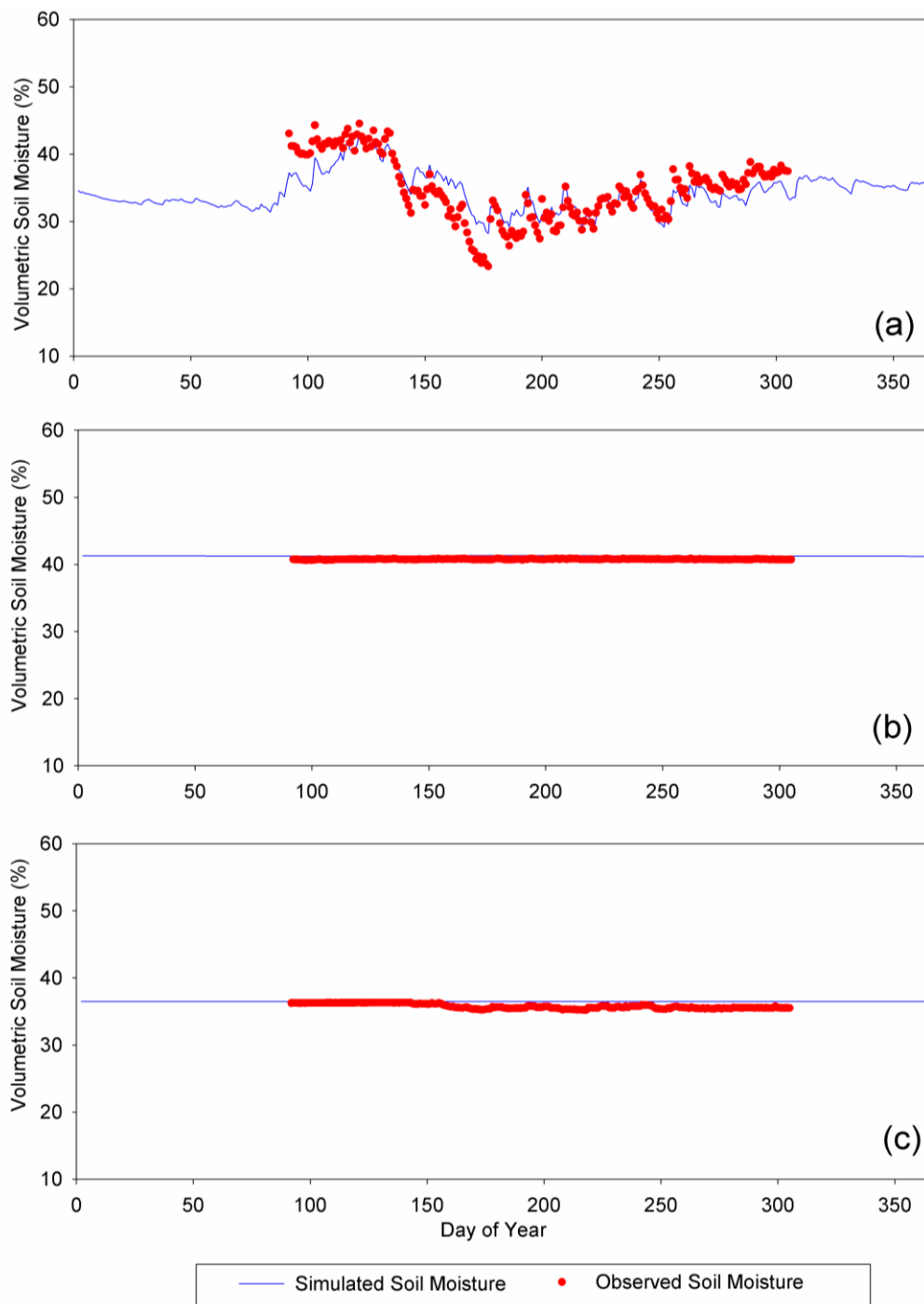


**Figure 2.7 Calibrated vs. observed volumetric soil moisture content (average daily value for 6 years) in Boone, IA. (a) 0-20 cm, (b) 46-58 cm, (c) 94-119 cm**

#### 2.4.7 Weekly biomass accumulation validation

Reasonable annual yield can also be achieved by adjusting harvest index even if the biomass accumulation is incorrect (equifinality in crop yield calibration). Under such situations, the model either consistently over or underestimates daily biomass accumulation, or incorrectly reflects crop responses under oversupplied/limited water conditions. Therefore, to overcome the potential for equifinality, the final biomass at maturity and the seasonal biomass curve are evaluated to ensure an appropriate model representation in daily biomass as well. However, due to the scarcity of field collected biomass data, it is difficult to calibrate daily biomass accumulation curves in the study plots. Singer et al. (2011) evaluated radiation use efficiency near Ames, Boone County, IA, which provides a total of 16 consecutive weekly biomass samples in maize for year 2005. Since SWAT simulates biomass at a daily scale, it is reasonable to compare our simulation results with their observed data.

#### 2.4.8 The relationship between crop yield and climate variability

When the model is not only able to capture the annual yield amount and variation, but also a reasonable daily biomass accumulation rate, it can be considered as a valuable tool to explore how climate variability affects annual crop yield. We extend model application to a longer period (1941-2010) to investigate climate stress to crop yield.

To better explore the role of climate variability (limited/excess water) on annual crop yield, the whole crop growing season is divided into six stages based on corn phenology (Table 2.6). Each period includes 2-3 phenological stages, which are controlled by GDD. The beginning and ending GDD values are defined by Neild and Newman (1990). For all six stages, the total amount and intensity of aeration stress (*astrs*) and drought stress (*wstrs*) were calculated from the SWAT simulation as indices to represent climate variability. Stress intensity is calculated from total stress amount divided by days with stress (days with non-zero stress). Stress indices were also calculated for the entire vegetative stage (first three phenological periods), entire reproductive stage (last three phenological periods) and entire crop growing period (all six phenological periods). Both Pearson and Kendall-Tau correlation coefficients were used to quantify the relationship between detrended observed crop yields and simulated climate variability for all nine periods in four counties.

**Table 2.6 Growing degree day requirements for different phenological stages of 2700 GDD corn**

<b>Phase</b>	<b>Stage</b>			<b>GDD (F)</b>
Vegetative	Planting	V2	V4	0-345
	V6	V8	V10	345-740
	V12	V14	V16	740-1135
Reproductive	Silking	Blister		1135-1660
	Dough	Denting		1660-2190
	Dented	Physiological maturity		2190-2700

To explore yield reduction due to individual stresses, the model was first run 70 years without crop stress using weather data from 1941 to 2010. The original SWAT source code has been modified to remove all stresses, so biomass accumulated in each day as reflected



in eq (2.2) is always the potential biomass. Simulated yield in this run is considered to be potential yield. Then only one stress (either drought or aeration stress) at a time is considered in the model simulation. This method allows us to compare yield reduction by the individual stresses to potential yield. All simulated crop yields are upscaled to county level based on the methods described in section 2.4.2. Then, simulated relative yield reduction is calculated as:

$$\text{Relative yield reduction} = (\text{Potential yield} - \text{Yield by only one stress}) / \text{Potential yield} \quad (2.9)$$

Similarly, relative yield reduction for county level observed data is also generated. First, a linear regression was applied to 70 years of NASS observed yield (Figure 2.8). Then the regression line is shifted upward until it intersects with the highest observed yield. The shifted line is considered the observed potential yield. Relative yield reduction for the observed data is calculated through the observed potential yield and NASS observed data.

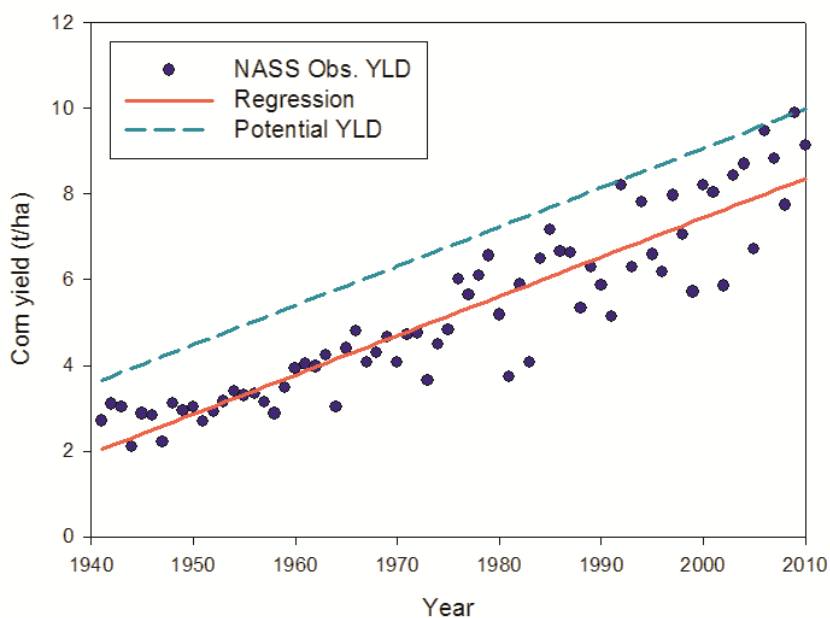


**Figure 2.8 Observed potential yield calculation**

For all 70 years, the non-exceedance probabilities are calculated using the Weibull formulation. Both simulated and observed yield reduction associated with the respective non-exceedance probabilities are then plotted in Figure 2.13. Similar to flood frequency analysis, the non-exceedance probabilities can be converted to a return period by inverting the values.

## 2.5 Results

### 2.5.1 Model performance in soil moisture prediction

Model performance at Boone, IA is shown in Figure 2.7 as a representative of the soil moisture calibration process for all SCAN sites. In order to better illustrate the overall model performance, only annual average daily values for the 5-6 year period are shown. Statistics for model performance for all four sites are summarized in Table 2.7. The model captures the interannual soil moisture variation and annual average amount very well in most years for most soil layers. At the Boone, Woodbury and Madison sites, simulation results are good for soil moisture, with d-statistics greater than 0.8 and MBE values less than 10%. A larger mean bias was found in Mason, IL when compared with the other three sites. The model also underestimates soil moisture in summer and fall in Mason. The relatively poor performance in this site is due to sandy soils and missing site precipitation. A high sand content at this site results in poor soil capacity to hold water. Therefore, the absolute value of soil moisture is much lower than the other three. Although the absolute difference is small, a large relative difference may occur. The SCAN site at Mason, IL only

has one year's site recorded precipitation, so the inverse distance method is used to generate site precipitation from another station. Unfortunately the nearest NOAA weather station is still 14.3 km away (Havana, IL), so the precipitation records are not as accurate as those from other sites resulting in the poorest performance for this site.

The soil in Boone, IA is poorly drained and there is no subsurface drainage at the field edge where the site is located, so the bottom layers are saturated. The model is able to reflect this after proper calibration. Poor d-statistic values in the bottom two soil layers at Boone are caused by variation of simulated and observed moisture around the saturated value. Under saturated conditions, the model generates relatively constant moisture, while the observed data fluctuates around this constant value due to instrument noise. The effect of noise could be covered if observed data itself varies. Therefore, the variance of simulated soil moisture is lower than observed data measured by soil sensors.

### 2.5.2 Model performance in crop yield/biomass prediction

The model captured annual average yield well. Mean bias error is less than 10% (Figure 2.9 and Table 2.8). Normalized root mean square error (N-RMSE) is less than 15%, indicating a good fit and accuracy in predicting yield (Tubiello et al., 2002; Maltais-Landry and Lobell, 2012). In addition, the model is able to capture the interannual variation of crop yield in Woodbury, Madison and Mason. For example, in Woodbury, IA, the d-statistic for both calibration and validation periods are higher than 0.8, and the simulation

predicts both higher (years 1999, 2008, 2009) and lower yields (1993, 2000, 2006) correctly.

**Table 2.7 Model performance in predicting soil moisture at the four SCAN sites**

	<b>Mass Balance Error (%)</b>	<b>d statistic</b>	<b>N-RMSE (%)</b>
<b>Boone, IA</b>	<b>2002-2008</b>	<b>2002-2008</b>	<b>2002-2008</b>
Layer1	-0.53	0.92	12.11
Layer3	1.24	0.27	1.40
Layer6	2.11	0.47	2.82
<b>Woodbury, IA</b>	<b>2004-2009</b>	<b>2004-2009</b>	<b>2004-2009</b>
Layer1	-4.74	0.82	21.49
Layer2	-2.25	0.87	14.16
Layer3	-0.29	0.79	14.60
Layer5	3.43	0.89	7.64
<b>Madison, OH</b>	<b>1998-2003</b>	<b>1998-2003</b>	<b>1998-2003</b>
Layer1	-8.83	0.84	19.94
Layer3	-3.85	0.82	10.40
Layer6	0.25	0.88	6.42
<b>Mason, IL</b>	<b>1998-2002</b>	<b>1998-2002</b>	<b>1998-2002</b>
Layer1	-14.42	0.77	24.52
Layer2	-4.77	0.64	14.33
Layer5	0.93	0.50	7.85

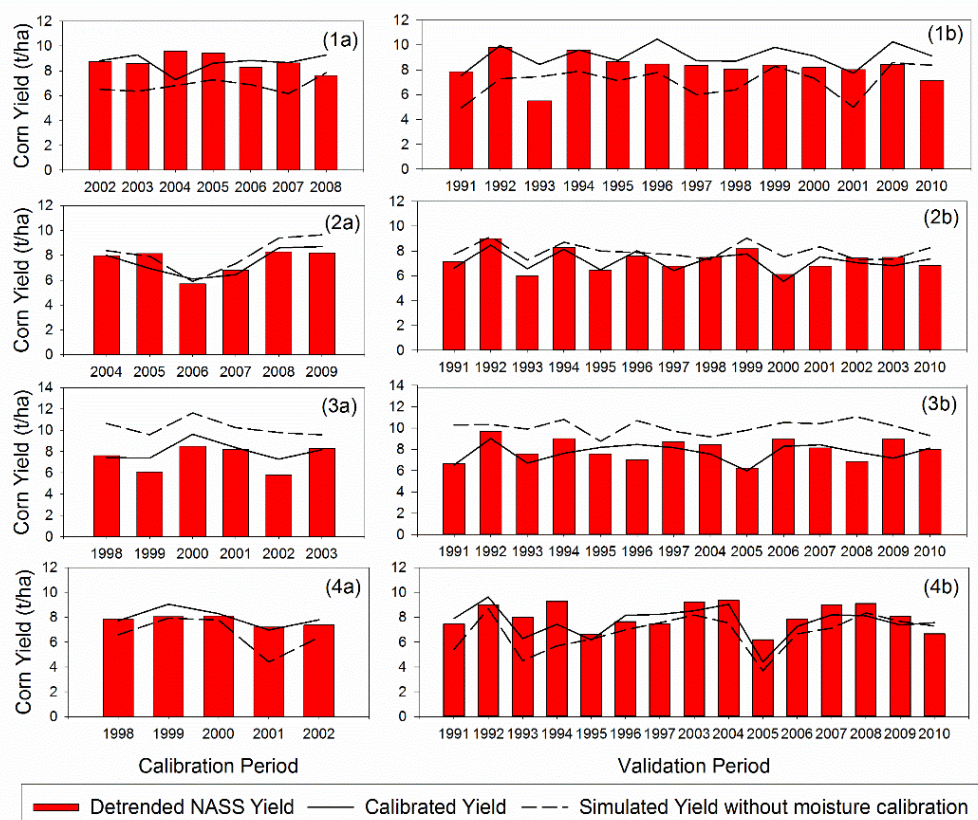


**Figure 2.9 Model performance in yield a) calibration and b) validation for: 1) Boone, IA, 2) Woodbury, IA, 3) Mason, IL 4) Madison, OH. Solid line indicates the simulated yield after following the crop yield calibration strategy (Figure 2.3). Dash line indicates simulated corn yields, if moisture calibration was skipped (hydrologic parameter adjustment in Figure 2.3).**

**Table 2.8 Model performance in predicting corn yield in the four SCAN counties**

	Calibration Period			Validation Period		
	N-RMSE(%)	MBE(%)	d	N-RMSE(%)	MBE(%)	d
Boone, IA	11.99	-3.81	0.09	12.07	-1.21	0.66
Woodbury, IA	8.74	-5.82	0.92	7.64	-2.04	0.84
Madison, OH	12.40	7.14	0.77	9.86	-4.41	0.76
Mason, IL	6.26	-1.61	0.78	13.94	-4.80	0.75

Although for some specific years and plots, the model has trouble, SWAT still does a good job at predicting the annual yield amount and variation in the study area. Compared to previous yield modeling studies (Heng et al., 2009; Mkhabela and Bullock, 2012; Sun and Ren, 2013), the model overall performance is satisfactory. We also compare model performances with and without moisture calibration in Figure 2.9. We found that model performance in corn yield estimation is poor for all four sites if soil moisture evaluation is skipped. For Woodbury and Mason, the model has trouble capturing the interannual variability in crop yield, while for Boone and Madison, the model either underestimates or overestimates crop yield. This indicates the importance of evaluating soil moisture in crop yield predictions.

To check the performance of simulated daily biomass accumulation, model output from Boone, IA was compared with Singer's observed data (Figure 2.10). They match very well, indicating a good model performance in simulating daily biomass accumulation at Boone, IA in 2005. Since daily biomass accumulation data is very limited, there is not enough available data to evaluate daily biomass simulation in other sites at other years.

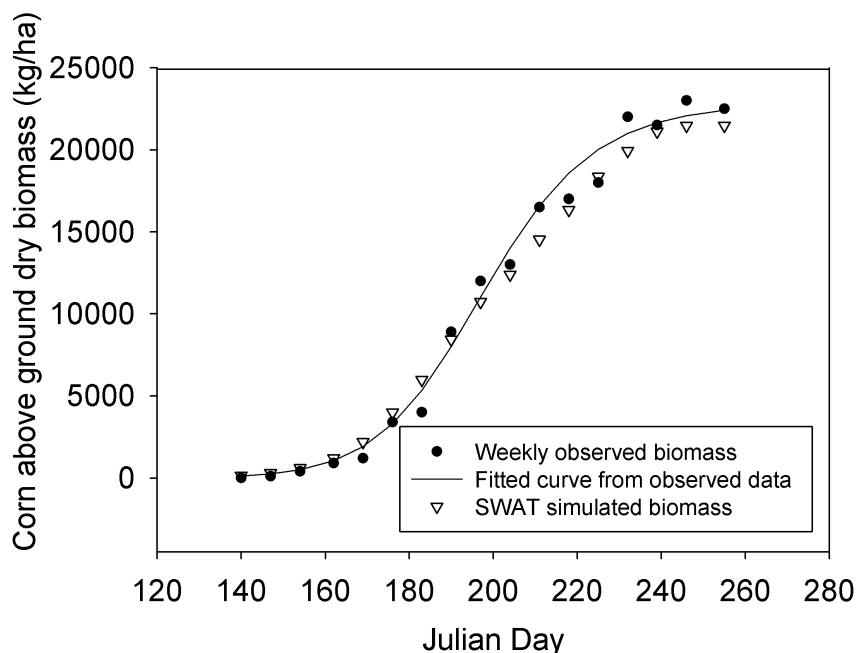


**Figure 2.10 Model performance in daily biomass accumulation in 2005 at Boone, IA.**

### 2.5.3 Role of climate variability on crop yield

The relationship between the climate variability indices and annual crop yield are summarized in Tables 2.9 and 2.10. Yield versus drought/aeration stress for specific growth stages are plotted in Figure. 2.11 and 2.12. Statistically significant correlations between yield and drought stress intensity were found in early reproductive (silking to blister) and middle reproductive (dough, denting) periods. Person's  $r$  is -0.38, -0.54 and -0.41 for silking and blister stage at Woodbury, IA, Mason, IL and Madison, OH, respectively. For Madison, OH, significant correlation ( $r=-0.48$  and  $-0.43$ , respectively) between drought stress intensity and corn yield was also observed in the V12-V16 and dough -denting periods. Corn yield in both Woodbury and Madison is significantly correlated with drought stress intensity during the reproductive period ( $r=-0.37$  and  $-0.55$ , respectively) Results

indicate that crops are more sensitive to drought stress from V12 to denting stage than during other phenology stages, especially compared to the early vegetative period. Drought stress intensity in those stages could serve as a good indicator for crop yield.

**Table 2.9 Correlation coefficient (Pearson's r) between corn yield and drought stress intensity for different growth stages**

	Boone, IA	Woodbury, IA	Mason, IL	Madison, OH
Planting , V4	0.25	0.33	-0.06	-0.11
V6, V8, V10	0.32	-0.29	-0.03	-0.28
V12, V14, V16	0.15	-0.28	-0.26	<b>-0.48**</b>
Silking, Blister	0.11	<b>-0.38**</b>	<b>-0.54**</b>	<b>-0.41**</b>
Dough, Denting	-0.03	-0.28	-0.19	<b>-0.43**</b>
Dented, Maturity	0.18	-0.02	0.01	-0.19
Vegetative stage	0.19	0.07	0.06	-0.32
Reproductive stage	0.22	<b>-0.37**</b>	-0.22	<b>-0.55**</b>
Whole growing period	0.20	-0.23	-0.15	-0.35

**\*\* means significant correlation with  $p < 0.05$**

**Table 2.10 Correlation coefficient (Pearson's r) between corn yield and aeration stress intensity for different growth stages**

	Boone, IA	Woodbury, IA	Mason, IL	Madison, OH
Planting , V4	0.04	0.13	-0.29	0.19
V6, V8, V10	0.22	0.21	0.38	0.30
V12, V14, V16	0.08	0.17	0.39	-0.25
Silking, Blister	0.15	-0.06	-0.09	0.03
Dough, Denting	0.23	-0.03	-0.35	0.31
Dented, Maturity	-0.71**	0.18	0.02	-0.07
Vegetative stage	0.23	0.38	0.27	0.26
Reproductive stage	-0.72**	0.02	-0.22	0.21
Whole growing period	-0.72**	0.27	-0.02	0.34

**\*\* means significant correlation with  $p < 0.05$**



Reproductive organs are formed in the late vegetative period (V12 – V16). Any drought stress in this period will negatively affect ear formation and tassel emergence. Pollination and fertilization happen in the early reproductive period (silking and blister). Success during this stage of development is critical to the final harvest in fall. In contrast, environmental stress occurring in this period can easily abort kernels and in turn reduce crop yield. Kernel abortion in dough and denting stage is not as common as at blister stage, but stress can still continue to reduce kernel weight and finally results in yield reduction (Nielsen, 2008). Therefore, our representation of drought stress is consistent with real conditions.

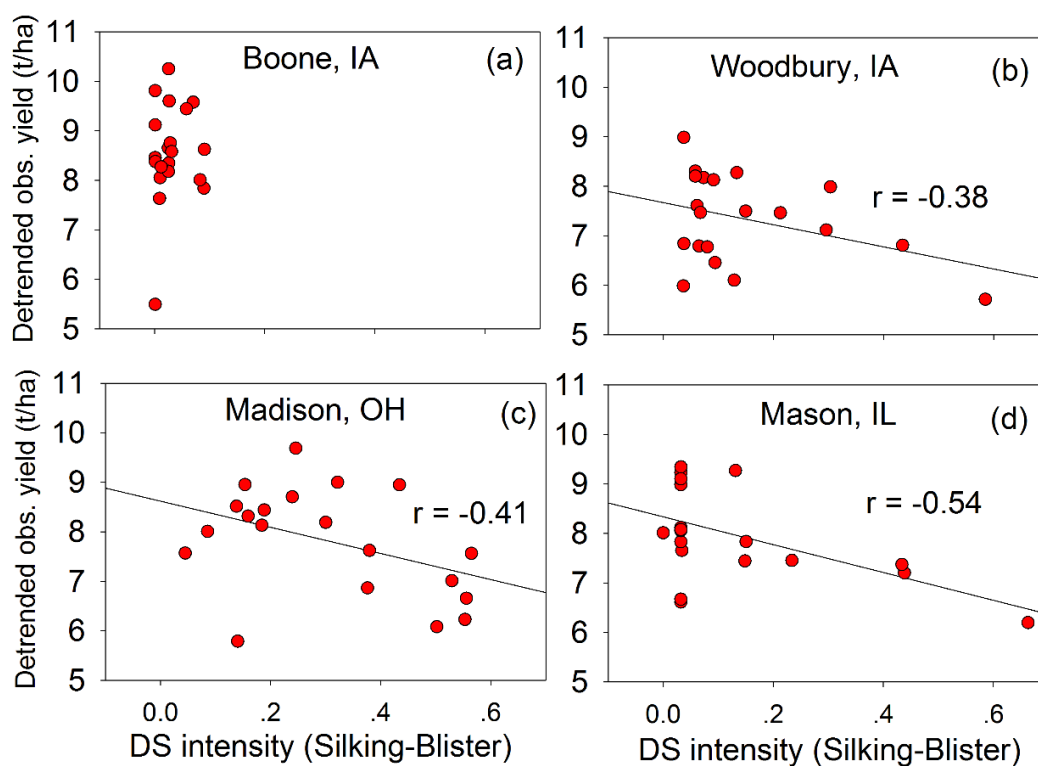


**Figure 2.11 Relationship of corn yields with drought stress intensity in silking-blister period at a) Boone, IA; b) Woodbury, IA; c) Madison, OH; d) Mason, IL.**

Compared to drought stress, no clear relationship was detected between aeration stress and yield. The significant relationship ( $r=-0.72$ ) in the reproductive period at Boone, IA is caused by one outlier (Figure 2.12a). Although yield reduction due to increasing of aeration stress is expected, the county-level statistics do not show this. The impact of aeration stress on yield may be more easily found at plot scale, but is masked by other fields when yield information is at the county level. More detailed explanation on aeration stress impacts on yield are addressed in the discussion section.

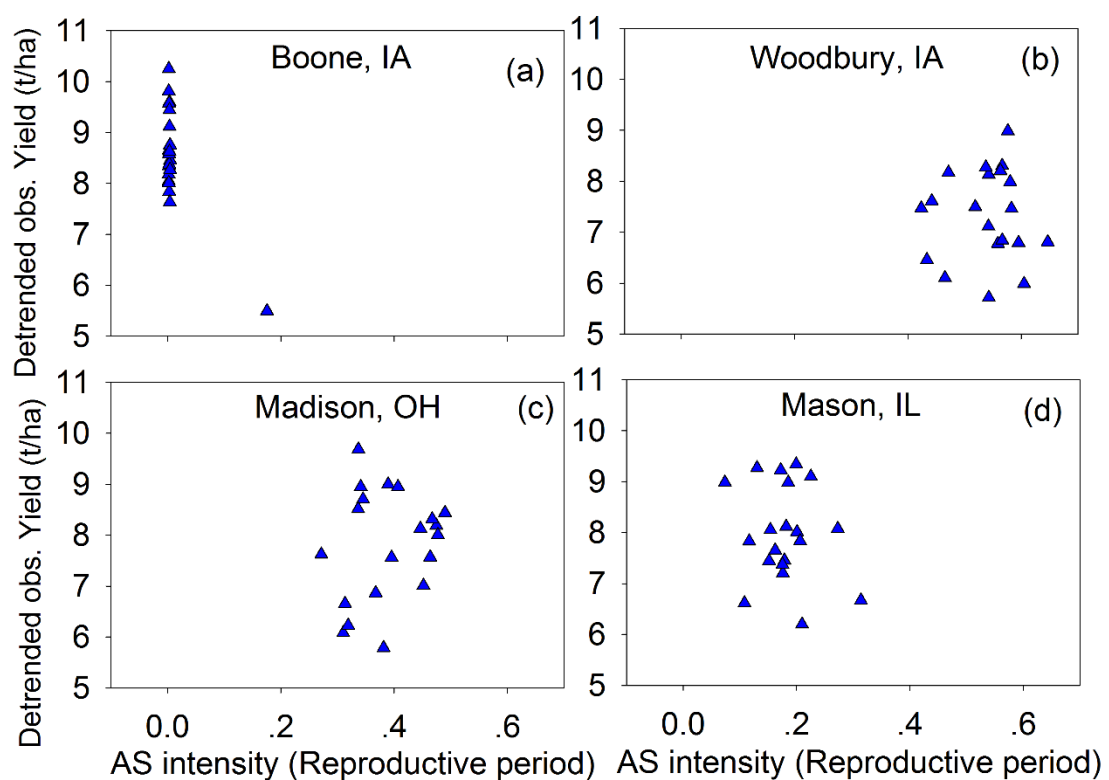


**Figure 2.12 Relationship of corn yields with aeration stress intensity in reproductive period at a) Boone, IA; b) Woodbury, IA; c) Madison, OH; d) Mason, IL.**

### 2.5.4 Long term crop yield reduction due to climate stress

Figure 2.13 reflects the relative crop yield reduction due to individual stresses (either drought or aeration stress) based on 70 years data. The relative yield reduction based on observed data is also shown in the same figure, which is higher than the simulated yield reduction by either individual stress. Under natural conditions yield reduction is caused by the interaction of many factors including water availability but also nutrient deficiency, temperature, disease, pest infestation and weed problems, so it is not surprising that the relative yield reduction based on observed data is the highest among the three.

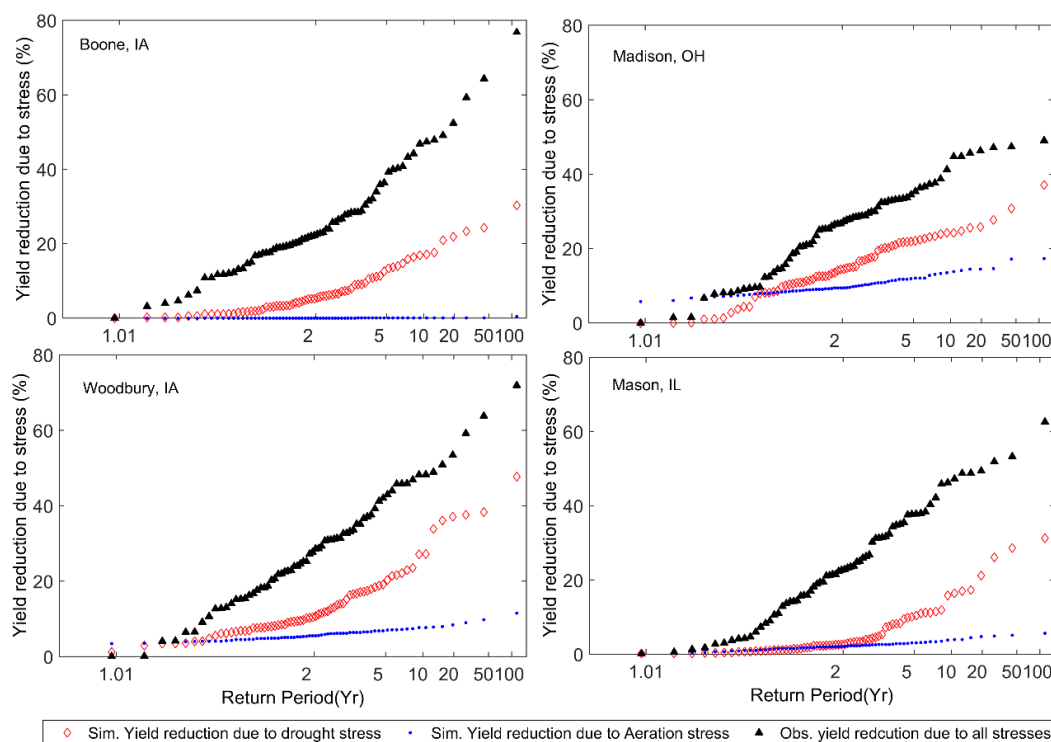


**Figure 2.13 Relative crop yield reduction due to drought stress or aeration stress. Relative yield reduction is calculated by eq. (2.9), which is shown on the y-axis. Recurrence probability which is represented as “return period” associated with the amount of yield reduction is shown in the x-axis. Red diamonds and blue dots represent the relative yield reduction caused by drought and aeration stress. Black triangles are relative yield reduction of observed data.**

In all four sites, yield reduction caused by drought stress is much higher than aeration stress, especially for long return periods. For a 100 year return period, the relative yield reduction caused by drought stress ranges from 30% to 50%, however the biggest yield reduction caused by aeration stress is still less than 30%. Compared to the relative yield reduction due to drought stress, aeration stress causes relatively stable yield reductions, ranging from 0 to 20% in all return periods. The yield reduction in Boone, IA caused by aeration stress is always close to zero, due to the simulation of subsurface drainage conditions at this site. Under natural conditions, the yield reduction is most likely higher than zero for long return periods. Generally speaking, compared to aeration stress, drought stress is still the dominant factor impairing crop yield in the historical period.

## 2.6 Discussion

Although overall the model successfully reflects the annual yield amount and interannual variability in crop yield, there are still some sites and years for which the model did not capture yield very well. For instance, in Madison, OH, the model underestimates corn yield by around 2 t/ha in 1993, 1994 and 2005, but for the year 2010, higher yields are predicted by the model (Figure 2.9-4b). A similar situation happens in Boone, IA where SWAT estimates of yield are higher in 2010 than 2004, while detrended NASS observed data indicates the reverse.

Madison, OH experienced a severe drought in 2005. In addition to the drought stress parameters  $c1$  and  $c2$ ,  $HI_{min}$  is also used to adjust yield. Therefore, yield reduction by

drought is considered by the model twice, which may lead to underestimation of corn yield. For 1993 and 1994 in Mason, IL, even when all stresses are turned off, the model potential yield is 6.3 and 8.3 t/ha, which is still below the detrended NASS yield. Therefore, yield underestimation in these two years is not caused by inappropriate stress functions. Though adjusting growth parameters may increase yields in 1993 and 1994, this would lead to bias in the simulated mean yield amount.

Warm daily minimum temperatures between silking and denting in 2010 might be responsible for the low yield observed in Boone, IA (Elmore, 2010). Since heat stress in SWAT is a function of daily mean temperature, such an impact cannot be clearly reflected in the simulation, which overestimates yield.

Besides those specific reasons mentioned above, yield inconsistency can be attributed to two other aspects: 1) missing site precipitation data and 2) upscaling from field to county level for yield comparisons. The most extreme over/underestimation years occurred during the yield validation period, when site recorded meteorological data was not available. Since crop yield is first modelled at the plot scale, any site missing direct local climate observations has increased uncertainty in the final simulation result. The nearest NOAA weather station is 14.3 km and 8.7 km away from the SCAN plots in Mason, IL and Madison, OH respectively. For Mason, IL, even in the calibration period, only one year's site climate record is available, which also explains why model performance in this site is relatively poorer than Woodbury and Madison. For yield comparison purposes, plot simulated yield was upscaled to county level considering soil varieties across the county. In the upscaling method, the same calibration offset ( $Y_{plot}^{cali} - Y_{plot}^{def}$ ) was added for different

soils across the county. However, due to the differences in soil properties, the calibration influence for different soils may diverge from each other. Due to the lack of data, it is hard to refute or prove this assumption.

Model performance at Boone, IA is the poorest among all four sites (Table 2.8). First, the model has trouble capturing the yield trend in the calibration period. Secondly, it overestimates yield in the validation period, by as much as 3 t/ha in 1993 (Figure 2.9). There are a couple of possible explanations for this difference. 1) SWAT is unable to handle extreme flooding situations well. Flooding is different from aeration stress because it may kill plants instead of reducing biomass. Other effects caused by flooding, such as leafy tassel (crazy top), ear rot and premature kernel sprouting are not considered in SWAT. The year 1993 is recorded as having experienced extreme flooding in Boone, IA (Iowa flood recovery coordination team, 1994). In addition, SWAT cannot represent the effects of flooding caused by neighboring streams (Srinivasan et al., 2010).

In addition, the model may poorly represent the soil moisture of the drained field. The soil used in plot simulation is not arable without the installation of subsurface drainage due to the saturation of the deeper monitored soil layers. Although tile drainage was introduced into the simulation to more accurately reflect soil conditions experienced by crops, no observational data was available to evaluate the simulated condition. Inappropriate tile drainage parameters will affect the sensitivity of the crop to aeration. For this application we used typical values for subsurface drainage ( $D_{\text{drain}}=1200$  mm,  $T_{\text{drain}}=52$  hr,  $G_{\text{drain}}=25$  hr) as recommended by Du et al., (2005). Additionally, tile drainage can affect

soil properties, though not significantly (Jia et al., 2008), introducing additional uncertainty into our simulations for the site.

Compared to drought stress intensity, no significant relationships were found between simulated aeration stress and observed crop yield at any evaluated phenology stage. Since aeration stress is more localized within the field rather than at the county scale, when investigating the relationship between aeration stress and yield, it is more likely to be identified when tested against field collected yield data, which was not available for this analysis. Additionally, if the soil is too wet for planting in the spring, farmers may delay planting, replant, change to faster maturing hybrids, or switch fields from corn to soybeans that need fewer days to mature. For example, Dohleman and Long (2009) found that in 2008, the corn planting date was delayed until June 18<sup>th</sup> compared to May 11<sup>th</sup>, 2007 in Urbana, IL due to very wet soil, and farmers changed hybrid from PI CV 34H35 to Dekalb 61-69. No significant difference was found in final corn biomass production (18.4 vs. 19.2 t/ha). Such hybrid change is not considered in the model simulations. In the simulations presented here, planting date is assigned by heat unit, so simulated planting date only considers temperature but not soil moisture. Therefore, the model may underestimate simulated yield under wet conditions and the aeration stress function alone may be insufficient to capture the impact of wet conditions on corn production.

Finally, although it has been established that the sensitivity of yield to stress is different for different growth stages, the same drought/aeration stress transformation algorithm is used. In other words, instead of using the same stress transformation function for all stages, it is better to use a steeper s-curve in critical/susceptible periods to intensify stress, while using

a mild transformation in other stages. In this study, yield calibration does not consider susceptibility. Furthermore, “crop death” is not considered in the simulation process. “Crop death” never happens, even under extreme stress (flooding year 1993 in Boone, IA). Plants can always recover until the date of harvest.

## 2.7 Summary and conclusions

In this study, the SWAT model was used to explore the relationship between climate variability and crop yield at four sites in the Midwestern USA. Soil moisture was first calibrated at plot scale. The calibrated model was used to extend the observational records between 1991 and 2010 to better capture the effect of climate variability on crop yields. The relative yield reduction in a longer period (1941-2010) due to individual stresses was also explored.

After appropriate parameter calibration, SWAT is capable of reproducing observed soil water content at different depths in all study sites, even when the site is faced with a serious excess water problem (Boone, IA). Mason, IL has the poorest model performance, which is due to the missing of site precipitation. Overall, absolute values of mass balance error (MBE) are less than 10%, d-statistics are greater than 0.6, N-RMSE<25%, for most soil layers at most sites, indicating a decent model performance in soil moisture estimation.

Before calibrating crop yield in the study area, the fraction of heat units was adjusted to ensure that the timing of important management practices (planting and harvest) and maturity dates are consistent with NASS crop progress data. After this management timing



parameterization, the crop growth period is more reasonable, especially for maturity date, which was too early before adjustment for all four sites. This step is also the prerequisite to clearly define important phenology stages in the study area. Drought and aeration stress parameters ( $b_1$ ,  $b_2$ ,  $c_1$ ,  $c_2$ ) accompanied with other traditional biophysical parameters ( $HI_{opt}$ ,  $RUE$ ,  $HI_{min}$ ) were used to adjust site crop yield, which was then upscaled to county level. The model did a good job capturing the average crop yield for all study areas. Annual yield variation is also successfully reflected in Woodbury, IA, Mason, IL, and Madison, OH. The difference in simulated yield before and after soil moisture calibration highlights the importance of considering both hydrological parameters and crop growth parameters in the yield calibration process.

Based on this work, we can conclude the following:

1. Annual yield is inversely correlated with drought stress intensity in the early and middle reproductive stage in most sites (Woodbury, Mason and Madison), indicating that early and middle reproductive periods are more critical than other stages. Reproductive organs are formed in the late vegetative stage, while pollination and fertilization happen in the reproductive period, making the crop more susceptible in those stages.
2. There is no significant relationship between crop yield and aeration stress at any of the four sites. This might be due to the different impact of aeration stress with respect to spatial scales, as well as the low frequency of events in the historical record. The impact of aeration stress on crop yield reduction may be more easily found at plot scale, and may be mitigated by delayed planting, replanting or replacement of hybrid.

3. Observed yield reductions vary between about 20% for 2 year return periods to 50-80% for 100 year return periods. The relative yield reduction of observed data is caused by the interaction of nutrient deficiency, moisture and temperature conditions, diseases, pest and weed problems, which should be higher than any individual stress. Analysis of long term simulated yield reduction indicates that drought stress is the dominant factor affecting yield in the historical period when compared with aeration stress both at short and long return periods (high/low probability of exceedance). For a 70 year return period, total yield reduction due to drought stress is 8.1%, 17.5%, 15.2% and 9.7%, respectively, for Boone, Woodbury, Madison and Mason.

## 2.8 References

- Andersson JCM, Zehnder AJB, Jewitt GPW, Yang H. 2009. Water availability, demand and reliability of in situ water harvesting in smallholder rain-fed agriculture in the Thukela River Basin, South Africa. *Hydrology and Earth System Sciences* **13**: 2329-2347
- Arnold JG, Srinivasan R, Muttiah RS, Williams JR. 1998. Large area hydrologic modeling and assessment part I: Model Development. *Journal of the American Water Resources Association* **34**: 73-89.
- Bannayan M, Hoogenboom G. 2009. Using pattern recognition for estimating cultivar coefficients of a crop simulation model. *Field Crops Research* **111**:290-302.
- Benjamin JG, Nielsen DC, Vigil MF. 2003. Quantifying effects of soil conditions on plant growth and crop production. *Geoderma* **116**:137-148
- Blann K, Anderson J, Sands G, Vondracek B. 2009. Effects of Agricultural Drainage on Aquatic Ecosystems: A Review. *Critical Reviews in Environmental Science and Technology* **39(11)**: 909-1001.
- Boyer JS. 1982. Plant productivity and environment. *Science* **218**: 443-448
- Crutchfield S. 2012. U.S. Drought 2012: Farm and Food Impacts. USDA Economic Research Service.
- Du B, Arnold JG, Saleh A, Jaynes DB. 2005. Development and application of SWAT to landscapes with tiles and potholes. *Transaction of ASABE* **48(3)**:1121-1133
- Dohleman FG, Long SP. 2009. More productive than maize in the Midwest: How does Miscanthus do it? *Plant Physiology* **150**:2104-2115
- Elmore R. 2010. Reduced 2010 corn yield forecasts reflect warm temperatures between silking and dent. *Integrated Crop Management New* <http://www.extension.iastate.edu/CropNews/2010/1008elmore.htm>
- FAO (Food and Agriculture Organization of the United Nations). 2002. World agriculture: towards 2015/2030. Summary Report. Rome, Italy.
- Gupta HV, Sorrooshian S, Yapo PO. 1999 Status of automatic calibration for hydrologic models: Comparison with multilevel expert calibration. *Journal of Hydrologic Engineering* **4(2)**:135-143.
- Heng LK, Hsiao T, Evett S, Howell T, Steduto P. 2009. Validating the FAO AquaCrop Model for Irrigated and Water Deficient Field Maize. *Agronomy Journal* **101(3)**:488-498.

- Han XW, Shao MA, Horton R. 2010. Estimating van Genuchten model parameters of undisturbed soils using an integral method. *Pedosphere* **20(1)**:55-62.
- Iowa flood recovery coordination team. 1994. The Floods of 1993: Iowa flood Disaster Report. Johnston, Iowa, USA
- Jia X, Scherer TF, DeSutter TM, Steele DD. 2008. Change of soil hardness and soil properties due to tile drainage in the Red River Valley of the North. ASABE Annual International Meeting. Rhode Island, June 29- July 2, 2008.
- Kirkham D, Powers WL. 1972. Advanced Soil Physics. Wiley: New York.
- Kozak JA, Ma L, Ahuja LR, Flerchinger G, Nielsen DC. 2006. Evaluating various water stress calculations in RZWQM and RZ-SHAW for corn and soybean production. *Agronomy Journal* **98**:1146-1155.
- Legates DR, McCabe GJ. 1999. Evaluating the use of the goodness-of-fit measures in hydrological and hydroclimate model validation. *Water Resource Research* **35**:233-241.
- Loague K, Green RE. 1991. Statistical and graphical methods for evaluating solute transport models: overview and application. *Journal of Contaminant Hydrology* **7**:51-73.
- Maltais-Landry G, Lobell DB. 2012. Evaluating the contribution of weather to maize and wheat yield trends in 12 U.S. Counties. *Agronomy Journal* **104(2)**: 301-311
- Matthews KB, Rivington M, Buchan K, Miller D, Bellocchi G. 2008. Characterizing the agro-meteorological implications of climate change scenarios for land management stakeholders. *Climate Research* **37**:59-75
- Muenich MR. 2011. The impacts of soil properties, subsurface drainage and surface depressions on streamflow in a recently glaciated landscape. Master Thesis. Purdue University
- Mishra V, Cherkauer KA (2010) Retrospective droughts in the crop growing season: Implications to corn and soybean yield in the Midwestern United States. *Agricultural and Forest Meteorology* **150**:1030-1045.
- Mkhabela MS, Bullock PR. 2012. Performance of the FAO AquaCrop model for wheat grain yield and soil moisture simulation in Western Canada. *Agricultural Water Management* **110**:16-24

- Nair SS, King KW, Witter JD, Sohngen BL, Norman RF. 2011. Importance of crop yield in calibrating watershed water quality simulation tools. *Journal of the American Water Resources Association* **47(6)**:1285-1297
- Narasimhan B, Srinivasan R. 2005. Development and evaluation of Soil Moisture Deficit Index (SMDI) and Evapotranspiration Deficit Index (ETDI) for agricultural drought monitoring. *Agricultural and Forest Meteorology*. **133**:69-88.
- Naz BS, Ale S, Bowling LC. 2009. Detecting subsurface drainage systems and estimating drain spacing in intensively managed agricultural landscapes. *Agricultural Water Management* **96(4)**:627-637
- Neild RE, Newman JE. 1990. Growing season characteristics and requirements in the corn belt. National Corn Handbook-40. Retrieved from <http://www.extension.purdue.edu/extmedia/nch/nch-40.html>
- Neitsch SL, Arnold JG, Kiniry JR, Williams JR. 2009. Soil and Water Assessment Tool: Theoretical Documentation, version 2009.
- Nielsen RL. 1998. Unusual senescence in Corn: Another Thought. The Chat'n Chew Café (Purdue University). Retrieved from <http://www.agry.purdue.edu/ext/corn/news/articles.98/p&c9830.html>
- Neilsen RL. 2008. Grain fill stages in corn. Corny News Network, Purdue University. Retrieved from <http://www.agry.purdue.edu/ext/corn/news/timeless/grainfill.html>.
- Rosegrant MW, Tokgoz S, Bhandary P. 2012. The new normal? A tighter global agricultural supply and demand relation and its implications for food security. *American Journal of Agricultural Economics*. **95(2)**: 303-309
- Rosenzweig C, Hillel D. 1998. Climate change and the global harvest: potential impacts of the greenhouse effect on agriculture. Oxford University press. New York. 324pp.
- Saseendran SA, Nielsen DC, Ma L, Ahuja LR, Halvorson AD. 2004. Modeling nitrogen management effects on winter wheat production using RZWQM and CERES-wheat. *Agronomy Journal*. **96(3)**: 615-630.
- Schilling KE, Helmers M. 2008. Effects of subsurface drainage tiles on streamflow in Iowa agricultural watersheds: Exploratory hydrograph analysis. *Hydrological Processes* **22(23)**: 4497-4506.
- Sinclair TR, Muchow RC. 1999. Radiation Use Efficiency. *Advances in Agronomy* **65**:215-265.

- Singh B, Maayar ME, Andre P, Bryant CR, Thouez JP. 1998. Impacts of a GHG-induced climate change on crop yields: effects of acceleration in maturation, moisture stress and optimal temperature. *Climate Change* **38**: 51-86.
- Singh R, Helmers MJ, Qi Z. 2006. Calibration and validation of DRAINMOD to design subsurface drainage systems for Iowa's tile landscapes. *Agricultural Water Management* **85(3)**: 221-232
- Singer JW, Meek DW, Sauer TJ, Prueger JH, Hatfield JL. 2001. Variability of light interception and radiation use efficiency in maize and soybean. *Field Crops Research*. **121**:147-152
- Srinivasan R, Zhang X, Arnold J. 2010. SWAT ungauged: hydrological budget and crop yield predictions in the upper Mississippi river basin. *Transactions of the ASABE* **53(5)**: 1533-1546.
- Steduto P, Hsiao TC, Raes D, Fereres E. 2009. AquaCrop – The FAO Crop Model to Simulate Yield Response to Water: I. Concepts and Underlying Principles. *Agronomy Journal* **101(3)**: 426-437.
- Steglich, EM, Williams JR. 2008. Agricultural Policy/Environmental eXtender Model: User's manual version 0604 DOS and WINAPEX interface. BREC Report # 2008-16. Temple, TX: Texas AgriLIFE Research, Texas A&M University, Blackland Research and Extension Center.
- Stockle CO, Martin SA, Campbell GS. 1994. CropSyst, A cropping systems simulation model: Water nitrogen budgets and crop yield. *Agricultural Systems* **46(3)**: 335-359.
- Sun C, Ren L. 2013. Assessment of surface water resources and evapotranspiration in the Haihe river basin of china using SWAT model. *Hydrological Processes* **27**:1200-1222.
- The Ohio State University Extension. 2005. Ohio Agronomy Guide. 14th Edition. Bulletin 472. Retrieved from <http://ohioline.osu.edu/b472/>
- Thompson JA, Bell JC. 1988. Hydric conditions and hydromorphic properties within a Mollisol catena in southeastern Minnesota. *Soil science Society of America Journal* **62(4)**:1126-1133.
- Torell LA, McDaniel KC, Koren V. 2011. Estimating grass yield on blue Grama range from seasonal rainfall and soil moisture measurements. *Rangeland Ecology and Management* **64**:56-66.
- Tubiello FN, Rosenzweig, Goldberg C, Jagtap RA, Jones JW. 2002. Effects of climate change on US crop production: simulation results using two different GCM scenarios. Part I: Wheat, potato, maize, and citrus. *Climate Research* **20**: 259-270.

- Warrick RA. 1984. The possible impacts on wheat production of a recurrence of the 1930s drought in the U.S. Great Plains. *Climatic Change* **6**:5-26
- Willmott CJ. 1982. Some comments on the evaluation of model performance. *Bulletin of the American Meteorological Society* **63**:1309-1313.
- Visser J. 1977. Soil aeration capacity, an index for soil structure, tested against yield and root development of apple trees at various soil treatments and drainage conditions. *Plant and Soil* **46**: 221-237.
- Yang HS, Dobermann A, Lindquist JL, Walters DT, Arkebauer TJ, Cassman KG. 2004. Hybrid-Maize – a maize simulation model that combines two crop modeling approaches. *Field Crops Research* **87(2-3)**: 31-154.

## CHAPTER 3. CORN RESPONSES TO CLIMATE STRESS DETECTED WITH SATELLITE-BASED NDVI TIME SERIES

### 3.1 Abstract

Corn growth conditions and yield are closely dependent on climate variability. Leaf growth, measured as the leaf area index, can be used to identify changes in crop growth in response to climate stress. This research was conducted to capture patterns of spatial and temporal corn leaf growth under climate stress for the St. Joseph River watershed, in northeastern Indiana. Leaf growth is represented by the Normalized Difference Vegetative Index (NDVI) retrieved from multiple years (2000-2010) of Landsat 5 TM images. By comparing NDVI values for individual image dates with the derived normal curve, the response of crop growth to environmental factors is quantified as NDVI residuals. Regression analysis revealed a significant relationship between yield and NDVI residual during the pre-silking period, indicating that NDVI residuals reflect crop stress in the early growing period that impacts yield. Both the mean NDVI residuals and the percentage of image pixels where corn was under stress (risky pixel rate) are significantly correlated with water stress. Dry weather is prone to hamper potential crop growth, with stress affecting most of the observed corn pixels in the area. Oversupply of rainfall at the end of the growing season was not found to have a measurable effect on crop growth, while above normal precipitation earlier in the growing season reduces the risk of yield loss at the watershed



scale. The spatial extent of stress is much lower when precipitation is above normal than under dry conditions, masking the impact of small areas of yield loss at the watershed scale

### 3.2 Introduction

Crop yield in the US Corn Belt is strongly affected by climate variability, primarily through the influence of climate on water availability as soil moisture. The summer warming trend from 1891 to 1936 adversely affected crop yields, while a cooling trend accompanied by increased summer rainfall decreased variability in yield and accounted for a 20% increase in yield from 1936 to 1972 (Thompson, 1988). Crop yields during the period of 1980–2007 were strongly correlated with the occurrence of meteorological drought and maximum daily temperature during the grain filling and reproductive growth period (Llano et al., 2012; Mishra and Cherkauer, 2010). Soil moisture that is either higher or lower than normal conditions can cause crop water stresses, which are harmful for crop growth over shorter spatial and temporal scales.

Despite clear evidence that soil moisture conditions cause billions of dollars of crop loss per year, the impact of water stress on crop growth is difficult to quantify. In part this is because the extreme events that cause yield loss are by definition infrequent in nature. Field-scale studies designed to investigate the impact of water stress must use artificial manipulation of moisture conditions (Kang et al., 1998; Saseendran et al., 2015) or they will far exceed the typical lifetime of a research grant. The available regional datasets are too coarse in spatial resolution. For example, the USDA National Agricultural Statistics

Service's (NASS) Crop Progress and Condition data is compiled at the state or sub-state level. Such datasets can capture the effects of region-wide environmental impacts such as drought, but events that are frequent at small scales (i.e. flooding in the field low spot) are particularly hard to detect due to the coarse nature of the datasets.

Corn phenology, the timing of corn growth and development each year, is weather and hybrid specific. For the same corn hybrid under similar management practices, growth conditions are strongly related with climate variability. When the hydroclimate is suitable, corn develops well and has higher yield potential, but when faced with biophysical stresses related to climate extremes many aspects of crop development can be affected. Observations related to the spatial variability in crop development can give insights into crop response to hydroclimate factors because of the spatial variability in soil water conditions, reducing the need for multi-year studies.

Analyzing corn phenology using remotely sensed satellite image provides an opportunity to investigate the linkage between the spatial variability in crop development and water stresses. Satellite data are increasingly used to monitor agricultural fields (Liu et al., 2012; Bhattarai et al., 2015) and can provide a powerful tool to record phenological trends and detect the effect of climate variability. Compared to hand-held optical sensors, satellite images offer a valuable perspective at the field-scale instead of individual plants, revealing regional crop conditions that are difficult to detect from limited ground measurements. On the other hand, compared to coarse state level crop statistical reports, remote sensing imagery reveals substantially more about the spatial variability of corn development within a region. An additional benefit of satellite imagery is that data can be collected and

processed in a repeatable and non-biased method. Additionally, spatial information, such as soil moisture from satellite images, can also be merged into crop modeling studies for improving regional crop yield forecasts (Ines et al., 2013; De Wit et al., 2007).

Interest in studying crop phenology using satellite data has been growing in recent research (You et al., 2013). Crops exhibit different features as they develop, many of these features are distinguishable from remote sensing imagery. For example, the area of green leaves associated with a plant strongly absorbs wavelengths of visible (red) light while reflecting near-infrared wavelengths (Knipling, 1970). The ratio of absorption to reflectance also varies from the early growing season through to maturity and senescence. Such changes in spectral properties are the theoretical basis for relating reflected radiation from satellite images to crop growth (Nguy-Robertson, et al., 2012). Vegetation indices are more widely used than direct light reflectance in remote sensing algorithms for monitoring crop characteristics (Hatfield and Prueger, 2010; Huang et al., 2012) because of their simplicity and the ease of data processing. A vegetation index is an indicator that describes a visible characteristic, for example, the greenness of a plant, which is correlated with the health of the vegetation. One widely used vegetation index is the Normalized Difference Vegetative Index (NDVI), which has been related to nitrogen status and chlorophyll content at micro scale and biomass, leaf area and grain yield at macro scale (Shanahan et al., 2003; Ma et al., 1996; Solari et al., 2008; Shnahan et al., 2001).

NDVI generated from remote sensing can be used to estimate crop growth under various climate conditions, which in turn can be used to improve and evaluate crop models (Fang et al., 2011; Casa et al., 2012). Constructing time series of vegetation indices, such as NDVI,

from satellite imagery can also help in the development of region specific phenologies for multiple crop types while limiting the necessity of intensive field monitoring. By merging NDVI values for the same region over multiple years, researchers can also establish “normal” growing conditions in a region for a specific time of year. Then by studying significant deviations from this “normal” phenological curve within any year, changes to crop phenology due to climate stresses can be quantified.

The overarching goal of this study is to evaluate variability in corn growth conditions and phenology both spatially and temporally in the St. Joseph River watershed, which is located in the Eastern Corn Belt, USA using an 11-year time series of Landsat 5 TM imagery. Corn growth conditions were identified using NDVI values from multiple years of satellite images, and linked with climate stresses and county level yield observations. By quantifying the variability in corn growth response in the presence of water stress, the phenologies extracted from the satellite data can be used to evaluate the ability of current generation crop growth models to represent plant responses to the more frequent occurrence of weather extremes under projections of climate change in the Corn Belt.

### 3.3 Method

#### 3.3.1 Study Area

The St. Joseph River watershed (Figure 3.1) with a drainage area of 2821 km<sup>2</sup> is located in northeastern Indiana, northwestern Ohio and southeastern Michigan. This watershed spans portions of eight counties. Agricultural land, including row crops and pasture occupy 67% of the basin area. Rainfed agriculture is predominant in the region, and just 5% of the

cropland in the eight county area is irrigated (USDA-NASS, 2012). Three NOAA weather stations recording daily air temperature and precipitation are located in Steuben, IN, Williams, OH and DeKalb, IN. The watershed is fully contained in a single Landsat 5 scene (path 21, row 31).

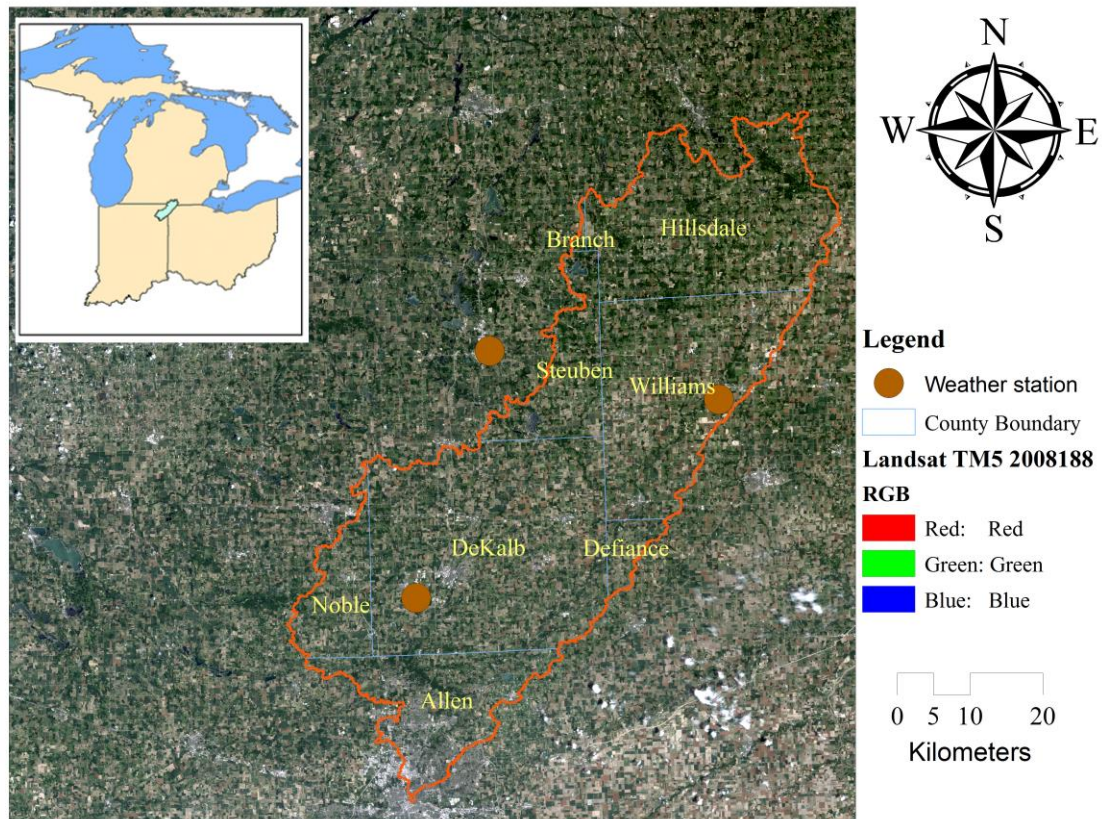


**Figure 3.1** Subset from the July 6th, 2008 Landsat TM5 image showing the St. Joseph River Watershed

### 3.3.2 Data

#### 3.3.2.1 Land cover and crop progress data

The Cropland Data Layer (CDL) product is a raster-formatted, geo-referenced, crop-specific, land cover map produced by the USDA National Agricultural Statistics Service (NASS). The purpose of the CDL program is to use satellite imagery to provide acreage estimates of major crop commodities for each state (Boryan et al., 2011). The resolution for CDL products is 30 m, so the area of each pixel is 900 m<sup>2</sup>. The CDL is available for Indiana beginning from 1999, and for Ohio and Michigan from 2006 and 2007, respectively. The CDL products are used to identify corn pixels in the St. Joseph River watershed for each year of analysis. These are in turn used to extract the spectral signature (NDVI) for corn only, which is the focus of this study.

USDA/NASS releases basic phenological information for corn in weekly Crop Progress and Condition Reports at the state or agricultural statistic district level (USDA-NASS, 2010). The latter is a sub-state region comprised of multiple counties. These reports show the percent of crop fields (by area) that have reached or completed a specific phenological stage (planted, emerged, silking, dough, dent, mature and harvested) each week during the growing season. The weekly progress reports were used to identify the range and median in growing season length in the Northwest District of Indiana using the dates for corn planting and harvesting each year. Ohio and Michigan do not report district level crop progress data, so information from those states were not used for defining the growing season.

### 3.3.2.2 Remote Sensing observations

Eleven years of Landsat-5 Thematic Mapper (TM) images (Path 21, Row 31) were downloaded from the USGS EarthExplorer (<http://earthexplorer.usgs.gov/>, latest access date is 2015-5-17) for the duration of the CDL data in the St. Joseph River watershed (2000-2010). The resolution of the Landsat 5 TM image pixel is 30 m by 30m. The Landsat satellite collects images for the same location every 16 days, so there are approximately 10 images spanning the corn growing season each year. Only images with cloud coverage less than 60% were kept for analysis. Table 3.1 lists the 63 Landsat 5 TM images used for this analysis with their acquisition dates and cloud coverage.

### 3.3.3 Data Processing

The NDVI is developed from two important wave bands: the red and near infrared, and has been widely used for agricultural mapping and yield monitoring (Bolton and Friedl, 2013; Rasmussen, 1992; Mkhabela et al., 2011; Johnson 2014; Chipanshi et al., 2015). The NDVI is calculated as:

$$NDVI = \frac{(R_{NIR} - R_{red})}{(R_{NIR} + R_{red})} \quad (3.1)$$

Where  $R_{nir}$  is the reflectance in the near infrared spectrum, and  $R_{red}$  is the reflectance in the red band spectrum. Values of NDVI range from 1.0 to -1.0 (Crippen, 1990). Barren land, sand or snow usually present very low NDVI values (for example, less than 0.1). Sparse vegetation such as shrubs and grassland or senescing crops may result in moderate NDVI

values (approximately 0.2 to 0.5). High NDVI values (approximately 0.6 to 0.9) correspond to dense vegetation such as that found in temperate and tropical forests or crops at their peak growth stage. Since the NDVI shows a close relation to canopy chlorophyll content, it can also be used to estimate Leaf Area Index (LAI) (Broge and Leblanc, 2001; Gitelson et al., 2003), which is an important vegetation biophysical characteristic.



**Table 3.1 Selected Landsat TM5 images during the growing season, path 21, row 31**

Year	Date	Day of year	Cloud Coverage (%)	Year	Date	Day of Year	Cloud Coverage (%)	
2000	27-Apr*	118	0	2005	Apr-9*	99	0	
	13-May	134	0		27-May	147	23	
	29-May	150	0		30-Jul	211	19	
	14-Jun	166	30		18-Oct	291	0	
	30-Jun	182	10		Apr-28*	118	0	
	2-Sep	246	20		15-Jun	166	7	
	18-Sep	262	0		1-Jul	182	21	
	20-Oct	294	0		17-Jul	198	0	
2001	30-Apr*	120	0	2006	2-Aug	214	1	
	17-Jun	168	0		5-Oct	278	12	
	4-Aug	216	0		Apr-15*	105	0	
	20-Aug	232	10		May-1*	121	49	
	5-Sep	248	0		18-Jun	169	4	
2002	7-Oct	280	10	2007	20-Jul	201	0	
	May-3*	123	0		22-Sep	265	0	
	20-Jun	171	0		May-3*	124	22	
	6-Jul	187	0		20-Jun	172	37	
	22-Jul	203	30		6-Jul	188	2	
	7-Aug	219	0		23-Aug	236	10	
	8-Sep	251	0		24-Sep	268	0	
	24-Sep	267	0		2008	10-Oct	284	0
2003	6-May	126	30	Apr-4*		94	13	
	22-May	142	0	May-22*		142	17	
	23-Jun	174	0	23-Jun		174	3	
	25-Jul	206	3	9-Jul		190	7	
	11-Sep	254	0	2009		11-Sep	254	5
	27-Sep	270	14			9-May	129	13
	13-Oct	286	0			10-Jun	161	0
	2004	8-May	129		60	Jun-26	177	23
25-Jun		177	22		29-Aug	241	3	
2010		13-Sep	257		4	Sep-14	257	0
						30-Sep	273	10

\* Image date is earlier than the NASS recorded date for 50% of planting completed.

NDVI values also change during the plant growing cycle. During development from planting to physiological maturity, corn experiences several growth stages. These stages are separated into two groups: vegetative and reproductive periods. The vegetative period covers the timing from planting to the stage when the entire tassel is visible (the visible tassel or VT period) and leaves are fully developed. The reproductive period starts from the silking stage and ends at physiological maturity. For a single plant, the growth rate is slow at the beginning of the vegetative period, but increases when new leaves appear. It reaches the maximum canopy coverage in the early reproductive period. Corn NDVI values roughly follow the same trend, where the peak NDVI value is often observed during the silking period. Natural senescence usually begins at the end of the denting period; NDVI values decrease from the beginning of natural senescence to maturity.

#### 3.3.3.1 NDVI calculation for corn pixels

The first step for computing NDVI values for corn pixels is to remove non-clear land pixels for all Landsat TM5 images. The object-based cloud and cloud shadow detection software Fmask (Zhu and Woodcork, 2012) was utilized to identify cloud, shadow and unobstructed land surface pixels. Digital Number values from the visible and near-infrared bands in the raw Landsat 5 TM imagery are first converted to Top of Atmosphere (TOA) reflectance, while the thermal band is converted to Brightness Temperature (BT) using the Landsat Ecosystem Disturbance Adaptive Processing System (LEDAPS; Masek et al., 2006). The TOA reflectance and BT (in degrees Celsius) are used as Fmask input. Decision rules based on cloud and cloud shadow physical properties (brightness and temperature) are then used

to extract a potential cloud/shadow layer. Cloud potential layers are improved by eliminating edge cells. Then the base and top height of clouds are computed and used to calculate projected shadows. Shadow detection is refined via a shape similarity comparison, where geometric relationships are used to match the potential cloud shadow with the cloud. Clearly visible land pixels are identified by Fmask as those with data that are not covered by cloud, cloud shadow or snow. Pixels used for the analysis are further screened to make sure that they are clearly visible for every Landsat image for a specific year by merging the Fmask products for all TM images in each year. As corn is not grown consistently on the same fields on a year-to-year basis (as defined by local crop rotation practices), the pixels selected for analysis did vary between years.

The final outputs of Fmask are clear land pixels for all TM5 images in each year. Quick Atmospheric Correction (QUAC) from Exelis ENVI was used to remove the effects of the atmosphere on the reflectance values of all clear land pixels. QUAC determines atmospheric correction parameters using an in-scene approach without ancillary information, requiring only specification of sensor band locations and their radiometric calibration (Bernstein et al., 2005). The final product for NDVI calculation after running QUAC was reflectance from all clear land surface pixels.

NDVI for all land pixels was calculated based on the atmospherically corrected reflectance of band 3 (red, 630-690 nm) and band 4 (near infrared, 760-900 nm). Pixels identified as corn in each CDL data layer from 2000 to 2010 are used to extract the corn NDVI values for pixels within 15 km of the St. Joseph River watershed. The purpose of extending the selection area to include areas outside the watershed is to enlarge the sample size for corn

pixels. It is assumed that growing conditions within the 15 km buffer are similar to the ones inside the watershed boundary.

Three additional filters are applied to further refine the selection of corn pixels identified by the CDL data, to minimize the potential for mixed pixels and registration errors that can introduce noise into the data. The first filter improves the identification of pure corn pixels by removing any pixel that had more than one non-corn neighbor. These are assumed to be edge-of-field pixels with a greater likelihood of being mixed. The second filter checks for a minimum amount of change in NDVI between planting and silking when NDVI should peak., Here the median NDVI value for all corn pixels was calculated for all images for a year, and the image with the peak median NDVI (near silking stage) and minimum NDVI (near planting) were identified. The difference between median NDVI for those two images was set as a threshold. Any pixel with maximum NDVI range less than that threshold over all images in the year was excluded. The final filter checks that NDVI increased monotonically from planting date to peak NDVI stage, then decreased monotonically from peak stage to maturity stage. Due to the limited availability of images each year, the maximum NDVI value calculated from the Landsat images may not always be the peak NDVI for that year. It is possible to have a non-monotonic change for valid pixels if the peak growth period is missed due to the lack of available imagery. Therefore, the monotonic check is applied for images between the latest planting date and earliest silking date, and images between the latest silking date and earliest maturity date, where these dates have been extracted from the USDA NASS Crop Progress Reports (Table 3.2).

Since 2004 had only three available images, the third filter was not applied. Figure 2 illustrates the impacts on NDVI after each of these filters.

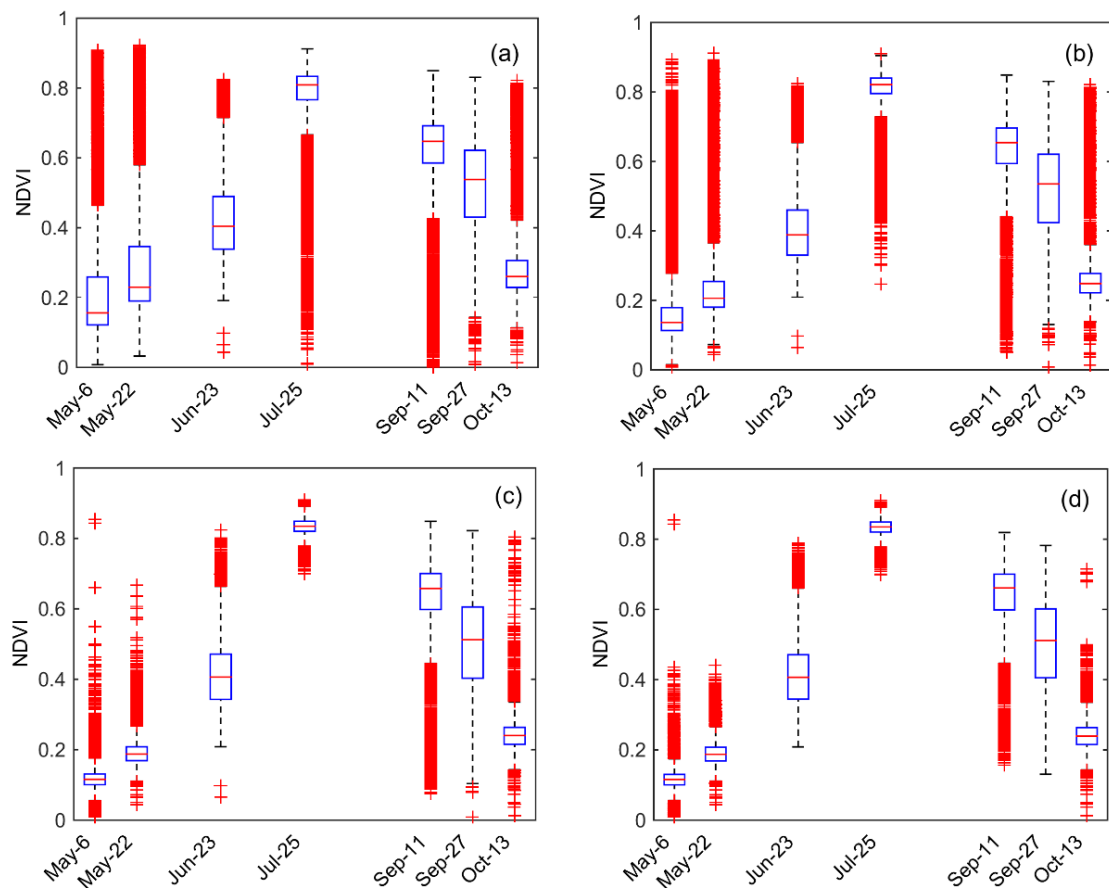


**Figure 3.2** Boxplot for corn NDVI values in 2003: (a) original data for all corn pixels within the region, (b) after applying the first filter: edge-of-field pixels are removed, (c) after applying filter 2: pixels without sufficient seasonal variation are removed, and (d) after applying filter 3: between images from May-22 and Jun-23. Pixels with decreasing NDVI values between the two dates were removed. The third filter was also applied between images from Jul-25 and Sep-11. Pixels with increasing NDVI values between two dates were removed.

**Table 3.2 NASS corn progress dates for the St. Joseph River Basin**

Crop Status	Year	Day of Year Status Begin	Day of Year Status End	50% progress status
Planted	2000	107	156	127
	2001	105	147	124
	2002	111	167	145
	2003	110	159	122
	2004	109	151	119
	2005	100	142	122
	2006	106	155	123
	2007	112	147	130
	2008	118	167	130
	2009	123	165	143
	2010	106	155	126
Silked	2000	184	219	200
	2001	196	217	201
	2002	195	223	206
	2003	194	229	207
	2004	179	221	192
	2005	191	219	199
	2006	190	218	199
	2007	189	217	197
	2008	195	230	205
	2009	193	228	208
	2010	183	218	199
Matured	2000	240	282	263
	2001	238	287	263
	2002	244	286	268
	2003	250	285	273
	2004	242	291	262
	2005	233	289	263
	2006	239	288	267
	2007	245	287	263
	2008	251	300	265
	2009	256	312	286
	2010	239	281	262

### 3.3.3.2 Normal curve generalization and NDVI residual calculation

Since corn phenology is more correlated with air temperature (or heat units) than Julian days since planting, development varies from year to year with respect to date (Abendroth et al. 2011). Therefore, the extracted NDVI data are associated with the Potential Heat Units (PHU) and Growing Degree Days (GDD) accumulated from the planting date to the date of image acquisition. PHU and GDD are both used as measures of the growth and development of plants based on daily average temperature. PHU is calculated based on degrees Centigrade, while GDD is based on degrees Fahrenheit. Development does not occur unless the daily average temperature is above a base temperature (lower limit). PHU/GDD start to accumulate from the planting date to the date of physical maturity for the plant as long as temperature is above the lower limit. The lower limit for corn is set as 8 °C (Kiniry et al., 1995). The GDD method also has an upper limit, which is set to 86 °F/30 °C (Nield and Newman, 1990), representing temperature above which the crop is too stressed to continue development towards maturity. Such a limit does not exist with the PHU.

A generalized corn NDVI growth curve is obtained using a robust version of LOESS (locally-weighted scatter plot smoothing; Cleveland, 1979) applied to median NDVI values from all 11 years' images plotted versus PHU and GDD. Due to data scarcity (3-7 images per year) and the timing difference of images, it is hard to describe the corn NDVI dynamics for specific growth periods using just one year's data. Therefore, all years of data are combined to create a general, regional corn growth curve. In this way, missing information for a specific period in one year can be compensated by other years. The

generalized NDVI curve via local regression method reflects the corn growth dynamics under “normal conditions” for 11 years. The differences between measured NDVI and the derived normal curve, the residual or “discrepancy score” (Sakamoto et al., 2011), can be treated as an index to reflect the influence of biophysical stresses on crop growth. If the residual has a negative value, corn development is below normal so can be assumed to have experienced more growth stress than in a normal year. The Sakamoto et al. (2011) “discrepancy score” was computed based on a rescaled shaped model from 7 years of continuous daily MODIS data and smoothed for each year. Therefore, their “discrepancy score” differs for each year, which is different from our image based residuals. By comparing the median NDVI for a specific image and the normal curve, we can roughly estimate basin level corn growth condition in a specific day. Interannual corn growth analysis can be conducted by averaging NDVI residuals based on satellite imagery. To obtain the spatial growth variability, the departure rate can also be computed based on NDVI and the normal curve for each individual pixel.

#### 3.3.3.3 Growth stress metrics

Actual crop growth is affected by various stresses occurring during the growing season, including those from extreme temperatures, oversupplied or limited water, insufficient nutrients, pest infestations, and weed competition. Actual growth is therefore always less than or equal to the potential growth even under optimal conditions.



In this research, only crop growth stresses from extremes of temperature and water, based on the approach used in the Soil and Water Assessment Tool (SWAT) were calculated (Neitsch et al., 2009).

Daily temperature stress ( $ts$ ) is calculated as:

$$ts = 1 \quad Tav > 2 * T_{opt} - T_{base} \text{ or } Tav \leq T_{base} \quad (3.2)$$

$$ts = 1 - \exp \left[ \frac{-0.1054 * (T_{opt} - Tav)^2}{(Tav - T_{base})^2} \right] \quad T_{base} < Tav < T_{opt} \quad (3.3)$$

$$ts = 1 - \exp \left[ \frac{-0.1054 * (T_{opt} - Tav)^2}{(2 * T_{opt} - Tav - T_{base})^2} \right] \quad T_{opt} < Tav < 2 * T_{opt} - T_{base} \quad (3.4)$$

Where  $Tav$  is the mean air temperature for day ( $^{\circ}\text{C}$ ),  $T_{base}$  is the plant's base or minimum temperature for growth ( $^{\circ}\text{C}$ ) (defined as  $8^{\circ}\text{C}$  for corn), and  $T_{opt}$  is the plant's optimal temperature for growth ( $^{\circ}\text{C}$ ) (defined as  $25^{\circ}\text{C}$  for corn).

Accumulated temperature stresses normalized by the number of days or heat units are used to quantify the cumulative effect of temperature on crop growth.

$$ts_{acc\_day} = \frac{\sum_i^n ts}{n-i} \quad (3.5)$$

$$ts_{acc\_PHU} = \frac{\sum_i^n ts}{\sum_{i=1}^n PHU} \quad (3.6)$$

$$ts_{acc\_GDD} = \frac{\sum_i^n ts}{\sum_{i=1}^n GDD} \quad (3.7)$$

Where  $ts_{acc\_day}$  is the accumulated temperature stress normalized by the number of days from planting date  $i$  to image collection date  $n$ ;  $ts$  is daily temperature stress;  $ts_{acc\_PHU}$  is the

accumulated temperature stress normalized by PHU; PHU is the accumulated heat units from day  $i$  to day  $n$ ;  $ts_{acc\_GDD}$  is the accumulated temperature stress normalized by GDD; GDD is the accumulated growing degree days from day  $i$  to day  $n$ .

Water stress ( $ws$ ) is computed based on the difference between average accumulated rainfall from long term historical data and accumulated rainfall for each year, as follows:

$$ws = \sum_{i=1}^n p_i - \sum_{i=1}^n \bar{p}_i \quad (3.8)$$

where  $p_i$  represents daily precipitation for a single year and  $\bar{p}_i$  is the daily normal precipitation for a 20 year period (1991-2010).  $ws$  is calculated by comparing the accumulation of precipitation from the average curve ( $\sum_{i=1}^n \bar{p}$ ) with that for the current year ( $\sum_{i=1}^n p$ ) relative to the planting date  $i$  for the year of interest, and can be calculated to any day  $n$  in that year. If  $ws$  is a negative value, it means the accumulated rainfall amount is below the average condition, so corn at that time may have suffered more from drought. On the other hand, if  $ws$  is a positive value, it indicates a wetter than average condition. As shown in Figure 3.3, the cumulative rainfall curve for year 2002 is below the long term average curve, which results in negative  $ws$  values in this dry year. Positive  $ws$  values are found for the year 2003, indicating it was wetter than average. Year 2006 is normal year, because the accumulation of precipitation in 2006 is close to the long term average.

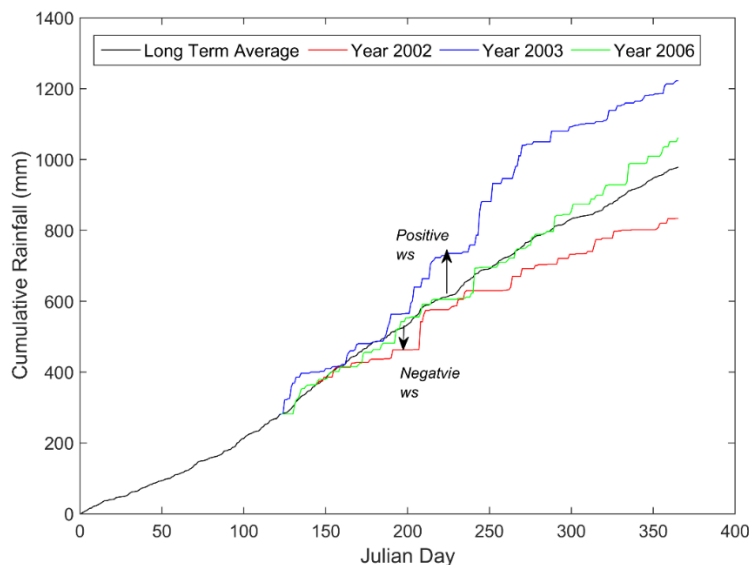


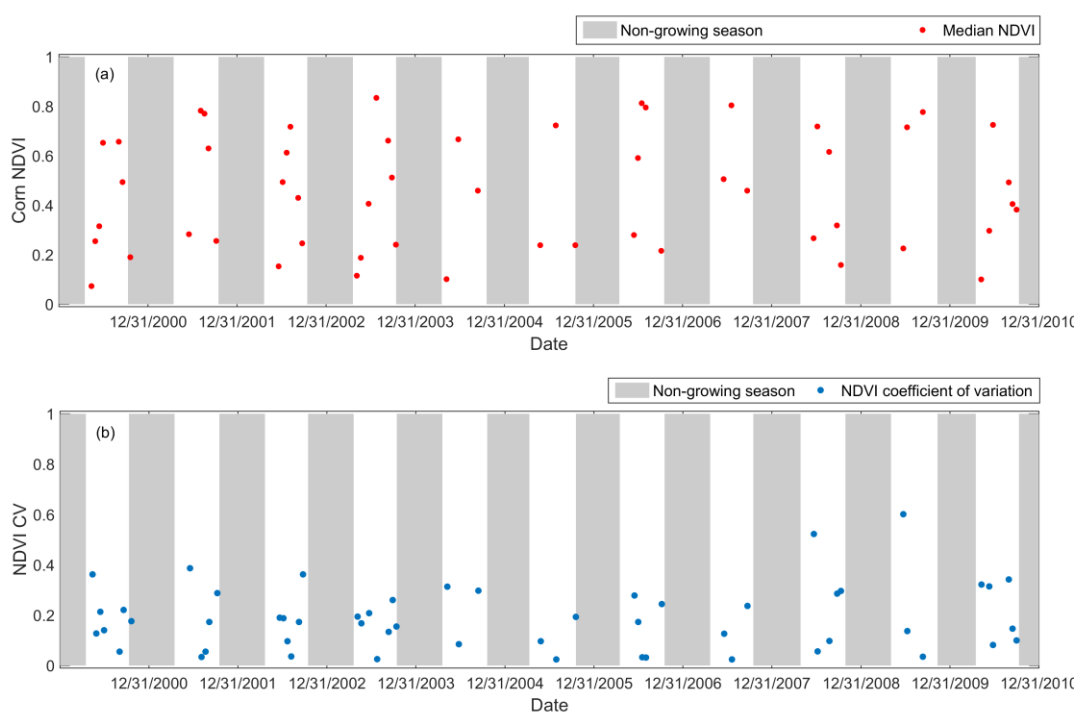
**Figure 3.3 Cumulative rainfall comparison between long term average (1991-2010) and specific years.**

### 3.4 Results

#### 3.4.1 Normalized Difference Vegetative Index with Time

Figure 3.4(a) illustrates the median growing season corn NDVI values for 11 years of images (2000-2010), and the 95% prediction interval of corn NDVI for each image. The median value of corn NDVI follows the expected phenology of the corn canopy. In the early growing period, as corn plants emerge, vegetation coverage per unit area is small, and the median NDVI value is low (0-0.2). As plants develop, the NDVI value grows rapidly (0.3-0.6) capturing the increase in leaf area as the growing plant spreads to cover the soil between the rows in the fields. The NDVI value is proportional to the canopy coverage during this stage. Corn NDVI reaches a peak value (0.7-0.8) at the end of July or early August, at the stage when all leaves are fully developed. As plants enter the end of

the reproductive stages and natural senescence occurs, NDVI decreases significantly. The 95% prediction interval highlights the 97.5 and 2.5 percentiles of NDVI values for available corn pixels in the St. Joseph watershed. This range is often small at the beginning of the growing season following planting, when the majority of fields are mostly bare and during the peak NDVI period when most fields have complete canopy closure. The range is much larger during the late vegetative growth stages and senescence, reflecting the large spatial variability during these periods of rapid change.



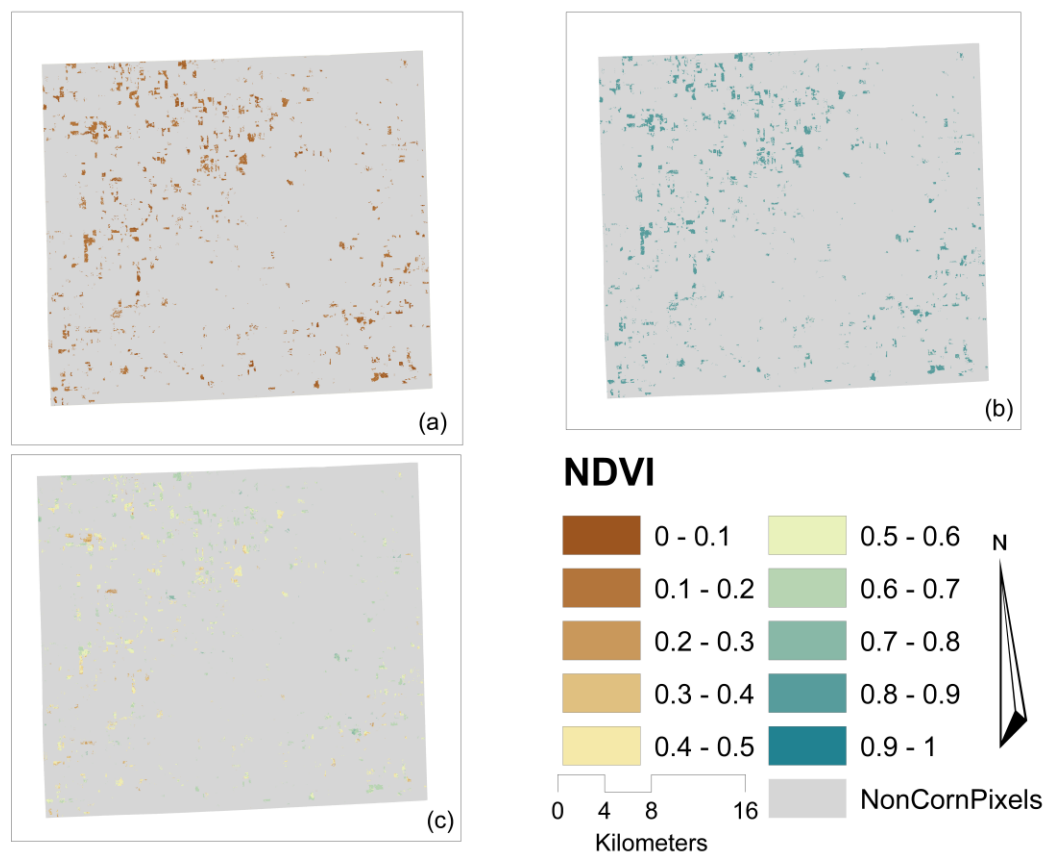
**Figure 3.4 (a) Median Normalized Difference Vegetative Index (NDVI) and (b) Coefficient of Variation (CV) from NDVI values in St. Joseph River watershed for 11 years.**

Figure 3.4(b) shows the Coefficient of Variation (CV) of corn NDVI with time. Minimum CVs for each year are found in the middle of the growing season associated with the peak

NDVI value. This period appears to be the most uniform stage, when the corn canopy is fully developed and spatial differences due to different planting dates are less pronounced. Peak CVs are often encountered either at the early or late growing season. In the early growing season when corn is just emerging, soil reflectance dominates the NDVI measurement, causing a very low mean NDVI value (e.g. Year 2000, 2003 and 2010), and therefore a higher CV. Secondly, due to different planting dates, NDVI values show greater variance in late June (around 30-40 days after planting), leading to higher CV values (Year 2001, 2008 and 2009). In the late growing season, as senescence occurs, the reflectance contains a wide range of green and non-green color intensities, also causing high CV values. Table 3.3 lists the date of the maximum NDVI variation for each year. Those dates are always found during either the leaf development stage or senescence period. This spatial variability in NDVI is illustrated in Figure 3.5 for De Kalb County in the year 2003. The spatial distribution pattern on June 23rd and September 27th appears more heterogeneous than on July 25th, when canopy coverage and leaf overlap were well-developed.

**Table 3.3 Date of maximum NDVI variation (range of the 95% prediction interval) for each year**

Date	Days after planting	95% interval	Median NDVI	CV
17-Sep-2000	133	0.4050	0.4938	0.2207
16-Jun-2001	43	0.4565	0.2833	0.3868
05-Jul-2002	41	0.3561	0.4934	0.1875
26-Sep-2003	147	0.4677	0.5117	0.2605
12-Sep-2004	136	0.5128	0.4591	0.2974
17-Oct-2005	168	0.1535	0.2387	0.1937
30-Jun-2006	58	0.3870	0.5906	0.1728
21-Sep-2007	134	0.4343	0.4588	0.2368
19-Jun-2008	40	0.5690	0.2665	0.5225
22-Jun-2009	30	0.5841	0.2253	0.6017
28-Aug-2010	114	0.5783	0.4930	0.3415



**Figure 3.5** Spatial distribution of NDVI as observed from Landsat 5 TM imagery for De Kalb County, IN on the following dates in 2003: (a) May 22nd, NDVI mean=0.19, CV=0.16; (b) Jul 25th, NDVI mean=0.83, CV=0.02; (c) Sep 27th, NDVI mean=0.54, CV=0.20.

### 3.4.2 Normal growth condition

The generalized corn NDVI growth curve obtained from all 11 years' images is shown in Figure 3.6. Since different planting dates each year may affect the starting point of the NDVI curve, the NASS recorded planting date (50th percentile value) is used as the starting point for each year's analysis. In addition, different lengths of the growing season (number of days vary from 122 days in 2002 to 151 days in 2003 based on the 50th percentile of

NASS crop progress records) may make it difficult to identify NDVI values for a specific growing period defined by Julian days. Therefore, NDVI dynamics are also regressed against PHU and GDD accumulated from the planting date (Figure 3.6). Two outliers (see Figure 3.6) were removed when generating the normal growth curve. The first is from 2005 imagery, and is removed because it associated with an extremely high PHU and GDD suggesting that it was collected well after crop maturity. The second one is from 2007 imagery, and yields extremely high NDVI values at the very end of the growing season, suggesting the NDVI value at this time does not correctly represent the corn growth condition.

The departure of image median NDVI values from the normal curve (NDVI residual) are calculated and plotted versus Julian days, PHU and GDD, respectively (Figure 3.7). For year 2002, most NDVI residuals are negative, indicating increased stress levels relative to the long-term average for almost the entire growing season, which can be attributed to the drought that occurred that year. For years 2008 and 2010, corn NDVI deviations are negative for the second half of the growing season, suggesting increased stress on crop growth in the later parts of the growing season. Years 2004, 2007 and 2009 all have positive residuals during the peak NDVI stage, indicating corn growth is above normal. Residuals for the other years are small so NDVI values are close to the normal curve, indicating an average growth year. Corn response to year to year variability is reflected in these departures from the normal curve. Therefore, positive NDVI residuals do not necessarily mean the corn is not in any way stressed, but that its growth is above the normal condition based on the multiple year record.

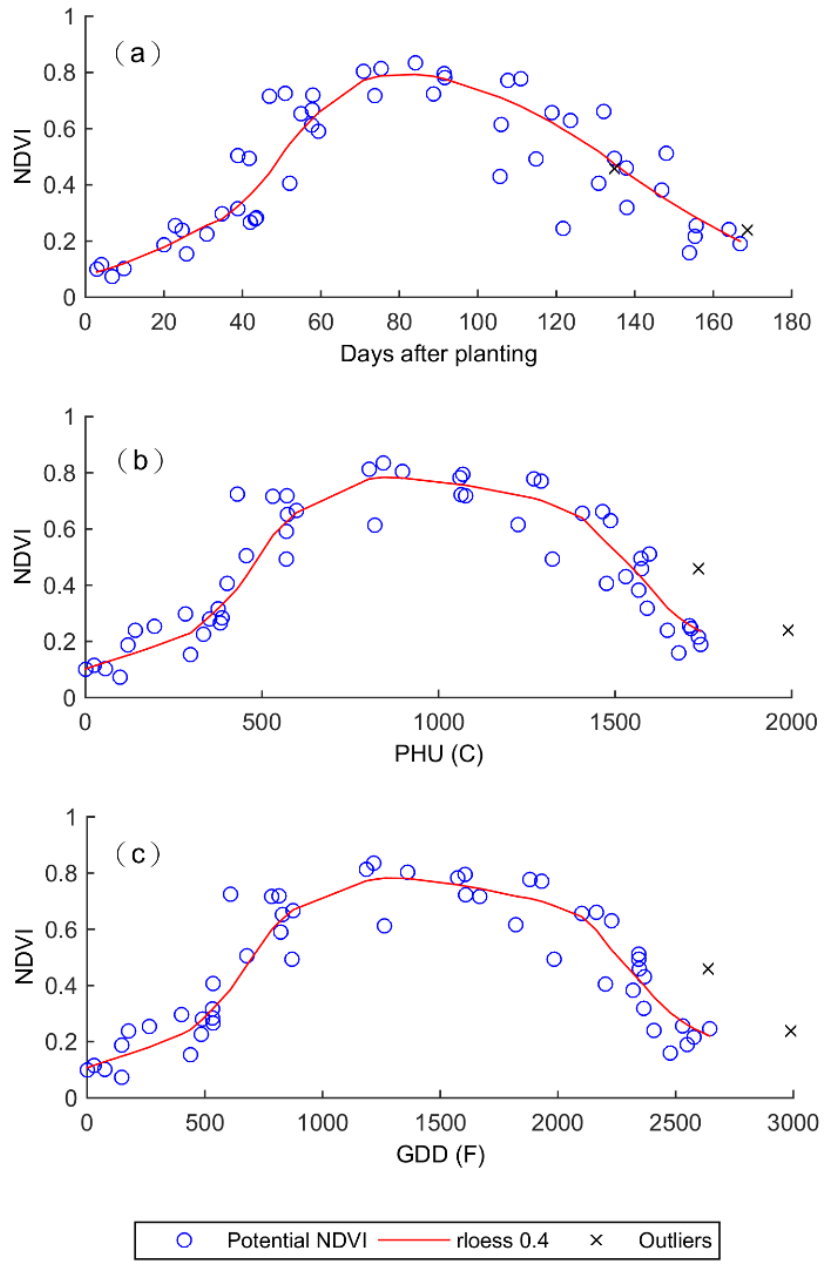


**Figure 3.6** Generation of normal NDVI curve based on 11 years data versus: (a) days after planting, (b) PHU, and (c) GDD. The normal curve is generated by smoothing NDVI using robust loess method, with a span of 40%.



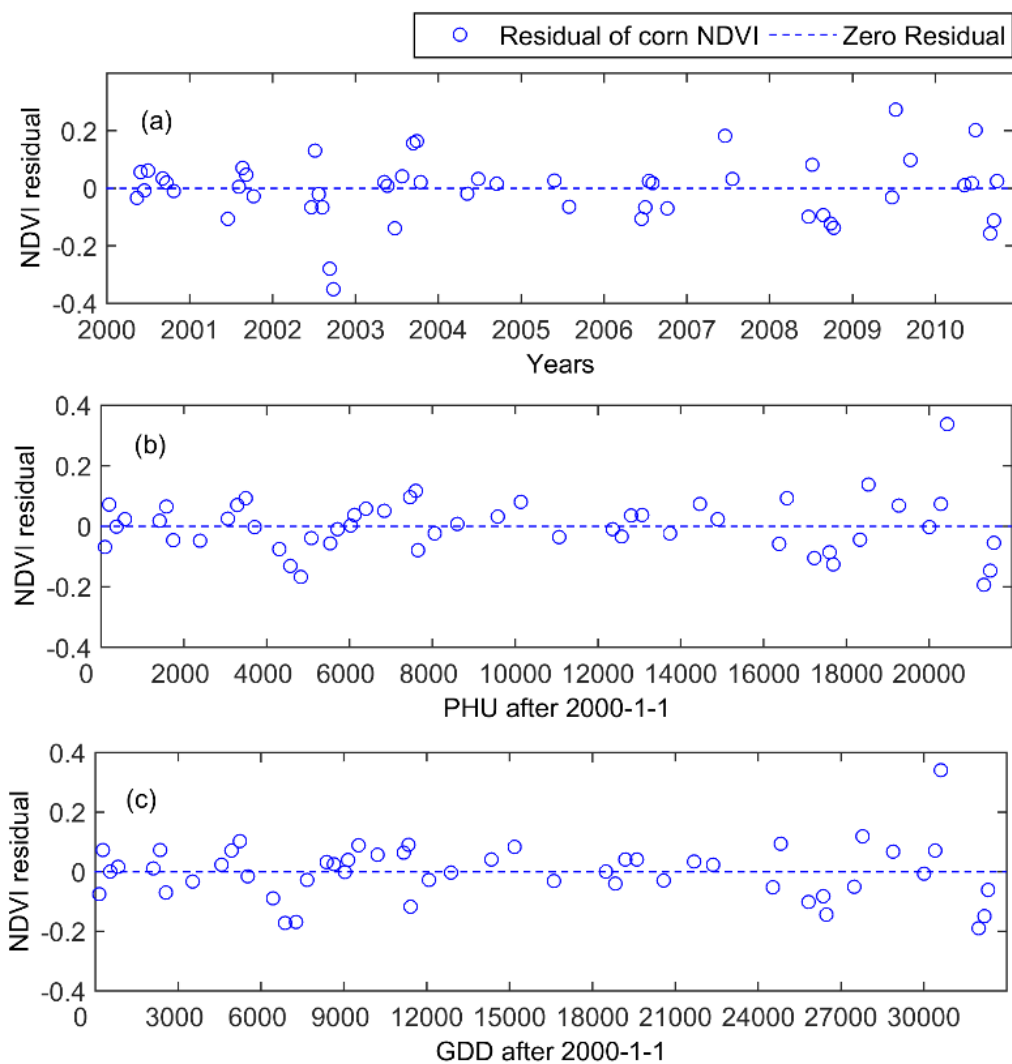


**Figure 3.7 Eleven year median NDVI values minus normal NDVI for the same: (a) number of days after planting, (b) PHU, and (c) GDD.**

The rank of the annual discrepancy score (average of the residual calculated for each image over a growing season) is summarized in Table 3.4. High rankings indicate positive residuals, meaning that the crop experienced higher NDVI than normal conditions, while low rankings indicate that crop experienced lower NDVI than normal conditions. Although there is some variation in ranks based on whether Julian days or heat units are used, the

relative positions in the rankings are quite consistent. For example, 2002 and 2008 are always the lowest ranked years, while 2009 and 2003 are more highly ranked regardless of the independent variable. The annual yield for 2002 and 2008 was 6.65 and 8.03 t/ha, which are around 1.5-3.0 t/ha lower than year 2003 and 2009 (9.51 and 9.48 t/ha respectively), confirming that corn in 2002 and 2008 may have experienced more growth stress, which negatively affected yield.

**Table 3.4 Rank of NDVI residual for each set of annual images. Rank 1 = best NDVIs, while Rank 11 = worst NDVIs.**

Year	Days		PHU		GDD		Growing Season Rainfall amount (mm)	Growing Season Mean Temperature (°C)
	Rank	Discrep. Score	Rank	Discrep. Score	Rank	Discrep. Score		
2000	4	0.0171	6	0.0090	6	0.0041	482	19.6
2001	6	-0.0019	4	0.0275	3	0.0301	460	19.9
2002	11	-0.1086	11	-0.0797	11	-0.0667	390	20.2
2003	3	0.0391	3	0.0407	2	0.0317	634	19.7
2004	5	0.0100	7	0.0054	7	0.0034	445	19.9
2005	8	-0.0183	5	0.0225	5	0.0262	287	21.6
2006	9	-0.0399	9	0.0011	8	0.0026	384	20.8
2007	2	0.1069	2	0.0480	4	0.0282	378	20.8
2008	10	-0.0743	10	-0.0563	10	-0.0573	394	19.8
2009	1	0.1134	1	0.0542	1	0.0450	490	18.0
2010	7	-0.0028	8	0.0029	9	0.0008	358	19.7

### 3.4.3 Yield-NDVI residual relationship

Biophysical stress at different crop growth stages produces different magnitudes of influence on final yields (Kebede et al., 2014; Ge et al., 2012). Therefore, the relationship between NDVI residuals averaged over various growth stages and county level corn yields

was investigated. Growth stages selected for analysis include: 1) The pre-silking period, where average NDVI residuals are calculated based on all available images from planting to the earliest silking date recorded by NASS data (Table 3.2). Average NDVI residuals during this period should reflect the corn growth condition during the corn vegetative period. Stress in this period reduces stem and leaf cell expansion resulting in lower plant height and less leaf area (Yang, 2009). 2) The pre-maturity period, where NDVI residuals are calculated based on available images from planting to the earliest maturity date recorded by NASS data. This period contains both the corn vegetative stage and the most important reproductive stages (silking, blister and dough) of the corn plant life cycle. Stress in the early and middle reproductive stages can abort kernels, reduce kernel weight, and increase lodging, and in turn impair final yield (Nielsen, 2008). 3) The silking period, where the NDVI residual are calculated for the image with the highest NDVI value for each year. This image is typically found in the silking period, when the canopy is fully developed. Early season stresses affect leaf area development, leading to differences in maximum NDVI values for each year. The NDVI residual for this image is caused by accumulated stresses during the vegetative period, which could also affect final yield. 4) The whole growing period where average NDVI residuals are calculated based on all available images. This is the same as the annual discrepancy score introduced previously.

The relationship between these four NDVI residuals, calculated from the three different generalized growth curves, and annual yield are summarized in Table 3.5. No significant relationship was found (for significance level,  $\alpha = 0.05$ ) for any period if Julian day is used to generate the normal curve. When PHU and GDD are used to generate the normal

growth curve, a significant relationship exists between NDVI residual and corn yield for the pre-silking, pre-maturity and entire growth periods. For the pre-silking period, a significant relationship ( $p < 0.01$ ) was detected between average NDVI residuals based on GDD and annual corn yield (Fig. 3.8). Average NDVI in the pre-maturity stage ( $p < 0.05$ ) and for the whole growing season ( $p < 0.05$ ) were also statistically significant predictors of annual yield. No significant relationship was found between the residual of the maximum NDVI image and annual crop yield, for any of the three normal growth curves. The relationship between annual basin level corn yield and NDVI residuals at different growing stages (GDD based) are also shown in Fig. 3.8.

**Table 3.5 Pearson correlation coefficient,  $r$ , between grain yield and average NDVI residuals for different growth stages**

	Day	PHU	GDD
Mean NDVI departure for pre-silking period images	0.067	<b>0.71*</b>	<b>0.76**</b>
Mean NDVI departure for pre-maturity period images	0.16	0.58	<b>0.62*</b>
Mean NDVI departure for all images in the growing period	0.50	<b>0.68*</b>	<b>0.69*</b>
Departure for Highest NDVI point for each year	0.28	0.36	0.36

\*means significant correlated when  $p < 0.05$ , \*\* means significant correlated when  $p < 0.01$

The correlation analysis summarized in Table 3.5 indicates that the NDVI residual derived from Landsat images reflects crop stress in the pre-silking period that in turn impacts final yield. This result is consistent with other studies that have found that NDVI from the middle to late vegetative period is significantly correlated with biomass and final yield (Martin et al., 2007; Teal et al., 2006). Therefore, it may be possible to predict corn grain

yield in-season for this study area, by comparing pre-silking period NDVIs to long-term normal growth curves.

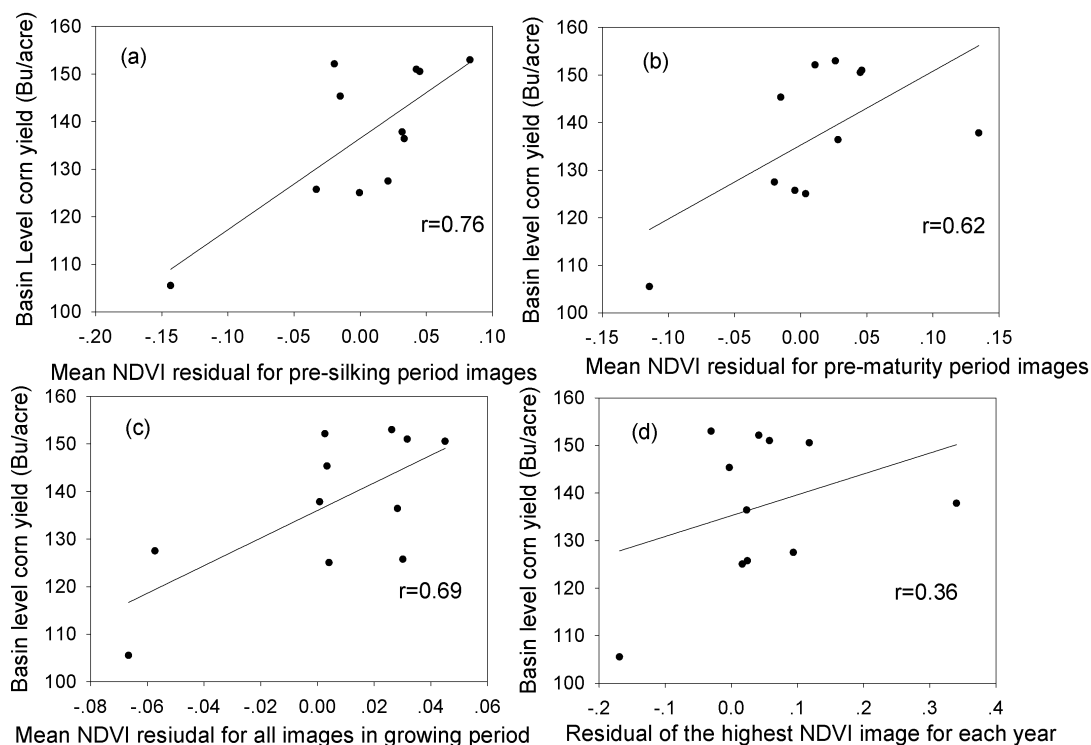


**Figure 3.8** The relationship between basin level corn yield and (a) mean NDVI residual for pre-silking period images; (b) mean NDVI residual for pre-maturity period images; (c) mean NDVI residual for all images in the growing period; (d) residual of the highest NDVI image for each year. Residuals are calculated based on GDD.

#### 3.4.4 Stress-NDVI residual relationship

As stated in section 3.3, annual corn yield is significantly related to the annual, pre-silking and pre-maturity NDVI discrepancy scores. The relationship between NDVI discrepancy and precipitation and temperature stress metrics are investigated in this section. The NDVI residuals calculated for all images in the 11-year period in section 3.2 are grouped into pre-

silking period, pre-maturity period and whole growing period. However, the residuals in those periods are not averaged as they were for the yield-residual relation, but rather regressed with normalized stress indices ( $ws$  and  $ts_{acc}$ ) on the date of image acquisition.

The relationship between NDVI residuals and water stress ( $ws$ ) is shown in Figure 3.9. Large negative values of water stress ( $ws$ ) represent dry conditions; positive  $ws$  represent wet conditions. There are no strong correlations found in the data (Figure 3.9), but it appears that points can be grouped into several clusters. Image averages in Cluster A have both negative NDVI residual and water stress, which indicates that the weather is dry and crop growth is below normal. Cluster C has both positive NDVI residuals and water stress, so precipitation and crop growth are both above normal. Images in Cluster B represent normal weather and crop conditions. Compared to Cluster B both cluster A and C have relatively larger absolute values (0.2-0.4) in NDVI residuals, indicating larger growth discrepancies (could be either under or above normal condition). When corn growth is way above or below normal, it is usually associated with extreme climate conditions. Images in cluster B do not have a clear relationship between water stress and NDVI residuals. Since crop growth can be affected by many environmental factors, for example, soil types and slopes, temperature, disease and pests, leaf growth in this cluster may not respond to water stress exclusively, but is influenced by other environmental factors. Figure 3.9(c) also has a fourth cluster, named Cluster D, that contains images collected from the end of the growing season (after middle September) in 2003. Images in this cluster have very large positive  $ws$  values, but an unclear relationship between  $ws$  and NDVI residuals. This indicates that an oversupply of rainfall at the end of the growing season did not have a

substantial effect on crop development. NDVI residuals at that time are more strongly related to the natural senescence process than water stress.

The relationship between NDVI residuals and normalized temperature stress indices ( $ts_{acc}$ ) are summarized in Table 3.6. No statistically significant relationship ( $p < 0.05$ ) was found between temperature stress and NDVI residuals at any period based on either time units or heat units. This might be caused by the temperature stress calculation method. Compared to average daily temperature, daily maximum temperature is more associated with crop growth (Mishra and Cherkauer, 2010). Leaf development is significantly affected by temperature when it is associated with water limitation. A more mechanistic analysis is needed to evaluate interactions between temperature, precipitation and other factors as they determine evapotranspiration, which is more closely related to NDVI (Srivastava et al., 1997)

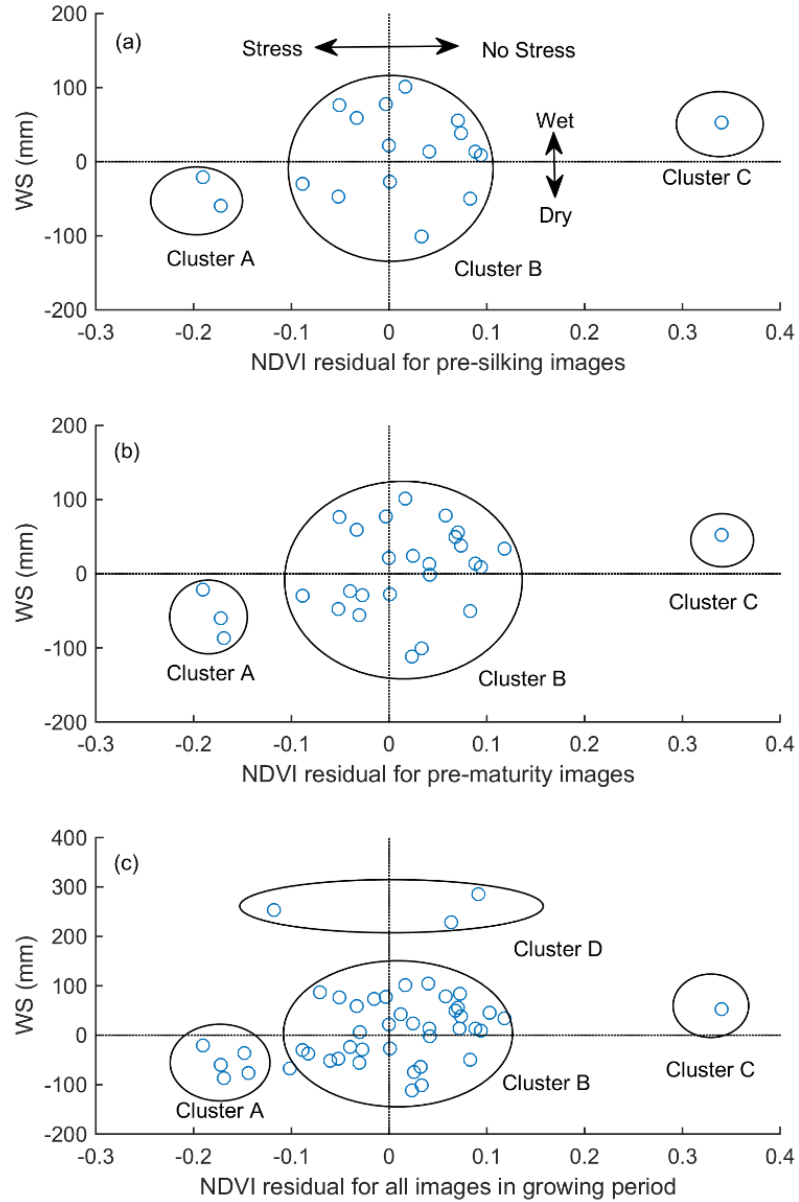


**Figure 3.9 Relationship between ws value and median image NDVI residuals at (a) Pre-silking period; (b) Pre-maturity period; (c) whole growing period.**



**Table 3.6 Pearson correlation coefficient,  $r$ , between stress indices and NDVI residuals for different growth stages**

	<b>Day</b>	<b>PHU</b>	<b>GDD</b>
NDVI departure for pre-silking period images vs. Normalized accumulated temperature stresses	-0.36	0.32	0.42
NDVI departure for pre-maturity period images vs. Normalized accumulated temperature stresses	-0.18	0.32	0.35
NDVI departure for all images in growing period vs. Normalized accumulated temperature stresses	0.07	0.27	0.27

#### 3.4.5 Risky pixel rate – stress relationship

In section 3.3 and 3.4, the relationship between image median NDVI residual and crop yield and climate metrics was investigated. Since NDVI residual was computed based on the image median NDVI value, the analysis neglected the spatial variability in crop stress. In this section, more emphasis is put on individual pixels under stress. Any corn pixel with NDVI less than the normal growth curve (Figure 3.6) is considered to be under stress. The percentage of pixels under stress (risky pixel rate) for each image is computed, and related to water stress (Figure 3.10).

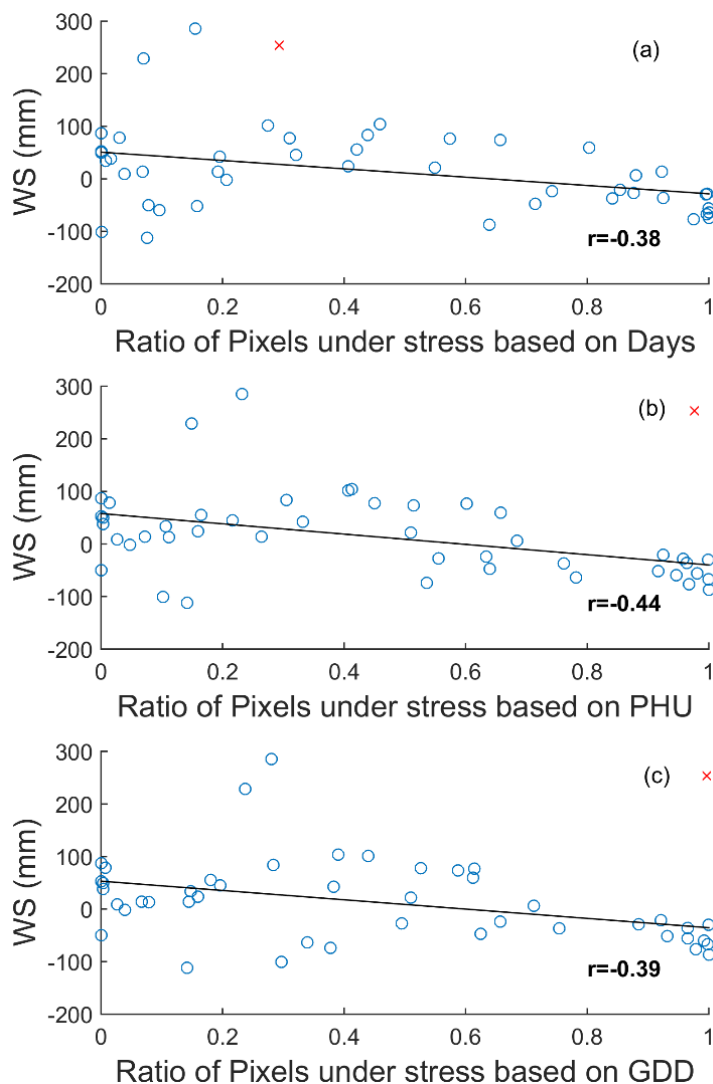


**Figure 3.10 Relationship between water stress and risky pixel rate based on a) days, b) PHU, c) GDD. Red cross indicates the outlier at the very end of the growing season (Oct. 13th) in wet year 2003.**

Statistically significant relationships ( $p < 0.05$ ) are detected between water stress and risky pixel rates, no matter which method was used to produce the normal growth curve. Therefore, the number of pixels experiencing growth limitations is strongly correlated with water stress. Based on Figure 3.10, images with risky pixel rates over 0.8 (80% of cells are under stress) have negative *ws* values, indicating drought condition is affecting crop

growth for most cells. Almost all images with low risky pixel rate (less than 0.2) are associated with positive  $w_s$  values, so above average rainfall reduced the threat of yield loss (less area experienced yield reduction). This difference in area affected under wet and dry stress is illustrated by comparing two images from the pre-silking stage for a dry year (2002) and a wet year (2003) (Figure 3.11), which clearly reflects the different impacts of rainfall on risky cell rates. If rainfall is limited, then most cells are under stress (Figure 3.11(a)). However, if rainfall is above average, only a small portion of cells are under stress (Figure 3.11(b)). This reflects the collection of runoff and ponding in depressional areas that may experience catastrophic yield loss, as opposed to the depressed growth over widespread areas in the case of water limitations.

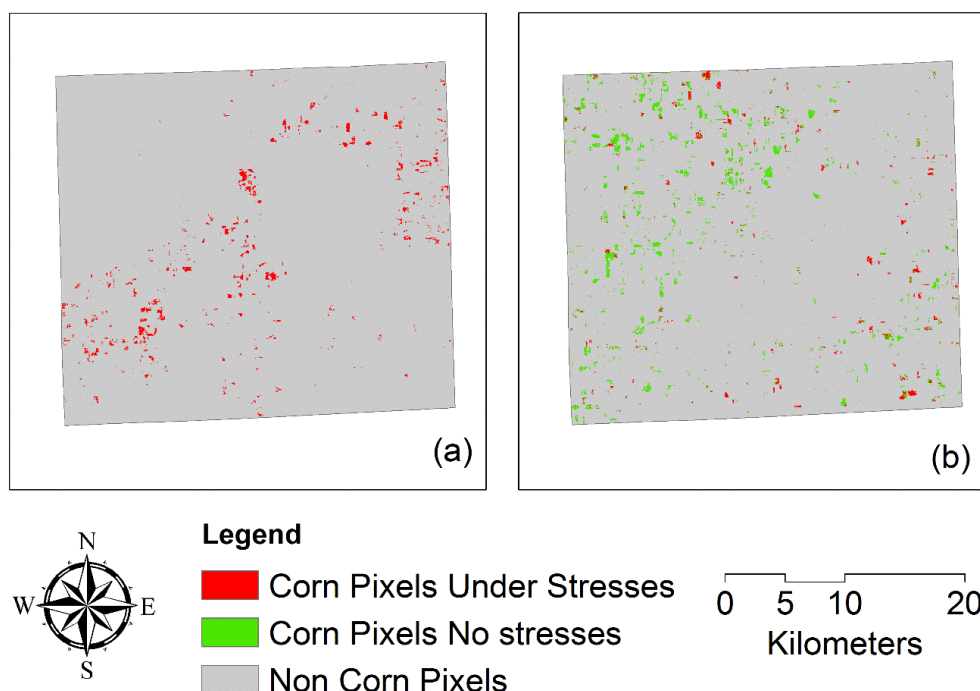


**Figure 3.11 Spatial distribution of corn pixels identified as being under stress and experiencing no stress (using the GDD based normal curve) in De Kalb county: (a) 2002 dry year, and (b) 2003 wet year.**

For wet years, although fewer cells are affected by stress (risky pixel rate  $< 0.2$ ), the potential yield loss in those cells with high stress rates could be huge. This is investigated using NDVI residuals that can represent potential yield, and  $w_s$ , for risky cells (negative NDVI residuals) only when the risky pixel rate is less than 0.2, and  $w_s > 0$  (Figure 3.12). Though there is no clear relationship between  $w_s$  and the NDVI residuals, in Figure 3.12(a), we found that very large  $w_s$  values ( $w_s > 200$  mm, both found in 2003) are always associated with large negative NDVI residuals, indicating potential yield loss in those cells. The overall yield in 2003 for the study area was the 3rd highest in the 11 year period (2000-2010), which means that yield losses in those few cells where water stress was high are compensated by increased yield in other cells that benefitted from sufficient rainfall.

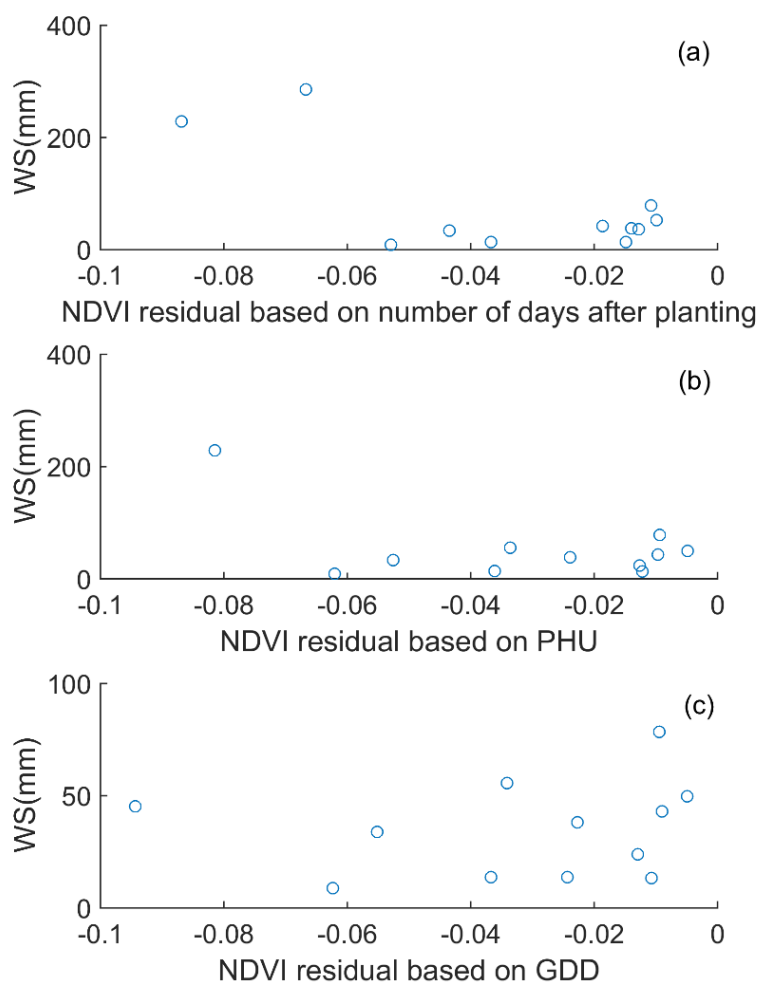


**Figure 3.12 Relationship between ws value and NDVI residual based on (a) number of days after planting, (b) PHU, (c) GDD for risky cells when risky pixel rate is below 0.2.**

### 3.5 Discussion

The information obtained from this study can be applied to three outcomes: 1) quantifying plant growth and environmental stress time series, which can be used to validate and

constrain crop growth models, 2) improving early in-season yield prediction, and 3) identifying areas, which have the potential risk to obtain lower yields.

NDVI time series can provide important information for crop modeling studies by providing an additional, sub-annual time series for evaluating models. NDVI residuals can serve as the observed data to evaluate simulated leaf development responses to climate stresses. In most dynamic crop models, biomass and final yield are a function of the daily predicted LAI. Understanding the LAI progression under stress and non-stress conditions is helpful to better estimate not only the annual yield but also interannual yield variation. Since LAI can be estimated from NDVI via various approaches (Cohen et al., 2003; Nguyen-Roberson et al., 2012), it is possible to adjust model predicted LAI based on NDVI from Landsat images and evaluate the accuracy of crop model performance in crop growth at different stages and under various climate stress conditions. This evaluation is especially important when exploring future climate change impacts. Crop modeling must be able to correctly reflect seasonal crop growth responses under various climate conditions (limited or oversupplied water). Validating crop growth model via information from this study can improve the reliability of model predictions under more frequent extreme weather in the future.

Results in Section 3.4.3 reflect a significant relationship between pre-silking stage NDVI residual and corn yield in the St. Joseph River Watershed. This indicates corn yield potential could be predicted in season without attaining whole life-cycle corn growth information. Although the residual-yield relationship may differ for different areas, this methodology could be applied to other regions in order to obtain their specific normal

growth curves. The corn industry can benefit from in-season yield prediction by producing better forecasts of corn prices. Since crop yield is linked with NDVI residual, which is spatially explicit when derived from satellite images, yield prediction could be conducted at the pixel level.

The advantage of a remote sensing method is the identification of crop developmental stages within 30 meter Landsat imagery, which can provide detailed patterns of spatial and temporal crop phenology variations. Local scale information about corn development stages can also be obtained. As an objective procedure, it holds potential to avoid reduce reliance on subjective, cost and labor intensive field observations. Since the spatial pattern of corn NDVI can be attained by analyzing satellite images, it is easier to accurately target areas which are suffering from stress (Figure 3.11). Therefore, proper crop management could be applied in the right place, improving cost and time efficiency.

This research could be further improved in two aspects:

- 1) The vegetation index, NDVI, used in this research has a potential to saturate when the leaf area index is high, thus limiting its ability to quantify LAI late in the growing season. This is one potential reason that no significant relationship is found between peak NDVI (high leaf area index) and crop yield. Applying other indices, such as EVI2 and MTVI2 (Liu et al., 2012) could overcome the saturation problem, and should be evaluated in future studies. Since our future focus is to improve crop growth model responses to climate stresses, and since most crop models apply LAI to represent seasonal growth, we still use NDVI in this study because of its well-established relationship with LAI.

2) Although detailed spatial information could be attained due to the fine resolution of Landsat images (30 m), the temporal coverage (16 days) is too infrequent to capture the rapid changes in biophysical processes during the early growth stages. Therefore, we have to overlay multiple years data to describe of the whole corn growth cycle in this study. Applying a fused MODIS/Landsat approach (Gao et al., 2006) could be an appropriate way to extend the temporal coverage for current mid-resolution images. Though new errors and uncertainties may still be introduced by such a fused approach due to differences in spatial and spectral band resolution, for example.

### 3.6 Conclusion

This research uses an 11 year time series of Landsat TM5 images to explore the spatial and temporal variability of corn growth in the St. Joseph River Watershed, in Indiana, Michigan and Ohio. Images during the corn growth period were first processed to remove cloud/shadow/snow pixels. Atmospheric correction was then applied to exclude the effect of atmosphere on the reflectance values. CDL data was used to extract all corn pixels in the study area. An 11 year time series of spatially-varying corn NDVI values was finally attained. The observed corn NDVI reaches its peak value ( $>0.7$ ) around the silking period, as identified using the NASS Crop Progress Data. Spatial variability in NDVI was also at its minimum ( $CV < 0.1$ ) at this time when the canopy is fully developed. The NDVI shows greater variation ( $CV > 0.2$ ) during the leaf development and senescence periods.

A normal corn growth curve was established for the region using the median values of the 11 year corn NDVI time series reflecting the whole life cycle of regional corn growth. NDVI residuals were calculated for individual image dates relative to the normal growth



curve and used to calculate pre-silking, pre-maturity and growing season discrepancy scores. Overall, the growth curve constructed using GDD on the image acquisition dates appeared to be the most robust.

The growing season average discrepancy was able to clearly identify years with above average and below average crop development. Regression analysis (Figure 3.8) indicates that grain yield is most significantly related to the pre-silking period NDVI residuals ( $p < 0.01$ ). Therefore, local stake holders can estimate in season corn yield even when only early images are available, and identify stress risk in early stages. Water stress is closely associated with NDVI residuals. At the scale of the entire image, dry weather (negative  $ws$ ) tends to result in crop growth below normal conditions (negative NDVI residuals), while plenty of rainfall reduces the risk of yield loss (positive yield loss). At this scale, no impact from excess water stress was detected. However, since corn pixels in this study are of very fine spatial resolution (30m), it is possible to identify individual pixels which have risks of yield loss due to stresses. The risky pixel rate is significantly correlated with water stress, as more corn pixels are under stress when precipitation is way below the long-term average curve. The spatial pattern of risky pixels is different between dry and wet years. Limited rainfall was found to affect most corn pixels, while the spatial extent of stress is much more limited when rainfall is plentiful or oversupplied. This difference in spatial extent is explains in part why yield limitation due to wet conditions is not detected for larger spatial scales.

This study lays a framework for using mid-resolution imagery to derive crop phenology and quantify corn responses to climate stresses. The methods derived from this study could

be applied to other areas for future research, especially climate sensitive areas, where crop growth is more easily affected by climate variability. Using remote sensing technology, corn responses to different climate stress (limited or oversupplied rainfall) were detected. Information conveyed from this research is recommended for crop modeling studies to quantify model performance under various climate conditions. A better parameterization to represent seasonal growth and annual yield under climate stresses is critical, especially to assess the impact of future climate change, where more extreme precipitation and drought are expected.

## 3.7 References

- Abendroth, LJ, Elmore RW, Boyer MJ, Marlay SK. 2011. Corn Growth and Development. Iowa State Univ. Extension Publication #PMR-1009. <https://store.extension.iastate.edu/Product/Corn-Growth-and-Development>
- Anthony L, Nguy R, Yi P, Anatoly AG, Timothy J, Arkebauer AP, Ittai H, Arnon K, Donald CR, David JB. 2014. Estimating green LAI in four crops: Potential of determining optimal spectral bands for a universal algorithm. *Agricultural and Forest Meteorology* **192**: 140–148.
- Bhattarai N, Quackenbush LJ; Dougherty M, Marzen, LJ. 2015. A simple Landsat–MODIS fusion approach for monitoring seasonal evapotranspiration at 30 m spatial resolution. *International. Journal of Remote Sensing* **36**: 115-143.
- Bernstein LS, Adler-Golden SM, Sundberg RL, Levine RY, Perkins TC, Berk A, Ratkowski AJ, Felde G, Hoke ML. 2005. Validation of the QUick Atmospheric Correction (QUAC) algorithm for VNIR-SWIR multi- and hyperspectral imagery. SPIE Proceedings, Algorithms and Technologies for Multispectral, Hyperspectral, and Ultraspectral Imagery XI. **5806**: 668-678.
- Bolton DK, Friedl MA. 2013. Forecasting crop yield using remotely sensed vegetation indices and crop phenology metrics. *Agricultural and Forest Meteorology* **173**: 74-84.
- Boryan C, Yang Z, Mueller R, Craig M. 2011. Monitoring US agriculture: the US Department of Agriculture, National Agricultural Statistics Service, Cropland Data Layer Program. *Geocarto International* **26(5)**:341-358
- Broge NH, Leblanc E. 2001. Comparing prediction power and stability of broad-band and hyperspectral vegetation indices for estimation of green leaf area index and canopy chlorophyll density. *Remote Sensing of Environment* **76**: 156–172.
- Casa R, Varella H, Buis S, Guérif M., De Solan B, Baret F. 2012. Forcing a wheat crop model with LAI data to access agronomic variables: evaluation of the impact of model and LAI uncertainties and comparison with an empirical approach. *European Journal of Agronomy* **37(1)**: 1–10.
- Chipanshi A, Zhang Y, Kouadio L, Newlands N, Davidson A, Hill H, Warren R, Qian B, Daneshfar B, Bedard F. 2015. Evaluation of the Integrated Canadian Crop Yield Forecaster (ICCYF) model for in-season prediction of crop yield across the Canadian agricultural landscape. *Agricultural and Forest Meteorology* **206**: 137-150.
- Cleveland WS. 1979. Robust Locally Weighted Regression and Smoothing Scatterplots. *Journal of the American Statistical Association* **74(368)**: 829-836.

- Cohen WB, Maieringer TK, Gower ST, Turner DP. 2003. An improved strategy for regression of biophysical variables and Landsat ETM+data. *Remote Sensing Environment* **84**: 561-571.
- Crippen RE. 1990. Calculating the vegetation index faster. *Remote Sensing of Environment* **34**:71-73.
- De Wit AJW, Van Diepen CA. 2007. Crop model data assimilation with the Ensemble Kalman filter for improving regional crop yield forecasts. *Agricultural and Forest Meteorology* **146**: 38–56
- Fang H, Liang S, Hoogenboom G. 2001. Integration of MODIS LAI and vegetation index products with the CSM-CERES-Maize model for corn yield estimation, *International Journal of Remote Sensing* **32(4)**: 1039-1065.
- Gao F, Masek J, Schwaller M, Hall F. 2006. On the blending of the Landsat and MODIS surface reflectance: Predicting Daily Landsat surface reflectance. *IEEE Transactions on Geoscience and Remote Sensing* **44**: 2207-2218.
- Ge T, Sui F, Bai L. 2012. Effects of water stress on growth, biomass partitioning, and water-use efficiency in summer maize (*Zea mays* L.) throughout the growth cycle. *Acta Physiologiae Plantarum* **4(3)**:1043-1053.
- Gitelson, AA, Vina A, Arkebauer TJ, Rundquist DC, Keydan GP, Leavitt B. 2003. Remote estimation of leaf area index and green leaf biomass in maize canopies. *Geophysical Research Letter* **30 (5)**: 1248.
- Hatfield JL, Prueger JH. 2010. Value of using different vegetative indices to quantify agricultural crop characteristics at different growth stages under varying management practices. *Remote Sensing* **2**:562-578.
- Huang N, Niu Z, Zhan Y, Xu S, Tappert MC, Wu C, Huang W, Gao S, Hou X, Cai D. 2012. Relationships between soil respiration and photosynthesis-related spectral vegetation indices in two cropland ecosystems. *Agricultural and Forest Meteorology* **160**: 80-89.
- Ines AVM, Das NN, Hansen JW, Njoku EG. 2013. Assimilation of remotely sensed soil moisture and vegetation with a crop simulation model for maize yield prediction. *Remote Sensing Environment* **138**: 149–164.
- Johnson DM. 2014. An assessment of pre-and within-season remotely sensed variables for forecasting corn and soybean yields in the United States. *Remote Sensing Environment* **141**: 116-128.
- Kang S, Liang Z, Hu W, Zhang J. 1998. Water use efficiency of controlled alternate irrigation on root-divided maize plants. *Agricultural Water Management*. **38(1)**:69-76.

- Kebede H, Sui RX, Fisher DK. 2014. Corn yield response to reduced water use at different growth stages. *Agricultural Sciences* **5(13)**: 1305-1315.
- Kiniry JR, Major DJ, Izaurrealde RC, Williams JR, Gassman PW, Morrison M, Bergentine R, Zentner RP. 1995. EPIC model parameters for cereal, oilseed, and forage crops in the northern Great Plains region. *Canadian Journal of Plant Science* **75**: 679-688.
- Knipling EB 1970. Physical and physiological basis for the reflectance of visible and near-infrared radiation from vegetation. *Remote Sensing Environment* **1**:155-159.
- Llano MP, Vargas W, Naumann G. 2012. Climate variability in areas of the world with high production of soybeans and corn: its relationship to crop yields. *Meteorological Applications* **19(4)**: 385-396.
- Liu JG, Pattey E, Jegou G. 2012. Assessment of vegetation indices for regional crop green LAI estimation from Landsat images over multiple growing seasons. *Remote Sensing of Environment* **123**: 347-358.
- Ma BL, Morrison MH, Dwyer LM. 1996. Canopy light reflectance and field greenness to assess nitrogen fertilization and yield of corn. *Agronomy Journal* **88**: 915-920.
- Martin KL, Girma K, Freeman KW, Teal RK, Tubana B, Arnall DB, Chung B, Walsh O, Solie JB, Stone ML, Raun WR. 2007. Expression of variability in corn as influenced by growth stage using optical sensor measurements. *Agronomy Journal* **99**:384-389.
- Masek JG, Vermote EF, Saleous N, Wolfe R, Hall EF, Huemmrich F, Gao F, Kutler J, Lim TK. 2006. A Landsat surface reflectance data set for North America, 1990-2000. *Geoscience and Remote Sensing Letters*. **3(1)**: 68-72.
- Mishra V, Cherkauer KA. 2010. Retrospective droughts in the crop growing season: Implications to corn and soybean yield in the Midwestern United States. *Agricultural and Forest Meteorology* **150**: 1030-1045.
- Mkhabela MS, Bullock P, Raj S, Wang S, Yang Y. 2011. Crop yield forecasting on the Canadian prairies using MODIS NDVI data. *Agricultural and Forest Meteorology* **151(3)**: 385–393.
- Neild RE, Newman JE. 1990. Growing Season Characteristics and Requirements in the Corn Belt. National Corn Handbook-40. Retrieved from: <http://www.extension.purdue.edu/extmedia/nch/nch-40.html>
- Neitsch SL, Arnold JF, Kiniry JR, Williams JR. 2009. Soil and Water Assessment Tool: Theoretical Documentation, version 2009.
- Nguy-Robertson A, Gitelson A, Peng Y, Vina A, Arkebauer T, Rundquist D. 2012. Green Leaf Area Index Estimation in Maize and Soybean: Combining Vegetation Indices to Achieve Maximal Sensitivity. *Agronomy Journal* **104**:1336-1347.

- Nielsen RL. 2008. Grain fill stages in corn. Corny News Network, Purdue University. Retrieved from <http://www.agry.purdue.edu/ext/corn/news/timeless/grainfill.html>.
- Rasmussen MS. 1992. Assessment of millet yields and production in northern Burkina Faso using integrated NDVI from the AVHRR. *International Journal of Remote Sensing* **13(18)**: 3431–3442
- Sakamoto T, Wardlow BD, Gitelson AA. 2011. Detecting spatiotemporal changes of corn developmental stages in the US Corn Belt using MODIS WDRVI data. *IEEE Transactions on Geoscience and Remote Sensing* **49(6)**: 1926-1936.
- Saseendran SA, Trout TJ, Ahuja LR, Ma L, McMaster GS, Nielsen DC, Andales AA, Chavez JL, Ham J. 2015. Quantifying crop water stress factors from soil water measurements in a limited irrigation experiment. *Agricultural Systems* **137**: 191-205.
- Shanahan JF, Holland KH, Schepers JS, Francis DD, Schlemmer MR, Caldwell R. 2003. Use of a crop canopy reflectance sensor to assess corn leaf chlorophyll content. *ASA Special Publication* **66**:135-150.
- Shanahan JF, Schepers JS, Francis DD, Varvel GE, Wilhelm W, Tringe JM, Schlemmer MR, Major DJ. 2001. Use of remote-sensing imagery to estimate corn grain yield. *Agronomy Journal* **93**: 583-589.
- Solari F, Shanahan J, Ferguson RB, Schepers JS, Gitelson AA. 2008. Active sensor reflectance measurements fo corn nitrogen status and yield potential. *Agronomy Journal* **100**: 571-579.
- Srivastave SK, Jayaraman V, Nageswara PP, Manikiam B, Chandrasekehar G. 1997. Interlinkages of NOAA/AVHRR derived integrated NDVI to seasonal precipitation and transpiration in dryland tropics. *International Journal of Remote Sensing* **18**:2931-2952.
- Teal RK, Tubana B, Girma K, Freeman KW, Arnall DB, Walsh O, Raun WR. 2006. In-Season Prediction of Corn Grain Yield Potential Using Normalized Difference Vegetation Index. *Agronomy Journal* **98**:1488-1494.
- Thompson LM. 1988. Effects of change in climate and weather variability on the yields of corn and soybeans. *Journal of Production Agriculture* **1(1)**: 20-27.
- USDA-NASS. NASS-National Agricultural Statistics Servies. 2012 Census of Agriculture. 2012, Available at <http://www.agcensus.usda.gov/Publications/>
- USDA-NASS. NASS-National Agricultural Statistics Servies. USDA-NASS, Washington, DC, 2010, Available at <http://www.nass.usda.gov/>

- Yang Y, Timlin DJ, Fleisher DH, Kim SH, Quebedeaux B, Reddy VR. 2009. Simulating leaf area of corn plants at contrasting water status. *Agricultural and Forest Meteorology* **149**:1161-1167.
- You X, Meng J, Zhang M, Dong T. 2013. Remote Sensing Based Detection of Crop Phenology for Agricultural Zones in China Using a New Threshold Method. *Remote Sensing* (**5**): 3190-3211.
- Zhu Z, Woodcock CE. 2012. Object-based cloud and cloud shadow detection in Landsat imagery. *Remote Sensing of Environment* **118**: 83-94.

## CHAPTER 4. IMPROVED SIMULATION OF ANNUAL CROP SENSITIVITY TO CLIMATE VARIABILITY IN THE EASTERN CORN BELT

### 4.1 Abstract

The representation of soil moisture is important when applying modeling methods to the study of climate variability and change on crop yields. When direct comparison is impossible due to scarcity of observed soil moisture datasets (a common problem), modelers could evaluate soil moisture indirectly via examining model performance in annual crop yield and seasonal growth information, because accurate prediction of seasonal development and annual yield reflects both ET and moisture required for vegetative growth. In this study, a multi-variable calibration strategy was employed in Soil and Water Assessment Tool (SWAT) simulation to regulate streamflow and crop growth simultaneously in St. Joseph River watershed, Eastern Corn Belt. Model representations of seasonal crop growth are evaluated by comparing satellite imagery-based time series LAI with SWAT output. Compared to streamflow only calibration strategy, the multi-variable calibration substantially improves crop seasonal growth and interannual crop yield variability, without hampering model performance in streamflow. Though soil moisture is not well represented by either methods, multi-variable calibration reduces the uncertainty in moisture prediction. Model performance in identifying climate sensitive cropland (CSC) is also compared between two different calibration approaches. Streamflow only calibration fails to identify CSC area in the study region due to simulated mean yield is too



high relative to actual yield. Multi-variable calibration strategy identified 146.79 km<sup>2</sup> CSC area with high possibility (>20%) to meet low yield threshold (6.43 ton/ha), occupying 5.14% of the basin area.

## 4.2 Introduction

Soil moisture dynamics, which serve as a source of long-term memory of past precipitation events (Entekhabi et al., 1996), are affected by climate variability. Soil moisture storage evolves on timescales of weeks to months, reflecting wetness/dryness longer than the atmosphere, and providing water for plants to grow (Koster and Suarez, 2001). Corn growth has a complicated relationship to soil moisture, both when limited and oversupplied, it introduces stress to corn development (Mishra and Cherkauer, 2010; Ren et al., 2014). Over shorter spatial and temporal scales, both limited and oversupplied soil moisture can be harmful for crop growth. To reflect crop responses to climate variability, ecohydrological modeling is often employed (Adejuwon, 2005; Steduto et al., 2009; Tao et al., 2009). When using modeling methods to evaluate crop sensitivities to climate variability that results in oversupplied or limited water, soil moisture needs to be well represented. If not, the interannual yield variability may not be well captured by the model (Wang et al., 2016). When extending model implementation under more extreme, future climate conditions, the model may have trouble accurately capturing crop responses under such circumstance.

Crop growth interacts with the surface water budget mainly through evapotranspiration. In a model application, incorrect prediction of daily crop growth, reflected for example by leaf growth, may affect predicted ET, and in turn affect the predicted water budget, leading

to incorrect representation of streamflow and soil moisture. Simulated streamflow is often regulated by comparing to observed data, provided by wide spread stations with well-established instrumentation. However, evaluating soil moisture at the watershed level is not straightforward due to data scarcity, for example, insufficient monitoring locations (Reichle et al., 2004; Draper and Reichle, 2015), or scale issues, for example, point observations are difficult to extend to the watershed level (Chen et al., 2014; Su and Ryu, 2015). Calibration of complex hydrologic models that contain multiple state variables through comparison to only one observed variable can result in “pseudo-optimal” solutions. (Rajib and Merwade, 2015). This is because the calibrated variable is usually associated with multiple processes, and in turn associated with many parameters controlling those process. When trying to adjust numerous parameters with limited observations, a good agreement between observed and simulated variable may attained by totally different parameter sets, which is known as “Equifinality” (Beven, 2006). A common example of “Equifinality” in hydrological modeling is similar streamflow simulations with very different simulated soil moisture states (Rajib and Merwade, 2015; Silverstro et al., 2015). Parameter set which fails to capture the soil moisture states is thought as “pseudo-optimal”. Though it has good agreement in streamflow, it does not correctly reflect hydrological processes including runoff generation, infiltration, or evaptranspiration. Then, calibration based on a single output variable or limited observation becomes an ill-posed inverse (Jakeman and Hornberger, 1993).

An indirect way to evaluate soil moisture storage is to compare observed and modeled crop yield (Srinivasan, et al., 2010). The idea is that crop yield reflects both ET and moisture

required for vegetative growth. Therefore, it could be used as an alternative method to evaluate the spatial variability in available soil moisture, instead of direct comparison with site recorded data. However, reasonable predictions of annual yield can be achieved by simply adjusting the parameter that controls the ratio of above ground biomass to final yield, which has no impact on simulated soil moisture. Therefore, unreasonable biomass accumulation may result in a reasonable yield through the choice of an inappropriate parameter set. Such a model may consistently over or under estimate biomass, or incorrectly reflect crop responses under various climate conditions (Cavero et al., 2000). Under such situations, the soil moisture associated with vegetative growth could be incorrect.

To overcome the possible equifinality on annual yield simulation and improve surface water budget estimation, seasonal crop growth information can be included in the model calibration. Satellite remote sensing is a potential source for crop seasonal growth information at regional scales. Many previous studies have suggested merging crop model output with satellite imagery to derive seasonal crop growth information (Sakamoto et al., 2011, Kotera et al., 2014). The most widely derived seasonal growth information used in modeling is leaf area index. For example, Zhang and Wegehenkel (2006) integrated MODIS LAI data into a simple grid-based soil water balance model, resulting in good agreement of soil moisture with in-situ measurements. For another example, Boegh et al. (2004) adjusted LAI simulated by the Daisy/MIKE SHE model based on remotely sensed LAI from the Landsat TM and SPOT satellites, which improved the prediction of crop yield and evapotranspiration. Therefore, it is possible to capture regional crop growth

dynamics by extracting LAI time series from multi-year remote sensing images, and integrating this information into crop modeling studies.

A model that represents crop responses to climate variability well can help to identify areas that have low yield or high interannual yield variability. Those areas are more sensitive to climate than other cropland in the same region. Since future climate change is predicted to introduce more growth stresses for crops in Midwest USA due to hotter summers and wetter springs (Christensen et al., 2007; Cherkauer and Sinha, 2010), these sensitive croplands may not continue to be suitable to for large-scale corn production due to the potential of yield loss under extreme climate condition or constant lower yield relative to other croplands. For example, these climate sensitive croplands (CSC) could be replaced by other less climate sensitive plants, such as cellulose biofuel crops to meet an increasing demand for biofuels. Some biofuel crops have higher land and water use efficiencies than traditional crops (VanLoocke et al., 2012; Heaton, et al., 2008), so that less land and water is needed for perennial grasses to match ethanol demands than corn. Secondly, compared to cash crops, cellulose biofuel crops may require less management and financial inputs, such as tillage, fertilization, and herbicide/ pesticide application (Hill et al., 2006), which has the potential to reduce non-point source pollution from management practices in cropland. Lastly, biofuel crops have higher biomass productivity due to their high adaptability to different soils and climates than corn, following the initial establishment period (Heaton, et al., 2004; Dohleman and Long, 2009). Therefore, clearly identifying CSC areas, and replacing corn with biofuel crops in those areas might be a sustainable

management practice to strike a balance between both food/fuel provision and environmental integrity, without jeopardizing food security.

Since the correct representation of crop growth under limited or oversupplied water conditions could improve surface water budget simulation and identification of CSC areas, it is worth constraining both crop growth and streamflow while doing hydrological modeling at the watershed scale. In this study, we evaluate a calibration approach to constrain both water and crop growth in order to represent water-plant relations under various climate conditions using the Soil and Water Assessment Tool (SWAT) (Arnold, et al., 1998). The main objective is to improve the simulation of annual crop sensitivity to climate variability by simultaneously constraining model performance in multiple variables (streamflow, seasonal crop development, and interannual crop yield) in the St. Joseph River watershed in the Eastern Corn Belt.

This objective is realized by an improved parameterization in regional leaf area growth from satellite images and a multi-variable calibration strategy to regulate both water and crop growth. Soil moisture is evaluated by comparing observed data from point locations with simulated HRU values. We will also examine the effect of different calibration strategies (streamflow calibration vs. multi-variable calibration) on representation of seasonal soil moisture. Finally, the spatial distribution of mean annual yield and inter-annual yield variability across the study area is investigated to locate climate sensitive cropland (CSC), which could be considered as areas to be replaced by other crops less sensitive to climate variability.

## 4.3 Method

### 4.3.1 Study area

The St. Joseph River Watershed (Figure 4.1) is located in the Eastern Corn Belt, draining 2,821 km<sup>2</sup> across northeastern Indiana, northwestern Ohio and southeastern Michigan. Agricultural land including row crop and pasture land, occupies 67% of the watershed area, and is the largest land use/cover type based on the USDA National Agricultural Statistics Service (NASS) Cropland Data Layer (CDL) for 2010. Other land use types in this watershed are forest (13.0%), urban areas (12.5%) and wetland (9.3%). There are seven precipitation gauges and three temperature gauges operated by National Oceanic and atmospheric Administration-National Climate Data Center (NOAA-NCDC) and National Soil Erosion Research Lab (NSERL) in this area that record daily precipitation, maximum and minimum air temperature from 1990. The watershed has three U.S. Geological Survey (USGS) streamflow measurement stations with long-term daily streamflow records. The National Soil Erosion Research Lab (NSERL) installed thirteen Stevens Hydra Probe II soil sensors in the Cedar Creek watershed, which is a tributary of the St. Joseph River. Each location records volumetric soil moisture data at multiple depths (51 mm, 203 mm, 406 mm and 610 mm) with beginning date varied from June, 2005 to Aug, 2013.

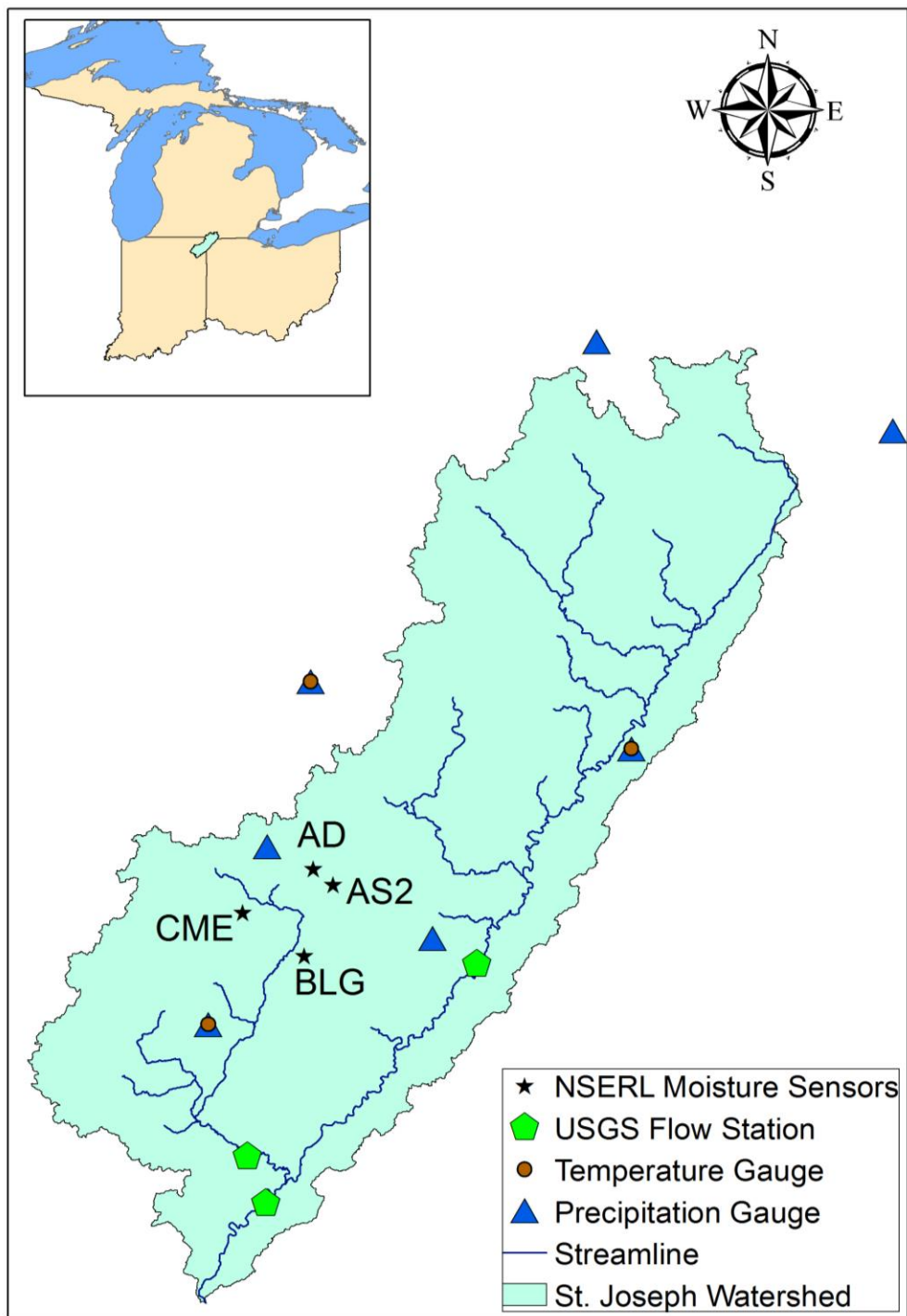


**Figure 4.1. Geographic location of St. Joseph River watershed and the distribution of observational stations used for the model simulation.**

### 4.3.2 Data Processing

#### 4.3.2.1 Soil moisture data preprocessing

To evaluate model performance in capturing soil moisture sensitivity to climate variability, multiple years of observed data are needed. Therefore, we chose four soil moisture sensors (AS2, BLG, AD and CME), which recorded at least four years continuous data. Sensor locations are shown in Figure 4.1. SWAT simulates soil moisture based on each soil layer defined in the SSURGO soil database, assuming soil moisture is evenly distributed inside each layer. The model begins to simulate saturated flow when the water content of a soil layer is over the field capacity for the layer. Saturated flow can percolate to an underlying layer or become lateral flow as long as soil temperature is above 0 °C. Since simulated soil moisture is homogeneous for each layer, if one layer, as defined in the model set-up has two sensors installed so that two measurements are provided when only one simulated value is available for comparison, we use the layer average (both sensor position and layer depth) observed data for analysis. SWAT also adds a 10 mm surface soil layer to the first layer from SSURGO database, which interacts with surface runoff. This topmost 10 mm soil has exactly the same properties like the first layer soil from SSURGO. However, since the depth is usually much less than the depth of SSURGO first layer, it could be neglected when computing layers based soil moisture. Take the first layer of AS2 (Figure 4.2) for example, layer average observed SM is computed based on Eq. (4.1).

$$SM_{layer\_obs} = (SM_{sensor1\_obs} * d1 + SM_{sensor2\_obs} * d2) / (d1 + d2) \quad (4.1)$$

Where  $SM_{sensor1\_obs}$  is the soil moisture data recorded by the sensor at 51 mm depth,  $SM_{sensor2\_obs}$  is the soil moisture data recorded by sensor at 203 mm;  $d_1$  is the depth from



soil surface to the middle position of two soil sensors (denoted by dash line), which is 127 mm in this case,  $d_2$  is the depth from the middle position of the two soil sensors to the bottom depth of the first layer, which is 103 mm; and  $d_1+d_2$  is the depth for the first layer, 230 mm. Since 230 mm is much greater than 10 mm, simulated soil moisture from topmost layer can be neglected when computing  $SM_{layer\_obs}$

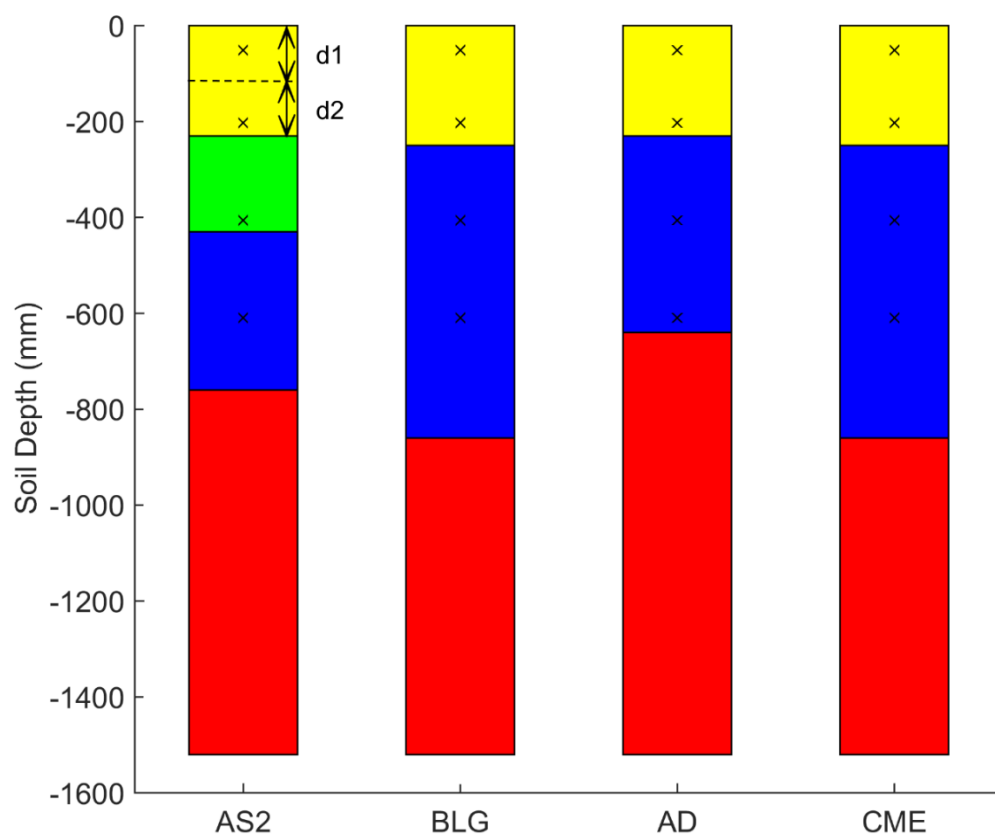


**Figure 4.2** NSERL soil moisture sensor position (denoted by 'x') and soil layer depth information from SSURGO database (each identified layer is given a unique color).

#### 4.3.2.2 Regional Leaf Area development curve

Regional corn leaf area development information was retrieved from 11 years (2000-2010) Landsat TM imagery (path 21, row 31) in the study area. All images during the corn growing season have been processed to remove cloud, snow and shadow pixels and were atmospheric corrected. Eleven years of CDL data was used to identify corn pixels in the study area. Several other edge and seasonality filters were also employed to further refine the selection of corn only pixels, rather than pixels that include grass waterways, for example. All 11 years data were merged based on potential heat units (PHU) to visualize a typical annual NDVI cycle based on multiple years of data. Detailed information on how corn NDVI was obtained can be found in Chapter 3.

Since the SWAT model computes leaf area growth based on leaf area index (LAI), NDVI values were converted to LAI based on a published empirical equation (Wiegand et al., 1990) for the Midwestern USA.

$$LAI = 0.1270 * \exp(4.1260 * NDVI) \quad (4.2)$$

SWAT simulates corn LAI dynamics in this way: Corn LAI increases rapidly in the early growing season, and then stays stable at its peak value before natural senescence. LAI drops from natural senescence point until physiological maturity. Parameters controlling the growth curve are listed in Table 4.1. The parameters  $fr_{PHU1}$ ,  $fr_{PHU2}$ ,  $fr_{LAI1}$  and  $fr_{LAI2}$  control the LAI rising limb,  $LAI_{mx}$  controls the peak LAI value,  $DLAI$  and  $PHU_{mat}$  control the senescence time and the slope of falling limb. By comparing the NDVI derived LAI with default SWAT potential LAI curve (Figure 4.3), we found the general development

shape is correct, but inconsistencies still exist between them. Peak LAI was overestimated, natural senescence arrives too early in the year. Therefore, the default LAI growth curve needs to be adjusted to better represent local conditions. The adjusted potential LAI growth curve (Figure 4.3), is more regionally specific, and consistent with observed data obtained from Landsat images. Updated SWAT parameters are shown in Table 4.1.

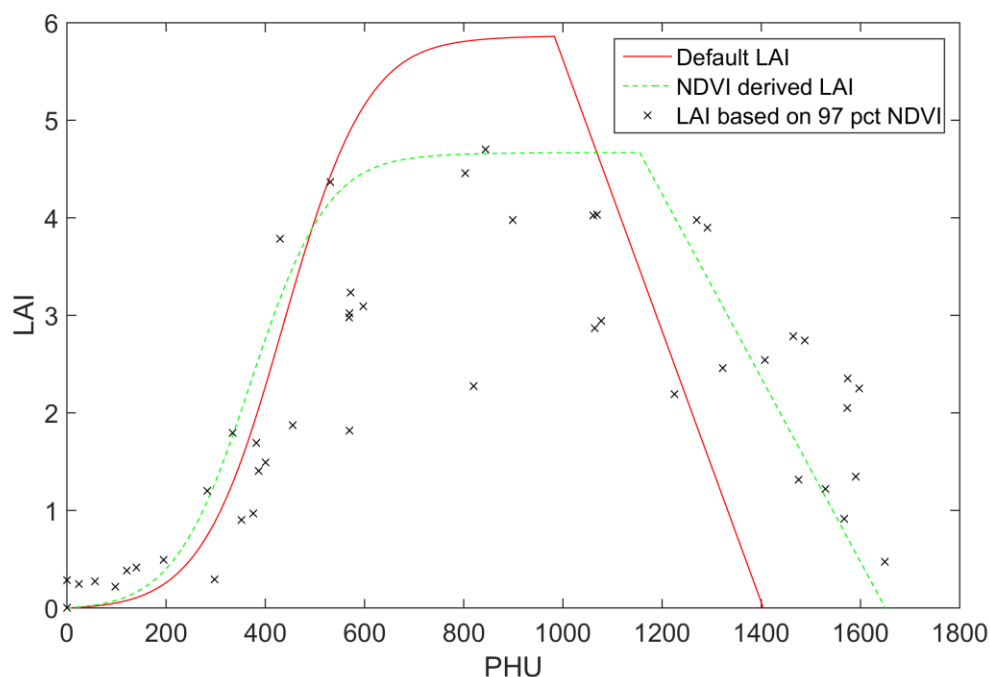


**Figure 4.3** The default SWAT potential LAI development curve and NDVI derived LAI from Landsat images (see Chapter 3 for details). The default curve is adjusted to better represent NDVI derived LAI.

**Table 4.1** Regional NDVI derived LAI versus default LAI development parameters

	$fr_{PHU,1}$	$fr_{LAI,1}$	$fr_{PHU,2}$	$fr_{LAI,2}$	$LAI_{mx}$	$PHU_{mat}$	$DLAI$
<b>Regional Parameters</b>	0.121	0.083	0.364	0.938	4.8	1650	0.68
<b>Default Parameters</b>	0.150	0.050	0.500	0.950	6.0	1400	0.70

### 4.3.3 Multi-variable calibration

Model implementation and initial parameters were based on research from Her and Chaubey (2015). They divided St. Joseph River watershed into 39 subbasins, each with an area of 5,000 ha as the stream initiation threshold area. Subbasins were then further divided into 498 hydrologic response units (HRUs) with threshold area proportions of 5% and 10% for land cover and soils, respectively. The initial calibration provided by Her and Chaubey (2015) focused on daily streamflow at multiple gauging stations (USGS 04180500 at St. Joseph River, USGS 04180000 at Cedar Creek, USGS 04178000 at Middle St. Joseph River), without consideration of interannual crop yield variation and seasonal crop growth dynamics. We will refer to this as the streamflow-only calibration. For the streamflow-only calibration, 34 parameters were chosen based on prior knowledge of the SWAT model. Most of these are hydrological parameters, for example, Alpha\_b (baseflow recession factor), ESCO (Soil evaporation compensation factor), OV\_n (Manning's n for overland flow), and CH\_NII (Manning's n for the main channel). A few of their selected parameters are related to both hydrology and water quality, such as RSDIN (Initial residue cover), and USLE\_K (USLE K factor). In order to better investigate the synergies between crop growth and the water cycle, biophysical and crop stress parameters (Chapter 2) were added to the calibration, and seasonal LAI (derived from NDVI in Chapter 3 via Eq. 4.2) and detrended annual yield were included in the objective functions. Detrending used the best fit least squares regression method of Goldblum (2009) to remove crop yield trends caused by improvements in genetics and management over time.

A multi-algorithm, genetically adaptive multi-variable (AMALGAM) method was employed for model calibration (Vrugt and Robinson, 2007). Model parameters were auto calibrated by AMALGAM to ensure the capturing of streamflow, seasonal crop growth and interannual crop yield from 2000 to 2010, simultaneously. Model performance was further validated from 1995 to 2000. Daily streamflow at the watershed outlet (USGS 04180500) was used as measured discharge. Nash-Sutcliffe (1970) efficiency was used to evaluate daily streamflow performance. Seasonal crop growth information is attained from an eleven-year (2000-2010) time series of watershed median LAI from Landsat images, which is used to evaluate model performance in seasonal crop growth. Annual corn yield at the watershed scale was aggregated from the USDA National Agriculture Statistic Service (NASS) county level crop yield (Srinivasan et al., 2010) based on a weighted average to reflect interannual crop yield variability. The d-statistic (Willmott, 1982), which reflects the degree to which the simulated variation represents the measured variation was employed as an indicator of model performance in seasonal LAI growth and inter annual crop yield.

#### 4.3.4 Yield adjustment

Since the soil survey is conducted at the county level and over the course of many years, the same soil type may be assigned a different soil series name in adjacent counties, which means the mapping of physical properties to what is really the same soil across the political boundary can result in artificial differences. This boundary or edge-matching issue (Luo et al., 2012) can cause trouble when simulating crop yields at fine spatial

scales. Soil property information (Figure 4.4) highlights a strong difference between counties within the St Joseph River watershed.

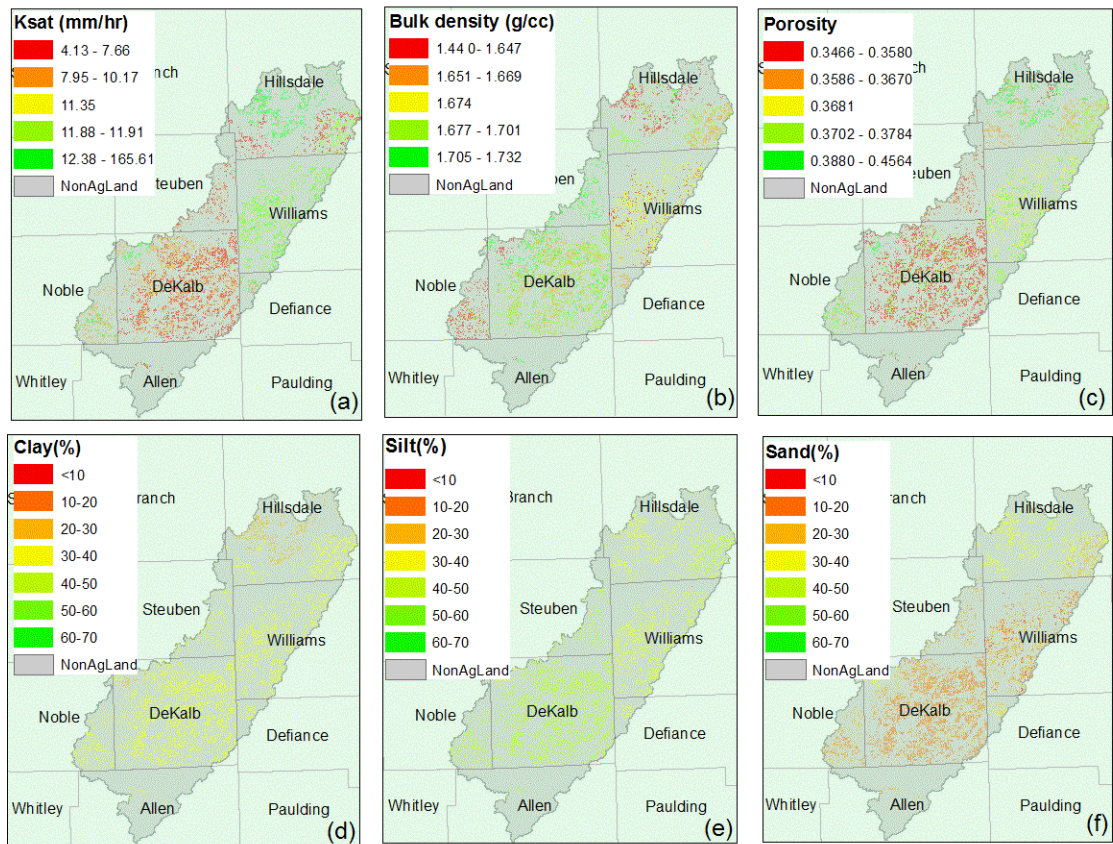


**Figure 4.4 Soil properties of corn HRUs in St. Joseph River watershed. a) soil saturated conductivity; b) bulk density; c) porosity; d) clay content; e) silt content; and f) sand content. All experience significant differences across county boundaries.**

If the inconsistent soil properties are used by the model, simulated yield may also have “boundary issues”. To overcome this inconsistency, we adjusted HRU (bias-corrected) simulated yield based on county level crop yield using Eq. 4.3:

$$Y_{adj\_HRU,i} = Y_{sim\_HRU,i} + (Y_{obs\_county,i} - Y_{sim\_county,i}) \quad (4.3)$$

$Y_{sim\_HRU,i}$  is the  $i$ th largest simulated annual corn yield at HRU level in 20 years period, ton/ha;  $Y_{obs\_county,i}$  is the  $i$ th largest county annual yield provided by NASS, unit converted from bu/acre to ton/ha using a moisture content of 15.5% (Srivansan, et al., 2010),  $Y_{sim\_county,i}$  is the  $i$ th largest county level simulated yield based on the average of  $Y_{sim\_HRU,i}$  inside each county, ton/ha;  $Y_{adj\_HRU,i}$  is the HRU level yield after adjustment, ton/ha.  $Y_{sim\_HRU,i}$  is shifted up or down based on the difference between observed and simulated county yield, making  $Y_{adj\_HRU,i}$  more realistic, solving the inconsistency in yield distribution across counties.

Eq. 4.3 is only used to bias-correct yield inconsistency for the multi-variable calibration. If applied to the streamflow-only calibration, the major simulation bias in mean yield between the two calibration strategies will be lost, therefore, yield for the streamflow-only calibration was adjusted relative to the bias correction for the multi-variable calibration simulation using Eq. 4.4:

$$Y_{adj\_HRU}^{so} = Y_{adj\_HRU}^{mv} - (Y_{sim\_HRU}^{mv} - Y_{sim\_HRU}^{so}) \quad (4.4)$$

$Y_{sim\_HRU}^{mv}$  and  $Y_{sim\_HRU}^{so}$  indicates simulated yield for multi-variable calibration and streamflow-only calibration strategy before any bias-correction.  $Y_{adj\_HRU}^{mv}$  is the bias-corrected yield value for multi-variable calibration after applying Eq.4.3.  $Y_{adj\_HRU}^{so}$  is the adjusted yield for streamflow only calibration.

## 4.4 Results and Discussions

### 4.4.1 Model performance in calibration/validation

Model performance in representing streamflow after multi-variable calibration (streamflow, LAI progression and crop yield) is shown in Figure 4.5, both log (Figure 4.5(a)) and linear (Figure 4.5(b)) scales are used to visualize model performance under low and high flow conditions, respectively. The model did a good job capturing both low and high flow conditions, with a daily Nash-Sutcliffe coefficient (NSC) of 0.82. The d-statistic for LAI is 0.83, and for crop yield is 0.76. After calibration, model performance was validated between 1995 through 1999. Daily Nash-Sutcliffe coefficient of streamflow was 0.86, and the d-statistic for annual crop yield was 0.64. Due to the data scarcity in LAI, we do not have another separate period to validate LAI. Our model performance in daily streamflow was similar to that of Her and Chaubey (2015), with NSCs of 0.82 and 0.86 for the calibration and validation periods, respectively. Figure 4.6 depicts model performance in seasonal LAI growth and interannual yield variability after calibration. Model representation of seasonal growth and annual yield is improved substantially. Simulated LAI was decreased and is more reasonable when compared with Landsat based LAI observations. Mean crop yield was also decreased and while inter annual increased when compared with simulations from the streamflow only calibration. Therefore, both seasonal crop growth and interannual yield variability was well captured via multi-variable calibration. Most parameters were the same as those used by Her and Chaubey (2015), but parameters that differ from their study, mostly biophysical and stress parameters, are summarized in Table 4.2.



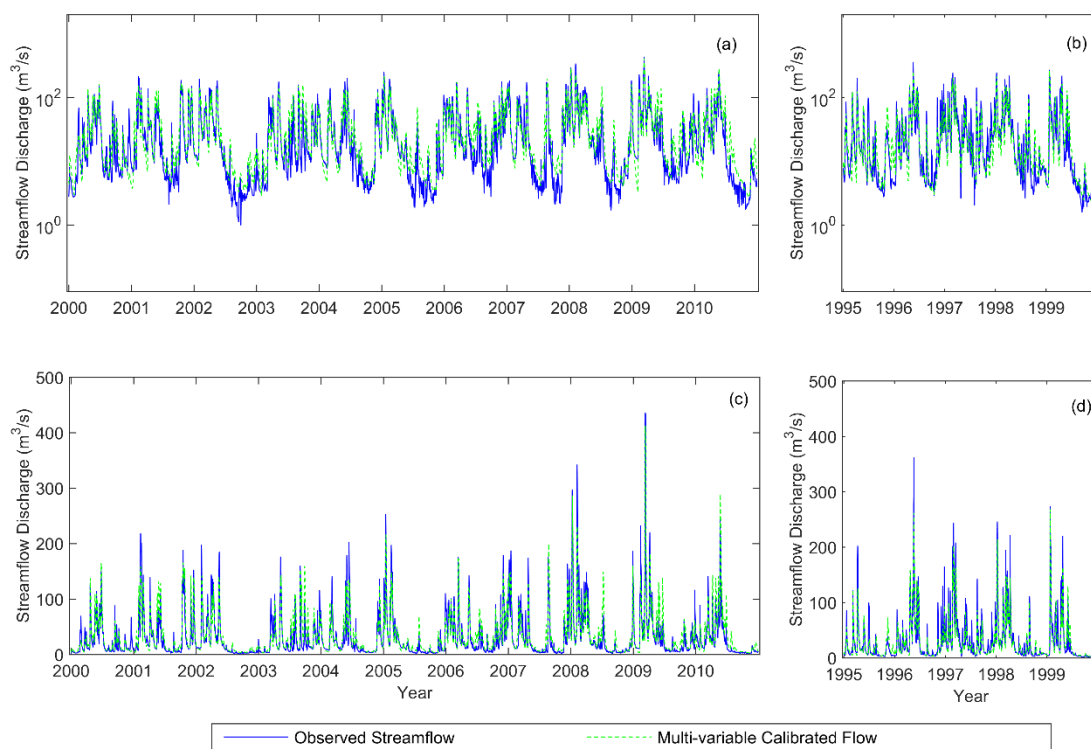


**Figure 4.5 Model performance in daily streamflow for the St. Joseph River near Fort Wayne, IN (USGS 04180500) during the a) calibration period with log scale, b) validation period with log scale, c) calibration period with linear scale; d) validation period with linear scale.**

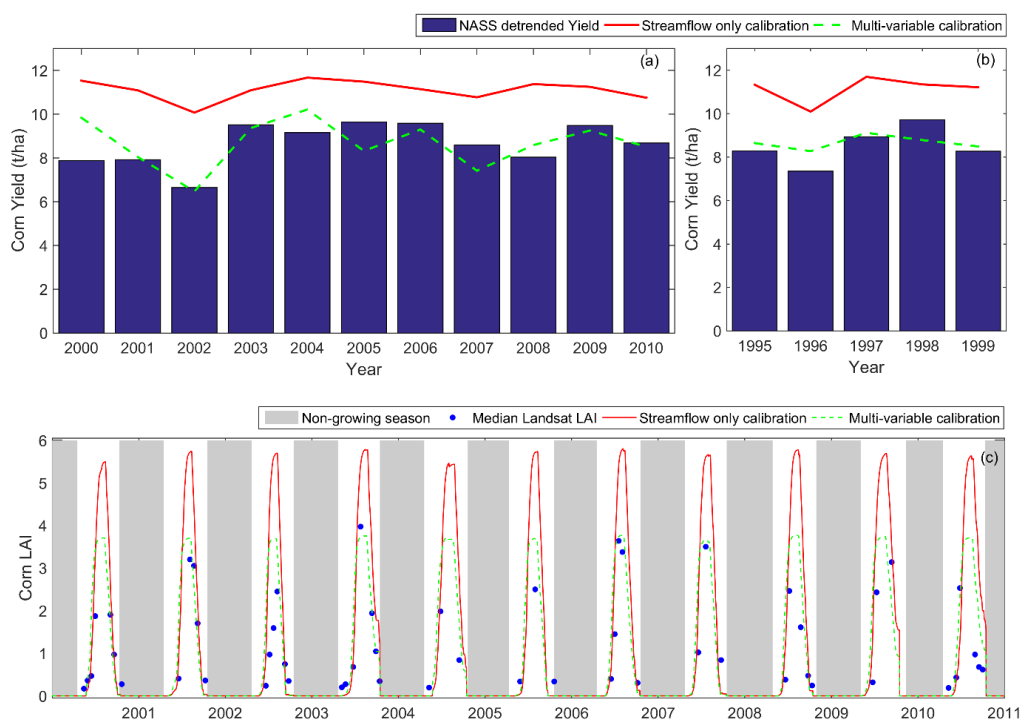


**Figure 4.6 Model performance in simulation of watershed average annual yield a) 2000-2010; b) 1995-1999; and c) corn leaf area index (LAI), 2000-2010.**

**Table 4.2 Parameter calibration values for streamflow, seasonal LAI and annual corn yield for parameters that differed from those used by Her and Chaubey (2015)**

Parameter	Description	Calibrated	Range
CN	Curve number (SF) <sup>a</sup>	-0.245	[-0.25, 0.25]
b1	Aeration stress S-shape transformation parameter 1 <sup>b</sup>	8.1664	[-2.9, 8.7]
b1-b2	Aeration stress S-shape transformation parameter 2	-3.0662	[-9.21, -2.18]
c1	Drought stress S-shape transformation parameter 1	1.835	[-0.4, 8.0]
c1-c2	Drought stress S-shape transformation parameter 2	-3.8133	[-9.21, -2.18]
RUE	Radiation-use efficiency ((kg/ha)/(MJ/m <sup>2</sup> ))	32.00	[32.00, 41.00]
BLAI	Maximum potential leaf area index	4.00	[4.00, 6.00]
HI <sub>opt</sub>	Harvest Index for optimal growing conditions	0.4823	[0.45, 0.55]
HI <sub>min</sub>	Harvest Index under highly stressed growing conditions	0.2901	[0.10, 0.35]

<sup>a</sup> Scale factor (SF) proportionally increases or decreases values of parameters

<sup>b</sup> Detailed information about stress parameters can be found in Wang et al., 2016.

#### 4.4.2 Parameter sensitivity to streamflow, LAI and interannual yield

In this section, we evaluate parameter sensitivity to calibration with all three objectives (streamflow, annual yield and seasonal LAI). The purpose for this analysis is to identify the relative importance of biophysical parameters in controlling model performance in both crop growth and water. Here we explore the variability of the parameter range in the last generation of the AMALGAM optimization routine, as the distribution of parameters in the last generation is indicative of model sensitivity to those parameters. A narrow range of final parameter values means that parameter is closely distributed in its parameter space, and that the model is sensitive to the parameter with respect to the objective function. A wide range in parameter values indicates that the model is less sensitive to the selected parameter, and therefore the variance of the final objective function is not highly dependent on the value of that parameter. The variability is quantified using the inverse of the coefficient of variation (CV) of the parameter values to represent the parameter sensitivity. This method allows for the direct comparison between parameter variations even when parameters have very different ranges and units.

Figure 4.7 ranks the sensitivity of the nine parameters used in multi-variable calibration. The model experiences higher sensitivity to the biophysical parameters BLAI,  $HI_{opt}$ , c1-c2, and RUE than to the other parameters. These parameters are critical in regulating seasonal crop growth (c1-c2, BLAI, RUE) and annual yield ( $HI_{opt}$ ), so it is not surprising that they have higher ranks. CN is the least sensitive parameter in the multi-variable calibration, indicating crop growth is not sensitive to CN. Although CN is the fifth sensitive parameter for the streamflow only calibration (other four are Alpha\_b, ESCO, OV\_N and CH\_NII),

all other hydrological parameters were adopted from the streamflow only calibration of Her and Chaubey (2015), and used as fixed values for our calibration. It was assumed that changing CN alone in the multi-variable calibration would significantly affect streamflow performance, however, it has been shown that it did not.

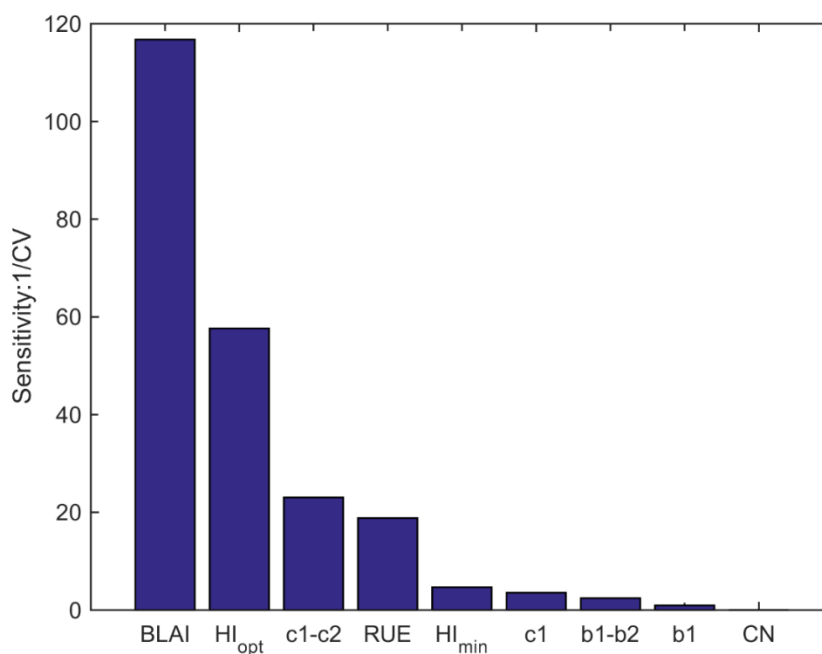


**Figure 4.7 Sensitivity of parameters to streamflow, seasonal LAI and interannual yield**

#### 4.4.3 Evaluation of soil moisture

To evaluate model performance in simulating soil moisture when different calibration strategies are applied, we re-run the model using all parameter sets from the last generation for both the Multi-variable and Streamflow only calibrations. Instead of comparing model performance for one parameter set from each strategy, we compared two populations,

which is helpful to explore the uncertainty in soil moisture performance brought by “equally good” (in streamflow, or in streamflow, LAI and yield) parameters.

Figure 4.8 depicts the moisture prediction from the two groups of parameter sets versus observed data for all three layers for site BLG. Generally speaking, both calibration strategies are able to capture the seasonal pattern of soil moisture during the growing season in the first and second layers. Multi-variable calibration improves model performance at some periods, for example, the drying trend in summers 2008 and 2010 are well captured when compared with the streamflow only calibration. However, for other periods, the underestimation of soil water for multi-variable calibration is worse than for the streamflow only calibration.

Tables 4.3 and 4.4 list the bias and uncertainty range of simulated volumetric soil moisture based on the two populations of parameter sets. Bias is computed as the difference between the population mean simulated soil moisture and the observed data recorded by soil sensors. The uncertainty range is taken from the 90% prediction interval from all simulated results. From Table 4.3, it seems that both parameter sets under estimate soil moisture in most of the sites, the bias ranges from -0.14 to -0.06, as a volumetric water content. For soil moisture, this bias is huge. Negative values mean more underestimation for the multi-variable calibration strategy, so overall the multi-variable calibration did not decrease bias in soil moisture prediction. The multi-variable calibration does reduce the uncertainty in soil moisture for all layers when compared to the streamflow only calibration, as shown in Table 4.4. This indicates that adding biophysical parameters to calibration and regulating

both water and crop growth can reduce the uncertainty in soil moisture prediction, though in this case it results in a less accurate prediction.

Neither of the two calibration strategies were able to capture observed soil moisture in the winter months and early spring. This mismatch is probably due to two reasons: 1) the installed TDR sensors are only sensitive to liquid water, so do not measure frozen soil moisture accurately, and 2) there is more missing meteorological information from the local weather stations during the winter. Note the nearest precipitation station is 12 km away from the soil moisture sensor, which could introduce errors in soil moisture prediction, especially in early spring, which is usually the rainfall season in this region.

**Table 4.3 Bias of simulated soil moisture versus observed data during corn growing season for different sites.**

Layer	Multi	Streamflow	Change	Multi	Streamflow	Change
	Variable	only		variable	only	
	calibration	calibration		calibration	calibration	
	AS2			BLG		
1	-0.124	-0.115	-0.009	0.008	0.015	-0.007
2	-0.105	-0.076	-0.029	-0.035	0.002	-0.037
3	-0.090	-0.074	-0.016	-0.025	-0.009	-0.016
	AD			CME		
1	-0.102	-0.094	-0.007	-0.106	-0.099	-0.007
2	-0.141	-0.104	-0.037	-0.111	-0.060	-0.051

**Table 4.4 Range of uncertainty in soil moisture prediction during corn growing season for different sites based on the final set of parameters for each calibration.**

Layer	Multi-objective calibration	Streamflow calibration	Uncertainty Pct. Difference	Multi-objective calibration	Streamflow calibration	Uncertainty Pct. Difference
	AS2			BLG		
1	0.001	0.007	-87.7	0.001	0.007	-86.5
2	0.003	0.012	-70.8	0.005	0.013	-64.3
3	0.005	0.011	-48.6	0.007	0.016	-54.9
	AD			CME		
1	0.001	0.007	-85.9	0.001	0.007	-83.1
2	0.003	0.012	-72.6	0.008	0.020	-60.1

Figure 4.8(c) shows that the model has the worst performance in the lowest soil layer (430-760 mm) at this location. Both parameter sets underestimate moisture systematically. We attribute this inconsistency to the lack of pedon information specific to where the soil sensor is installed. The field capacity and permanent wilting point are important parameters to control soil water content variation. However, SWAT computes permanent wilting point using the reported clay content for the soil series from the SSURGO soil database. SSURGO typically includes ranges of values based on field measurements from representative samples that might be far removed from the mapped location. Further, all soil information used for simulation comes from the SSURGO soil unit where the sensor is located, which ignores possible heterogeneity in such unit, using an area property to represent a point. Therefore, the discrepancy in soil moisture prediction can occur when SSURGO information does not match with local pedon information.

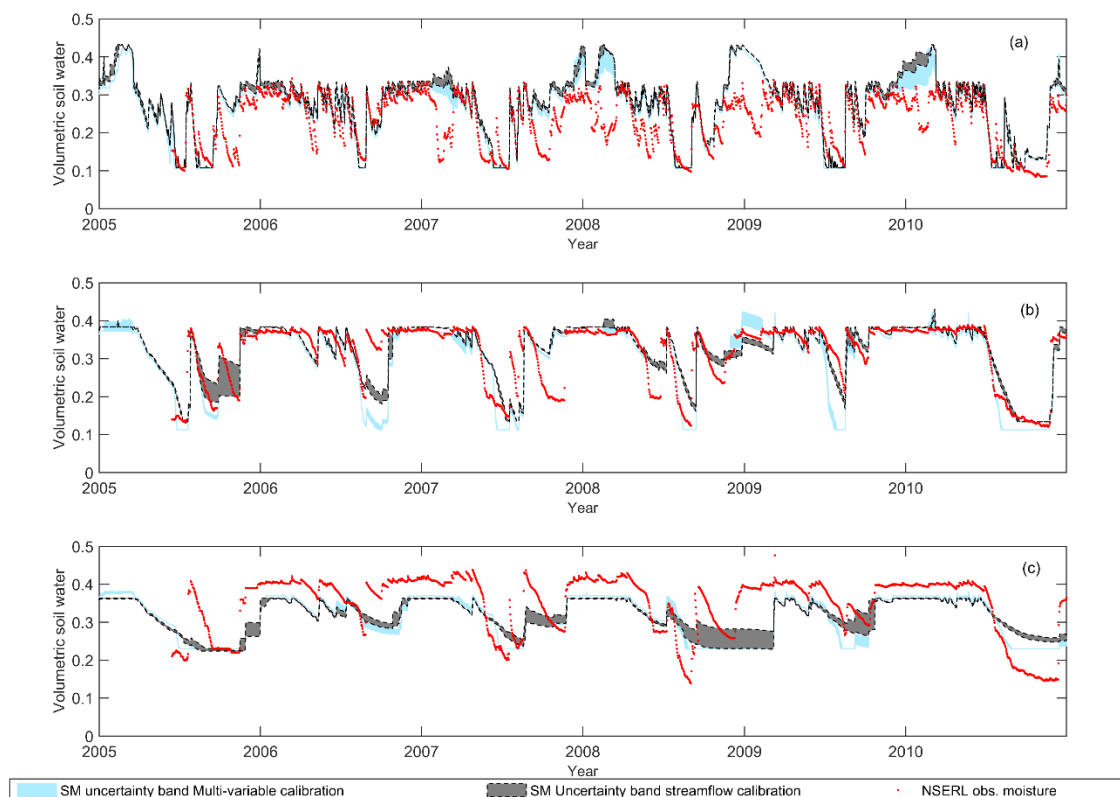


**Figure 4.8 Evaluation of soil moisture in site BLG at (a) First layer (0-230 mm); (b) Second layer (230-430 mm); (c) Third layer (430-760 mm)**

#### 4.4.4 Spatial distribution of corn yield

Figure 4.9 indicates the annual mean corn yield distribution and annual yield variance across the St. Joseph River watershed. The spatial maps of the two variables highlight different spatial patterns. The annual yield variance is evenly distributed across the watershed. No matter what calibration strategy is applied, the simulated mean yield shows a strong spatial distribution pattern: low yield is always associated with southwestern, while higher yield area is found in the Eastern part of the watershed. The state and county



boundaries can be clearly seen in Figure 4.9, which is consistent with the soil property distribution patterns seen in Figure 4.4. It seems that Ohio always has higher simulated yield than Indiana. However, a t-test on the difference in NASS county yield between Williams, OH and De Kalb, IN, found no statistically significant difference in mean yield. Therefore, although the basin average simulated yield from Figure 4.5 is reasonable, the spatial distribution of corn yield is problematic.

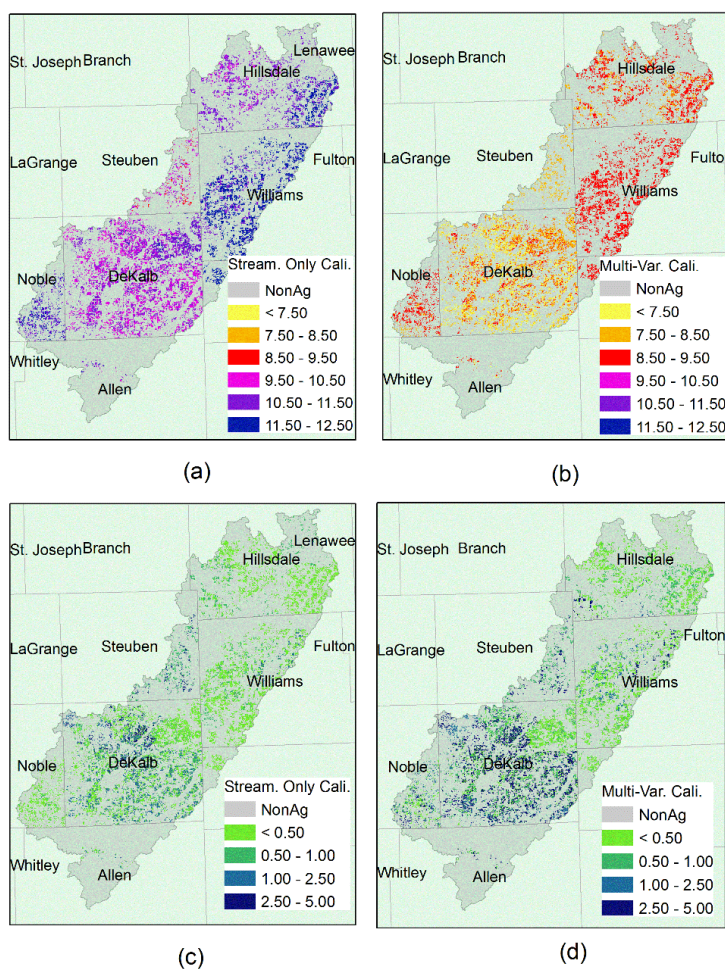


**Figure 4.9** The spatial distribution of annual mean yield by a) streamflow only calibration; b) multi-variable calibration; and the spatial distribution of interannual yield variation by c) only flow calibration. d) multi-variable calibration in the St. Joseph River watershed.

We therefore bias corrected HRU level corn yields using Eq. 4.3 and 4.4 to resolve the “boundary issue” (Figure 4.10). Abrupt yield differences were only found in the very northern part after bias-correction. It seems Hillsdale, MI has relatively lower yield than other counties in this region. This is consistent with the NASS observed yield data, indicating Hillsdale, MI, is the lowest yielding county in St. Joseph River watershed. The 20 year (1991-2010) mean yield is 117 bu/acre, which is significantly lower than De Kalb, IN, where yield is 128 bu/acre and Williams, OH where it is 131 bu/acre.

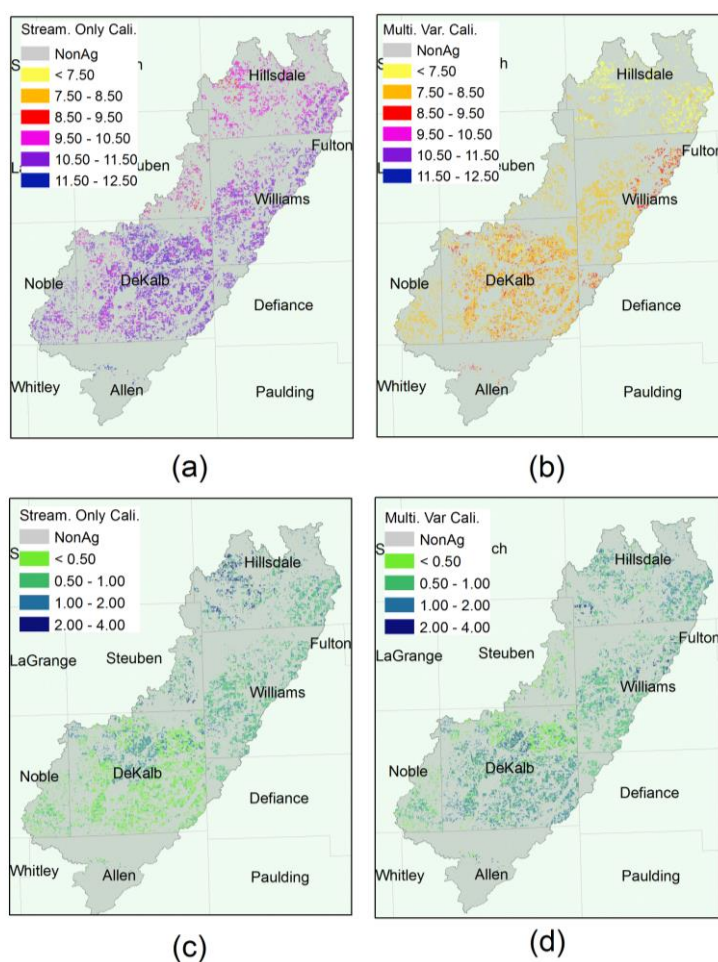


**Figure 4.10** The spatial distribution of adjusted annual mean yield after removing the effect of soil inconsistencies, for a) streamflow only calibration; b) multi-variable calibration; and the spatial distribution of interannual yield variation by c) streamflow only calibration. d) multi-variable calibration

After solving the abrupt yield inconsistency among counties, it is possible to locate specific areas that are sensitive to climate. We define climate sensitive cropland (CSC) based on frequency analysis. First, a fixed low threshold for crop yield was set. We defined this threshold as 80% of the 20 year average NASS harvest yield data at the basin scale, which is 6.43 ton/ha. Then the probability of HRU level yield lower than this threshold was computed based on a 20 year simulation. This method requires the computation of non-exceedance probability associated with long term simulated yield. Then the probability of yield lower than 6.43 ton/ha was identified. Some area may have low or zero probability, which indicates relative constant and higher yield. Areas with high probability indicates always lower yield or frequent yield variation.

Figure 4.11 indicates the spatial distribution of CSC in the St. Joseph River watershed as estimated from simulations using each of the two calibration strategies. We found a totally different spatial distribution pattern for two calibration strategies. For streamflow only calibration, most of the area crops have a 0 probability to reach the low yield threshold (6.43 ton/ha), indicating a reliably high yield for all years in the simulation. Only a limited area in the vicinity of Hillsdale, MI had a non-zero probability, still only reaching a 1 in 10 chance of experiencing yields lower than our threshold (< 10%). For the simulations using the multi-variable calibration parameters, a substantial portion of the watershed is at risk to experience yield below the threshold. Most HRUs in the vicinity of Hillsdale, MI are predicted to have between a 1 in 10 and 3 in 10 probability of having yield lower than 6.43 ton/ha in any given year. Parts of the DeKalb, IN are also have a high probability of crop

yields failing to meet the threshold, resulting from increased interannual variance, which is consistent with Figure 4.10 (d).

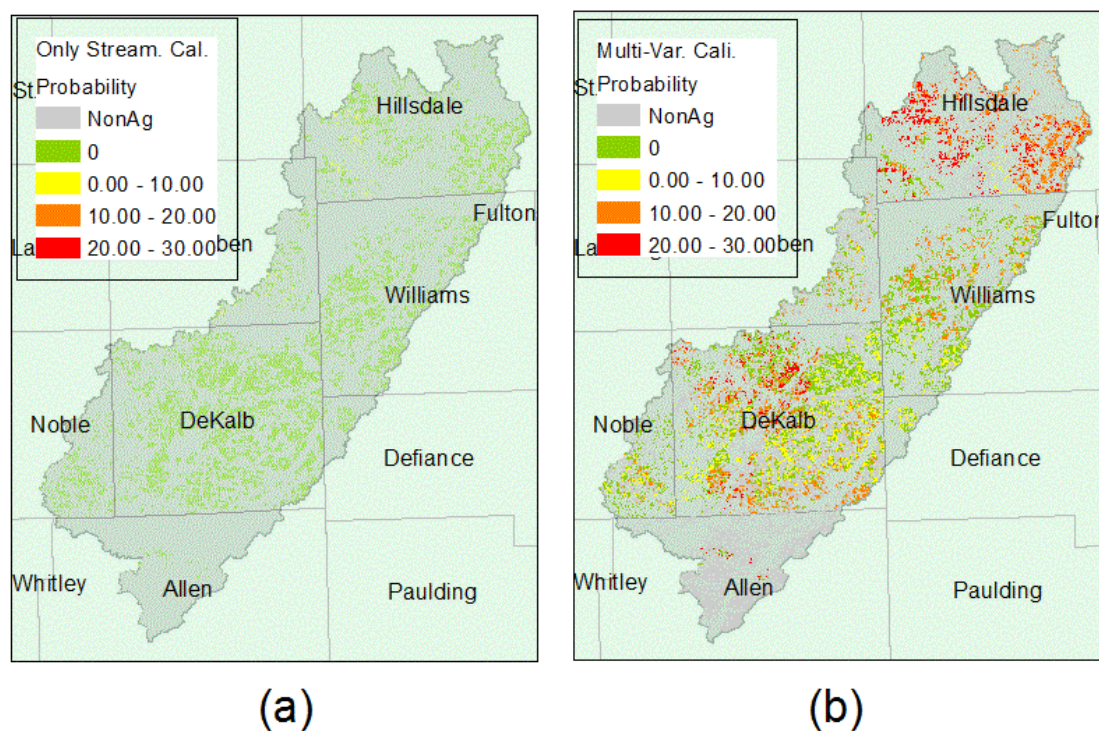


**Figure 4.11** The probability distribution of HRU with yield lower than threshold (6.43 ton/ha) based on a) streamflow calibration. b) multi-variable calibration.

Figure 4.12 indicates the yield variation and mean annual yield relationship for all corn HRUs after bias-correction based on different calibration strategies. Generally speaking, the multi-variable calibration strategy reduced the mean yield amount for all HRUs, to an average yield more consistent with observed NASS yield data (Figure 4.5). Visually, it is hard to identify any difference in interannual yield variability between the two calibration methods. However, a t-test indicates a significant difference in interannual yield variability. After bias-correcting the yield, the multi-variable calibration strategy experienced a higher

degree of interannual yield variability when compared to the simulation using streamflow only calibration parameters.

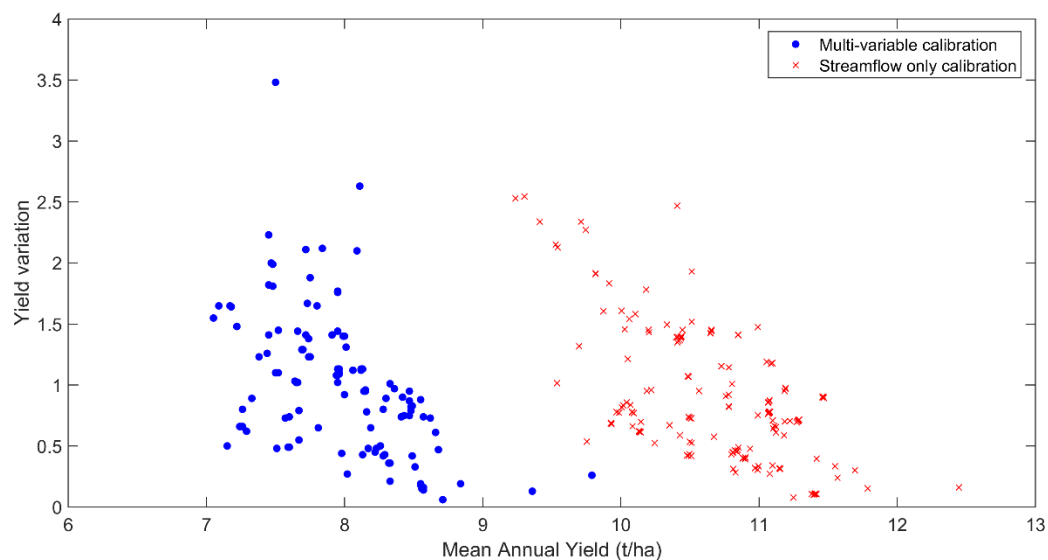


**Figure 4.12 Mean annual yield and interannual yield variability for all corn HRUs in St. Joseph River watershed, based on different calibration strategy after bias-correction.**

Areas with different probability to meet low yield threshold were summarized in Table 4.5. For simulations using streamflow only calibration parameters, 30.88 km<sup>2</sup> of the crop growing region is identified to have risk to reach low yield threshold (6.43 ton/ha), and the possibility is quite low (<10%), which is mainly due to its higher yield all over the watershed. More areas are expected to have low yield risk, which is identified by multi-variable calibration strategy. There are 146.79 km<sup>2</sup> area has higher possibility (>20%) to meet the low yield threshold (6.43 ton/ha), which is thought as CSC area. Those areas occupied 5.14% of the total basin area, which are recommended as potential places to plant more climate resistant crops to avoid yield loss.

**Table 4.5 Watershed area with a non-zero probability of failing to meet the low yield threshold (6.43 ton/ha) in any given year.**

	Probability to not meet threshold yield		
	<10%	10-20%	20-30%
Multi-var. Cali	141 km <sup>2</sup>	335 km <sup>2</sup>	147 km <sup>2</sup>
Stream. Only Cali.	31 km <sup>2</sup>	0 km <sup>2</sup>	0 km <sup>2</sup>

#### 4.5 Conclusions

In this research, SWAT was used to examine the simulation of annual crop sensitivity to climate variability by integrating crop seasonal growth information from satellite images in current model settings. Two model calibration strategies (streamflow only calibration vs. multi-variable calibration using streamflow and crop yield) were evaluated for their ability in reflecting climate variability in both crop growth and soil water. Simulated results were evaluated to identify the risk of crop yields falling below a defined minimum yield threshold (6.43 ton/ha) and areas where the probability of falling below the threshold exceeded 20% were identified as regions of Climate Sensitive Cropland (CSC).

Based on this work, we can conclude the following:

1. Compared to the streamflow only calibration, the multi-variable calibration strategy is able to capture seasonal crop growth development, and thus reduce the equifinality in final yield estimation due to incorrect parameter set. Simulation of annual yield variance is improved by multi-variable calibration, which correctly reflects the climate effects on final yield. Model performance in streamflow is reduced marginally (from a NSC of 0.820 to 0.817), but is still satisfactory.

2. By comparing in-situ sensor recorded soil moisture with simulation results, the SWAT model did capture the moisture seasonal pattern to some extent at several sites. However, both calibration strategies resulted in substantial bias, possibly due to the lack of in-situ soil physical properties. The multi-variable calibration strategy does not improved model performance in moisture prediction, but it reduces the uncertainty range in soil water
3. Before yield adjustment, the spatial distribution of simulated yield shows abrupt yield changes at state boundaries caused by the inconsistency of soil property representations among counties. However, interannual yield variability does not indicate such pattern. CSC identification cannot be conducted without the adjustment of HRU level yield.
4. The multi-variable calibration strategy increases the yield variability and reduces the mean yield at HRU level when compared with streamflow only calibration strategy. This improves the yield simulation relative to USDA NASSS county level yield reports.
5. No areas are identified as CSC area in the streamflow only calibration simulations as the mean yield is too high relative to actual yield. Areas of CSC are found in the simulations using the multi-variable calibration parameters both for areas with low overall mean (Hillsdale county in Michigan), and for regions with higher interannual variability (DeKalb County in Indiana). Total CSC area with high possibility (>20%) to meet low yield threshold is 146.79 km<sup>2</sup>, occupying 5.14% of the basin area which is identified by multi-objective calibration strategy.

Results from this analysis could provide valuable suggestions for better watershed management. For example, areas with low or zero probability to meet low yield threshold (the middle eastern part of the basin) should be always used for corn growth, because of their constant and productive performance. Identified CSC area with high probability to meet low yield threshold could be considered as potential places for more climate resistant crops to avoid yield loss.

There are still some limitation in this study, which could be improved with future work.

- 1) When executing multi-variable calibration in the St. Joseph River watershed, we fail to include more hydrological parameters in calibration strategy, only Curve Number is considered. Since all other hydrological parameters are fixed, it is hard to regulate the subsurface processes. Although model performance in surface water (streamflow) is satisfactory by only calibrating Curve Number and crop growth parameters, model performance in moisture is not improved.
- 2) Another problem in this study is the inconsistency of soil properties across counties. Though bias-correction in crop yield could solve the problem, it is still worth checking yield representation via more uniform soil datasets, for example gSSURGO (USDA-NRCS, 2014), or by developing SSURGO soil inputs based on landscape position (Muenich, 2011) or taxonomy properties (Luo, et al., 2012) rather than soil classification
- 3) Finally, we have not considered the uncertainty implicit in using empirical equations to derive LAI from NDVI time series. The LAI used in this study is not direct ground observations. As there is no physical relationship between NDVI and



LAI, empirical equations or statistical models are often employed based on regressions between field measured LAI and NDVI. Then the empirical model is used to predict or derive LAI from the NDVI values when field measurements are not available. For example, the coefficient of determination ( $R^2$ ) for the relationship used for this paper (Eq. 4.2) is 0.78, indicating that the model fits 78% of data well. Models for deriving LAI from NDVI may also vary spatially (e.g., Fortin et al., 2013; Walthall et al., 2004; Wiegand et al., 1990), introducing more uncertainty in to LAI estimates. Finally, NDVI has the potential to saturate when the LAI is high, thus limiting its ability to quantify LAI later in the growing season (Chapter 3).

## 4.6 References

- Adejuwon J. 2005. Assessing the suitability of the EPIC crop model for use in the study of impacts of climate variability and climate change in West Africa. *Singapore Journal of Tropical Geography* **26**: 44-60.
- Arnold JG, Srinivasan R, Muttiah RS, Williams JR. 1998. Large area hydrologic modeling and assessment part I: Model Development. *Journal of the American Water Resources Association* **34**: 73-89.
- Beven K. 2006. A manifesto for the equifinality thesis. *Journal of Hydrology* **320**:18–36
- Boegh E, Thorsen M, Butts MB, Hansen S, Christiansen JS, Abrahamsen P, Hasager CB, Jensen NO, van der Keur P, Refsgaard JC, Schelde K, Soegaard H, Thomsen A. 2004. Incorporating remote sensing data in physically based distributed agro-hydrological modeling. *Journal of Hydrology* **287**: 279–299.
- Cavero J, Farre I, Debaeke Philippe, Faci JM. 2000. Simulation of Maize Yield under Water Stress with the EPICphase and CROPWAT Models. *Agronomy Journal* **92**:679–690.
- Chen M, Willgoose GR, Saco PM. 2014. Spatial prediction of temporal soil moisture dynamics using HYDRUS-1D. *Hydrological Processes* **28**: 171–185.
- Cherkauer KA, Sinha T. 2010. Hydrologic impacts of projected future climate change in the Lake Michigan region. *Journal of Great Lakes Research* **36**: 33-50.
- Christensen JH, Hewitson B, Busuioc A, Chen A, Gao X, Held I, Jones R, Kolli RK, Kwon WT, Laprise R, Magana RV, Mearns L, Menendez CG, Raisanen J, Rinke A, Sarr A, Whetton P. 2007. Regional Climate Projections. In: *Climate Change 2007: The Physical Science Basis. Contribution of Working Group I to the Fourth Assessment Report of the Intergovernmental Panel on Climate Change* [Solomon S, Qin D, Manning M, Chen Z, Marquis M, Averyt KB, Tignor M, Miller HL (eds.)]. Cambridge University Press, Cambridge, United Kingdom and New York, NY, USA.
- Dohleman FG and Long SP. 2009. More productive than maize in the Midwest: how does Miscanthus do it? *Plant Physiology* **150**: 2104-2115.
- Draper C, Reichle R. 2015. The impact of near-surface soil moisture assimilation at subseasonal, seasonal, and inter-annual timescales. *Hydrology and Earth System Sciences* **19**:4831-4844.
- Entekhabi D, Rodriguez-Iturbe I, Castelli F. 1996. Mutual interaction of soil moisture state and atmospheric processes. *Journal of Hydrology* **184**: 3-17.

- Fortin JG, Anctil F, Parent LE. 2013. Comparison of physically based and empirical models to estimated corn (*Zea mays* L) LAI from multispectral data in eastern Canada. *Canadian Journal of Remote Sensing* **39**(1):1-11.
- Goldblum D. 2009. Sensitivity of corn and soybean yield in Illinois to air temperature and precipitation: The potential impact of future climate change. *Physical Geography* **30**:27-42.
- Heaton E, Voigt T and Long SP. 2004. A quantitative review comparing the yields of two candidate C4 perennial biomass crops in relation to nitrogen, temperature and water. *Biomass and Bioenergy* **27**:21-30.
- Heaton EA, Dohleman FG and Long SP. 2008. Meeting US biofuel goals with less land: the potential of *Miscanthus*. *Global Change Biology* **14**: 2000-2014.
- Her Y, Chaubey I. 2015. Impact of the numbers of observations and calibration parameters on equifinality, model performance, and output and parameter uncertainty. *Hydrological Processes* **29**: 4220-4237.
- Hill J, Nelson E, Tilman D, Polasky S, Tiffany D. 2006. Environmental, economic, and energetic costs and benefits of biodiesel and ethanol biofuels. *Proceedings of the National Academy of Sciences of the United States of America (PNAS)* **103**: 11206-11210.
- Jakeman AJ, Hornberger GM. 1993. How much complexity is warranted in a rainfall-runoff model? *Water Resources Research* **29**:2637-2649
- Koster RD, Suarez MJ. 2001: Soil Moisture Memory in Climate Models. *Journal of Hydrometeorology*, **2**: 558-570.
- Kotera A, Nguyen KD, Sakamoto T, Lizumi T, Yokozawa M. 2014. A modeling approach for assessing rice cropping cycle affected by flooding, salinity intrusion, and monsoon rains in the Mekong Delta, Vietnam. *Paddy and Water Environment* **12**: 343-354.
- Luo Y, Ficklin DL, Zhang M. 2012. Approaches of soil data aggregation for hydrologic simulations. *Journal of Hydrology* **464**:467-476.
- Mishra V, Cherkauer KA. 2010. Retrospective droughts in the crop growing season: Implications to corn and soybean yield in the Midwestern United States. *Agricultural and Forest Meteorology* **150**:1030-1045.
- Muenich MR. 2011. The impacts of soil properties, subsurface drainage and surface depressions on streamflow in a recently glaciated landscape. Master Thesis. Purdue University
- Nash JE, Sutcliffe JE. 1970. River Flow Forecasting Through Conceptual Models, Part I-A Discussion of Principles. *Journal of Hydrology* **10**:282-290.

- Rajib A, Merwade V. 2015. Multi-objective calibration approach for SWAT by using spatially distributed remotely sensed/in-situ soil moisture data. International Soil and Water Assessment Tool Conference. Oct 14<sup>th</sup> -16<sup>th</sup>, Purdue University, West Lafayette, IN, USA.
- Reichle RH, Koster RD, Dong J, Berg AA. 2014. Global soil moisture from satellite observations, land surface models, and ground data: implications for data assimilation, *Journal of Hydrometeorology* **5**: 430-442.
- Ren B, Zhang J, Li X, Fan X, Dong S, Liu P, Zhao B. 2014. Effects of waterlogging on the yield and growth of summer maize under field conditions. *Canadian Journal of Plant Science* **94**: 23-31.
- Sakamoto T, Wardlow BD, Gitelson AA. 2011. Detecting spatiotemporal changes of corn developmental stages in the US Corn Belt using MODIS WDRVI data. *IEEE Transaction on Geoscience and Remote Sensing* **49**: 1926-1936.
- Silvestro F, Gabellani S, Rudari R, Delogu F, Laiolo P, Boni G. 2015. Uncertainty reduction and parameter estimation of a distributed hydrological model with ground and remote-sensing data. *Hydrology and Earth System Sciences* **19**:1727–1751.
- Srinivasan R, Zhang X, Arnold J. 2010. SWAT Ungauged: Hydrological Budget and Crop Yield Predictions in the Upper Mississippi River Basin. *Transactions of the ASABE* **53**: 1533-1546.
- Steduto P, Hsiao TC, Raes D, Fereres E. 2009. AquaCrop - The FAO Crop Model to Simulate Yield Response to Water: I. Concepts and Underlying Principles. *Agronomy Journal* **101**: 426-437.
- Su CH, Ryu D. 2015. Multi-scale analysis of bias correction of soil moisture. *Hydrology and Earth System Sciences* **19**: 17–31.
- Tao F, Yokozawa M, Zhang Z. 2009. Modelling the impacts of weather and climate variability on crop productivity over a large area: A new process-based model development, optimization, and uncertainties analysis. *Agricultural and Forest Meteorology* **149**: 831-850.
- USDA-NRCS. 2014. Gridded Soil Survey Geographic (gSSURGO) Database User Guide. Available at [http://www.nrcs.usda.gov/wps/portal/nrcs/detail/soils/home/?cid=nrcs142p2\\_053628](http://www.nrcs.usda.gov/wps/portal/nrcs/detail/soils/home/?cid=nrcs142p2_053628)
- VanLoocke A, Twine TE, Zeri M, Bernacchi CJ. 2012. A regional comparison of water use efficiency for Miscanthus, switchgrass and maize. *Agricultural and Forest Meteorology* **164**:82-95.

- Vrugt JA, Robinson BA. 2007. Improved evolutionary optimization from genetically adaptive multimethod search. *Proceedings of the National Academy of Sciences of the United States of America (PNAS)* **104**: 708-711
- Walthall C, Dulaney W, Anderson M, Norman J, Fang H, Liang S. 2004. A comparison of empirical and neural network approaches for estimating corn and soybean leaf area index from Landsat ETM+ imagery. *Remote Sensing of Environment* **92**:465-474.
- Wang R, Bowling LC, Cherkauer KA. 2016. Estimation of the effects of climate variability on crop yield in the Midwest USA. *Agricultural and Forest meteorology* **216**: 141-156.
- Wiegand CL, Gerbermann AH, Gallo KP, Blad BL, Dusek D. 1990. Multisite analyses of spectral-biophysical data for corn. *Remote Sensing of Environment* **33**:1-16.
- Willmott CJ. 1982. Some comments on the evaluation of model performance. *Bulletin of the American Meteorological Society* **63**: 1309-1313.
- Zhang Y, Wegehenkel M. 2006. Integration of MODIS data into a simple model for the spatial distributed simulation of soil water content and evapotranspiration. *Remote Sensing of Environment* **104**: 393-408.

CHAPTER 5. BIOPHYSICAL AND HYDROLOGICAL EFFECTS OF FUTURE  
CLIMATE CHANGE INCLUDING TRENDS IN CO<sub>2</sub>, IN THE ST. JOSEPH  
RIVER WATERSHED, EASTERN CORN BELT

5.1 Abstract

Future climate change has the potential to significantly impact crop growth, both directly due to CO<sub>2</sub> enhancement and indirectly, through temperature and moisture impacts. This work investigates the biophysical and hydrological effects of future climate change, including trends in CO<sub>2</sub>, in the St. Joseph River watershed, Eastern Corn Belt. In this study, the Soil and Water Assessment Tool (SWAT) was first modified to take dynamic CO<sub>2</sub> concentration as input. A regional crop leaf development curve from Landsat TM imagery was also used to adjust model performance in corn leaf area development for the historical period. A multi-variable calibration strategy was employed to ensure the capturing of streamflow, seasonal crop growth and interannual crop yield simultaneously. The model was then driven by future climate change and CO<sub>2</sub> data from three Global Circulation Models (GFDL-CM2.1.1, NCAR-PCM1.3, UKMO-HADCM3.1), under three Special Report on Emissions Scenarios (SRES) Emission Scenarios (b1, a1b, a2) to investigate crop and streamflow response in two future periods: the near future (2021-2050) and the far future (2061-2090). The St. Joseph River watershed is expected to experience more winter and spring precipitation, but slightly decreasing summer precipitation. Due to increasing temperature and decreasing summer moisture, more drought stress is predicted.

Both annual total aeration and drought stress are projected to be more variable in both future periods. Although future CO<sub>2</sub> enhancement will benefit the crop growth and final yield by improving radiation use efficiency (RUE) and reducing drought stresses, corn yield is still expected to decrease by 6% in the near future period, and 16% in the far future period due to the combined effect of both climate change and CO<sub>2</sub> enhancement. Streamflow redistribution is also predicted in future. Stream discharge is projected to increase for the whole flow range in the near future period. For the far future period, high flows are expected to increase, while low flows are expected to decrease, indicating more hydrologic drought and flood events in the St. Joseph River watershed.

## 5.2 Introduction

Agricultural production is critically dependent on climate conditions. Temperature, precipitation and extreme events such as flooding or drought can seriously affect production, with risks often being higher for smaller farmers and some types of crops (Kling et al., 2003). The US Corn Belt is one of the biggest and most productive agricultural systems globally, with corn production occupying more than 20% of global maize areas. Any yield reduction due to climate variability and climate change may lead to a tighter food market and intensify food crisis (McMichael, 2009).

Many previous studies have investigated historical climate in the US Corn Belt and how it influences regional crop yield. In this area, mean temperatures have increased overall from 1900 to 2010 by approximately 0.059°C per decade. A rapid mean temperature shift

occurred in 1950 and 1979, which is similar to the temporal pattern of the global trend (Pryor et al., 2012). Current mean annual temperature for this region (1981-2010) varies from 3.3 °C in northern Minnesota to 15.6 °C in Missouri. Annual precipitation generally decreased from the late 1800's through the mid 1930's, followed by a general increasing trend until to the present (Groisman and Easterling, 1994; Andresen, 2012). The increase in the number of heavy precipitation events and number of wet days are two main reasons leading to the increase in precipitation from the 1930's (Kunkel et al., 2003; Grover and Soursounis, 2002).

Increased annual temperature is generally considered to benefit crop production in the Midwest, due to the longer growing season. Warmer winter temperatures will also reduce the frost season. A longer frost-free season generally implies increased agricultural productivity and the possibility for multiple plantings (Wuebbles and Hayhoe, 2004). However, the increased summer temperature may be detrimental to some crops. For example, Thompson (1988) found that the summer warming trend from 1891 to 1936 adversely affected crop yields, while the cooling trend accompanied by increased summer rainfall decreased variability in yield and accounted for a 20% increase in yield from 1936 to 1972. Increased weather variability since 1973 caused both higher and lower yields than previous periods. Mishra and Cherkauer (2010) also found that corn and soybean yields in the Midwest are significantly inversely correlated with drought indices and maximum daily air temperature in the grain filling and reproductive growth period.

For the grain fill period, cooler and wetter conditions are favorable for corn and soybean production (Lobell and Asner, 2003). However, this is not the case for spring months. If



soil is too wet in the spring, planting date is delayed. Later planting means grain ripening takes place as days become shorter in fall thus reducing grain filling time, and reducing crop yield (Arjal et al., 1978). Delayed planting also increases the risk of exposure to lethal cold temperatures late in the season before grain maturation (Nielsen et al., 2002). Planting crops in cold and wet soil is not good either. Oxygen transport rates in such soil are reduced, adversely affecting root metabolism and retarding root development. In some cases, a paradoxical phenomenon of the plant wilting may happen after soil submersion (Glinski and Stepniewski, 1983).

Historical climate information indicated that “cooler and wetter” condition in summer months and “warmer and drier” condition in spring months are optimal for crop growth in this area. However, projected seasonal changes in precipitation and temperature in this region are likely to lead to sub-optimal conditions for crop growth. Average US temperatures are expected to increase by 2 °C to 6 °C by 2100, depending on the level of future GHG emissions, and the results from various climate models (USGCRP, 2009). Patterns of precipitation and storm events, including both rain and snowfall will change. However, some of these changes are less certain than the changes associated with temperature. Projections show that future precipitation and storm changes will vary temporally and spatially (Meehl et al, 2007). Due to the enhancement of GHG concentrations, the Midwest USA is projected to face an increased in temperatures of 3-6 °C by the end of this century (Wuebbles and Hayhoe, 2004), a shift in the seasonal rainfall distribution to wetter springs (Christensen, 2007), and an increased frequency of intense

precipitation events and lower summertime soil moisture levels (Cherkauer and Sinha, 2010).

Many studies have investigated crop responses to possible future climate change in this region. Sinha and Cherkauer (2010) found that the duration of soil frost will decrease late in the century (2070-2099) accompanied by earlier occurrences of last spring frost and later first autumn frost. Southworth et al. (2000) indicate that crops in the northern part of the Midwest will have increased yields under climate change, because of the earlier planting date, but in some locations increased spring moisture will still delay planting despite warmer temperatures (Dohleman and Long, 2009; Rogovska and Richard, 2011). An increase in average temperatures also implies more frequent and intense extreme heat events, which may negatively affect crop yield (Goldblum, 2009). Possible decreases in summer rainfall during the critical growing periods or longer drought periods will also result in lower summer soil moisture (Mishra et al., 2010), and crop yield reduction (Wuebbles and Hayhoe, 2004). Increased heavy precipitation and flooding also has negative impacts on crop yield; Rosenzweig et al (2002) predicted 6% corn yield losses due to excessive precipitation and related events by 2030 in the Midwest.

Changes to precipitation and temperature are not the only factors impacting future crop yields, instead enhanced CO<sub>2</sub> levels in the atmosphere also affect crop growth. In 2013, CO<sub>2</sub> accounted for about 82% of all U.S. greenhouse gas emissions from human activities (USEPA, 2013). Since CO<sub>2</sub> is the substrate of photosynthesis, increased concentration stimulates photosynthetic rates directly. Crop production usually responds positively to the increased atmospheric CO<sub>2</sub> concentration, which is termed a “CO<sub>2</sub> fertilization effect”

(Oliver et al., 2009). Increased CO<sub>2</sub> concentration reduces the stomatal conductance, which leads to an improved plant-water productivity. As a result, transpiration loss is reduced, and higher soil water content is maintained during the growing season (less drought stress), which improves the drought tolerance by delaying the onset of water stress, and finally enhances the biomass production (Long et al., 2004).

Reduced transpiration also has a negative effect on corn growth, mainly due to the resulting increase in tissue temperature. Transpiration is reduced because of the decrease of stomatal conductance as a result of CO<sub>2</sub> concentration enhancement, which reduces the cooling via transpiration, and consequently increases canopy and leaf temperature (Wall et al., 2001). If leaf temperature is over 37 °C, the activity of phosphoenolpyruvate (PEP) is negatively affected (Rathnam, 1978) and thus photosynthesis decreases. Increased tissue temperature may have other microclimatic effects within the canopy such as decreasing humidity, which increases the leaf-to-air vapor pressure gradient. As a result, this may lead to a feedback that increases one of the driving forces for transpiration, negating the CO<sub>2</sub> effect and leading to increased water use at the canopy scale (Wullschleger and Norby, 2001).

Further, lower transpiration alone will not typically benefit a crop when soil moisture is available. Leakey et al. (2006) found that the productivity and yield of maize were not affected by the open-air elevation of CO<sub>2</sub> concentrations (550 ppm) in the absence of drought in Illinois, USA, although stomatal conductance was reduced by 34% and soil moisture was increased by 31% when compared with corn under ambient CO<sub>2</sub> concentrations (370 ppm).

In summary, crop growth and yield is influenced by precipitation pattern, growing season temperature, and CO<sub>2</sub> concentration. All of these factors directly impact crop water use, either through water availability, atmospheric demand or water productivity, resulting in feedbacks to the field water balance. As a result, their combined effects and relative importance are difficult to separate and varies from case to case. Therefore, the main objective of this study is to quantify the biophysical and hydrologic response to future precipitation change, temperature increase and CO<sub>2</sub> enhancement in an agricultural watershed.

The Soil and Water Assessment Tool (SWAT) (Arnold et al., 1998) was employed in the St. Joseph River watershed, Eastern Corn Belt. SWAT was modified to take a time series of dynamic CO<sub>2</sub> concentration as input. A regional crop leaf development curve from Landsat TM imagery was used to adjust model performance in corn leaf area development for the historical period during calibration. Finally, regional crop growth and streamflow responses due to changes in air temperature, precipitation, and CO<sub>2</sub> enhancement at two future periods (2031-2050; 2071-2090) were evaluated.

### 5.3 Method

#### 5.3.1 Study area

The St. Joseph River Watershed (Figure 5.1) is located in northeastern Indiana, northwestern Ohio and southeastern Michigan, with a drainage area of 2821 km<sup>2</sup>. Cropland, with coverage of 38% of the watershed area, is the dominant land use/cover type based on the USDA National Agricultural Statistics Service (NASS) Cropland Data Layer (CDL)

for 2010. Other land use types in this watershed are pasture (26.6%), forest (13.0%), urban areas (12.5%) and wetland (9.3%).

### 5.3.2 SWAT model overview

Developed by the USDA-ARS, the Soil and Water Assessment Tool (SWAT) is widely used to assess the impact of climate variability on hydrologic process and crop production. The basic simulation unit for SWAT is the hydrologic response unit (HRU), which is a lumped land area, possessing a unique combination of land use, soil and slope within a subbasin. At the HRU level, SWAT simulates the hydrologic cycle based on a water balance equation of soil water content including evapotranspiration, surface runoff, infiltration, percolation, shallow and deep aquifer flow (Arnold et al., 1998). A detailed description of SWAT hydrological simulation can be found in Neithsch et al. (2009).

SWAT simulates crop growth both under optimal and actual conditions. When no growth stress is considered, daily growth rate or daily biomass accumulation ( $\Delta bio$ ; kg/ha) is regulated by leaf area index (LAI) development, light interception ( $k_l$ ), photosynthetically active radiation ( $H_{day}$ ; MJ m<sup>-2</sup>), and radiation-use efficiency (RUE; 10<sup>-1</sup> g/MJ), as follows:

$$\Delta bio = 0.5H_{day} * (1 - \exp(-k_l * LAI)) * RUE \quad (5.1)$$

For annual crops, LAI accumulates following an optimal leaf area development curve for each day. LAI starts to accumulate from the planting date until it reaches the maximum LAI. It remains stable until the senescence point (DLAI) is attained, where LAI drops until maturity.

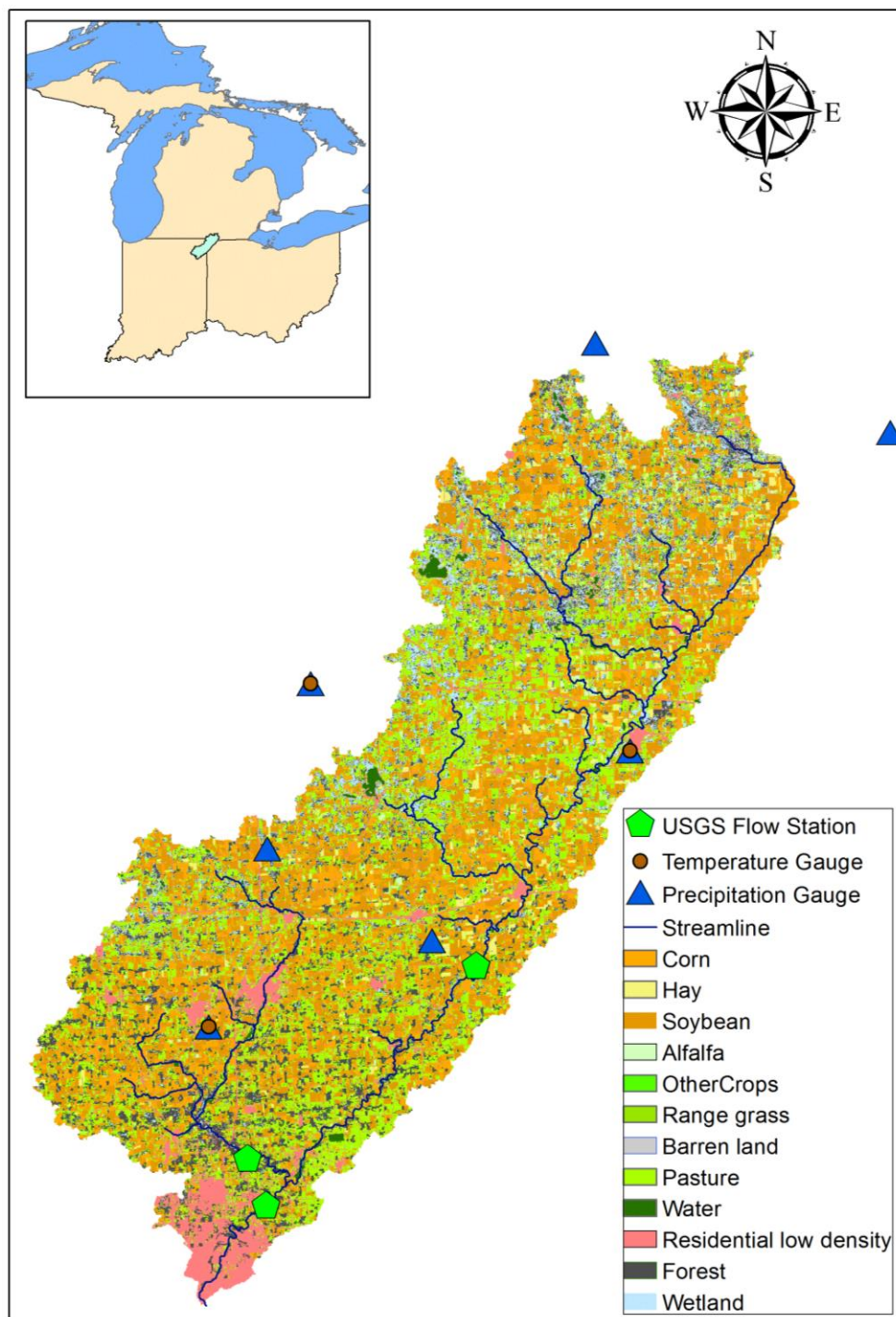


**Figure 5.1** Location and land cover of the St. Joseph River watershed. Land cover is from the USDA NASS Cropland Data Layer for 2010. The location of three USGS gauging stations and seven weather stations are also shown.

Actual daily growth varies from optimal growth due to various stresses. SWAT considers growth constraints from five aspects: drought, aeration, temperature, nitrogen and phosphorous stresses. The plant growth factor quantifies the fraction of potential growth achieved on a given day and is calculated as:

$$\gamma_{reg} = 1 - \max(wstrs, astrs, tstrs, nstrs, pstrs) \quad (5.2)$$

where  $\gamma_{reg}$  is the plant growth factor (0.0-1.0), *wstrs* is the water stress for a given day expressed as a fraction of optimal plant growth, *astrs* is aeration stress, *tstrs* is the temperature stress, and *nstrs* and *pstrs* are nitrogen and phosphorus stress, respectively. Therefore, the potential LAI, and biomass are adjusted daily if any individual stress is greater than 0.0. If there is no stress, then  $\gamma_{reg}=1$ . In this study, the auto fertilization option was applied to avoid nutrient limitation. Therefore, nutrient stress was not considered in this research. Unlike the original SWAT drought stress and aeration stress calculation method, an S-curve method is used to convert the physical measure of excess or low soil moisture to the aeration or drought stress factor (Wang et al., 2016).

### 5.3.3 The representation of CO<sub>2</sub> effects in the SWAT model

SWAT considers the biomass production enhancement due to elevated CO<sub>2</sub> concentration in two ways. The direct impact on stimulating photosynthesis is reflected in a change in radiation-use efficiency (RUE) under different ambient CO<sub>2</sub> levels. Radiation-use efficiency is sensitive to variations in atmospheric CO<sub>2</sub> concentrations. The relationship used to adjust the RUE for effects of elevated CO<sub>2</sub> (Stockle et al., 1992) is:

$$RUE = \frac{100 * CO_2}{CO_2 + \exp(r_1 - r_2 * CO_2)} \quad (5.3)$$

where  $RUE$  is the radiation use efficiency of the plant ( $10^{-1}$  g/MJ),  $CO_2$  is the concentration of carbon dioxide in the atmosphere (ppmv), and  $r_1$  and  $r_2$  are shape coefficients. For corn,  $r_1=5.7998$  and  $r_2=-0.00135$  (Stockle et al., 1992; Neitsch et al., 2009). According to equation 5.3, when  $CO_2$  is between 330 and 660 ppmv,  $RUE$  increases with increasing  $CO_2$  concentration, reflecting that plants can accumulate more biomass for the same amount of absorbed energy due to greater carbon intake.

The indirect impact of  $CO_2$  enrichment due to improving plant-water productivity is considered by modifying the canopy resistance term when using the Penman-Monteith equation to calculate potential/actual evapotranspiration. The Penman-Monteith method combines components that account for energy needed to sustain evaporation, the strength of the mechanism required to remove the water vapor and aerodynamic and canopy resistance terms. Based on this method, increased canopy resistance or reduced stomatal conductance leads to a decreased ET. Easterling et al. (1992) proposed the following equation to consider  $CO_2$  effect on canopy resistance:

$$r_c = \frac{r_l}{(0.5 * LAI) * (1.4 - 0.4 * \frac{CO_2}{330})} \quad (5.4)$$



where  $r_c$  is the canopy resistance (s/m),  $r_l$  is the minimum effective stomatal resistance of a single leaf (s/m), and LAI is the leaf area index of the canopy. Increased canopy resistance or reduced stomatal conductance leads to a decreased ET.

### 5.3.4 Input Data

#### 5.3.4.1 Historical climate input

Historical climate input (daily precipitation and air temperature) from 1991 to 2010 is provided from NOAA National Climate Data Center weather stations, as well as weather stations maintained by the USDA-ARS National Soil Erosion Research Laboratory. Seven precipitation and three temperature stations were selected around or inside the St. Joseph River watershed (Figure 5.1). Model calibration is based on observed historical climate data.

#### 5.3.4.2 GCM climate input

Three Global Circulation Models (GFDL-CM2.1.1, NCAR-PCM1.3, UKMO-HADCM3.1), under three Special Report on Emissions Scenarios (SRES) Emission Scenarios (b1, a1b, a2) were provided by World Climate Research Programme's (WCRP's) Coupled Model Intercomparison Project Phase 3 (CMIP3). Data was first bias corrected and then temporally disaggregated to daily scale based on resampling of the historic time series (Cherkauer and Sinha, 2010), before being utilized as weather input to evaluate climate change effects on crop growth and streamflow. The downscaled and bias-corrected

projected daily data is available from 1950 to 2099 for all three models and all three emissions scenarios.

#### 5.3.4.3 CO<sub>2</sub> input

Historical annual CO<sub>2</sub> concentration and future CO<sub>2</sub> concentration predicted for the three SRES emission scenarios are provided by the IPCC Third Assessment Report - Climate Change (Houghton et al., 2001). Concentration data is provided annually from 1970 to 2100 for each emission scenario.

#### 5.3.5 Model implementation

Model implementation and all parameters are based on multi-variable calibration from Chapter 4. Daily weather from the three selected GCMs under three emissions scenarios, including the dynamic CO<sub>2</sub> concentrations, were used to drive the SWAT model. Model applications were performed using calibrated parameters from the previous section for three 30-year time periods. The first period represents the baseline period (1981-2010). The second and third periods represent the near future (2021-2050) and far future (2061-2090). In order to explore how CO<sub>2</sub> enhancement and future climate change affect crop growth and streamflow, the following model experiments were conducted:

- 1) Baseline run: Baseline period daily precipitation and temperature data (1981-2010) plus baseline period (1981-2010) CO<sub>2</sub> concentrations ([CO<sub>2</sub>]).

- 2) Near future run: Near future daily precipitation and temperature data (2021-2050) plus near future (2021-2050) CO<sub>2</sub> concentrations ([CO<sub>2</sub>]).
- 3) Near future run, with CO<sub>2</sub> control: Near future daily precipitation and temperature data (2021-2050) plus baseline period (1981-2010) CO<sub>2</sub> concentrations ([CO<sub>2</sub>]).
- 4) Far future run: Far future daily precipitation and temperature data (2061-2090) plus far future period (2061-2090) CO<sub>2</sub> concentrations ([CO<sub>2</sub>]).
- 5) Far future run, with CO<sub>2</sub> control: Far future daily precipitation and temperature data (2061-2090) plus baseline period (1981-2010) CO<sub>2</sub> concentrations ([CO<sub>2</sub>]).

## 5.4 Results and Discussions

### 5.4.1 Future climate change and CO<sub>2</sub> enhancement

As shown in Figure 5.2, annual precipitation and temperature change prediction are quite different between models and scenarios. Figure 5.2 displays variations in average annual temperature and precipitation for the two future periods relative to the baseline period (1991-2010). Both future projections indicate a consistent rise in temperature, but distinct differences in magnitude. For the near future period (2021-2050), the change varied between +0.43 °C and +1.98 °C, with an average value of +1.20 °C, while for the far future period (2061-2090), the range is from +1.42 °C to 3.75 °C, with an average change of 2.79 °C. For precipitation, all of these scenarios experienced an annual increasing precipitation, with average change of +4.69% for the 2021-2050 period, and +7.51% for

the 2061-2090 period. The UKMO-HADCM 3.1 model always predicts lower precipitation change but higher temperature increases. On the contrary, higher precipitation change but lower temperature change was projected by the NCAR-PCM 1.3 model. Under the B1 scenario, all three models predict lower annual precipitation and temperature change than the other two scenarios in both the near future and far future periods.

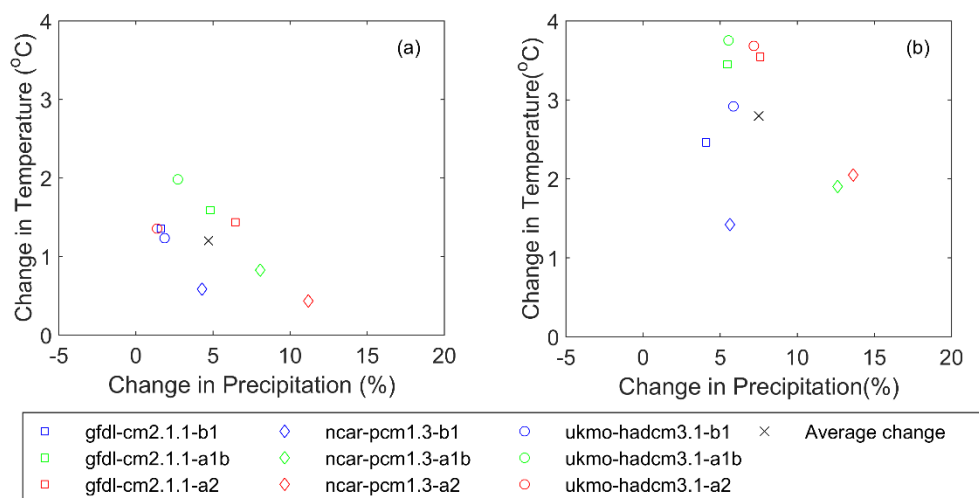


**Figure 5.2 Annual mean temperature and precipitation change from the baseline period (1981-2010) to a) the near future period (2021-2050) and b) the far future period (2061-2090) according to three GCMs under three GHG scenarios in St. Joseph River watershed**

The monthly temperature and precipitation change based on the three future emission scenarios is illustrated in Figure 5.3. Temperature increases are predicted for all months in the near future period (Figure. 5.3(a)). Temperature is expected to keep increasing in the far future period under all three scenarios (Figure. 5.3(b)). July, August and September are expected to experience greater temperature increases compared to the other months. Most

of the time, scenario B1 predicts a smaller increase in temperature when compared with the other two scenarios.

Precipitation change also varies seasonally in the study area. Precipitation increases are predicted in winter and spring months (November to March) for all scenarios in the two future periods, with the magnitude of the increase highest in the far future period. Marginal variations (could be positive or negative) in precipitation are predicted in June and July. For August, only scenario A2 predicted a moderate increase, on average (around 10%), all other scenarios report marginal precipitation variations. All three scenarios project different precipitation change patterns in September and October. Scenario B1 indicates a moderate decrease in both future periods. For the near future period, scenario A1B indicates moderate decreases in September but moderate increases in October, scenario A2 shows the revers. For the far future period, both A1B and A2 predict precipitation increases in September and October. Therefore, no clear direction of precipitation change is predicted for the fall months (September and October).

Based on Figure 5.2 and 5.3, the St. Joseph River watershed will more likely experience enhanced air temperature in both future periods, especially during the summer months (July, August, and September). Precipitation is expected to substantially increase in winter and spring, but show little change in summer months (July, June and August). Increased temperature accompanied with nearly unchanged precipitation in summer months indicate a higher evapotranspiration demand. Therefore, the study area may become much drier in the summer months, which are often critical corn growth periods, and an increase in drought stress during this critical period will lead to final yield reduction.

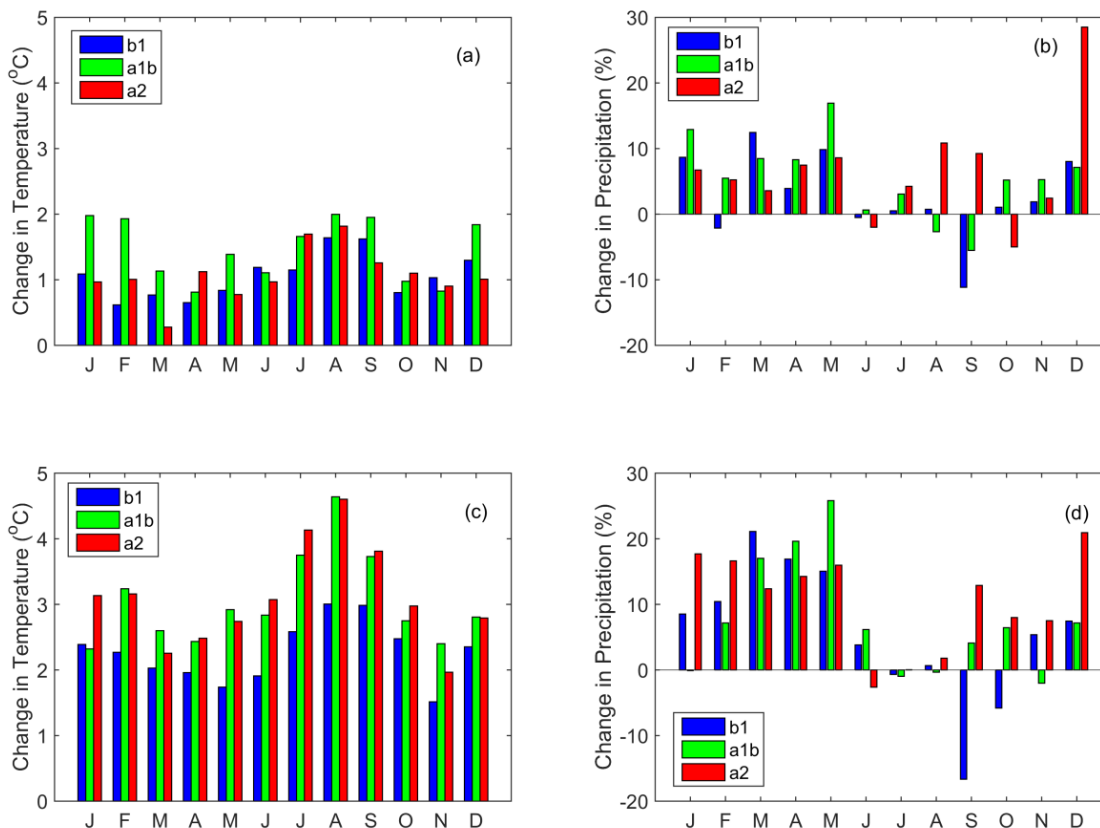


**Figure 5.3 Monthly mean: (a) temperature and (b) precipitation variation between the baseline period (1981-2010) and the near future period (2021-2050); Monthly mean: (c) temperature and (d) precipitation variation between the baseline period (1981-2010) and the far future period (2061-2090)**

Figure 5.4 depicts the CO<sub>2</sub> concentration prediction from 1970 to 2100 for different SRES scenarios. The A2 scenario has the highest CO<sub>2</sub> increasing rate. A2 and A1B have quite similar CO<sub>2</sub> concentrations until year 2050 (522 ppm), when A2 projects a much more rapid increase. The B1 scenario has the lowest concentration among all three SRES emission scenarios, and it reaches a relatively stable concentration (530 ppm) by the year 2080. Since biomass accumulation and final yield are closely related to Radiation Use Efficiency RUE (Eq. 5.1), which is a function of CO<sub>2</sub> level (Eq. 5.3), Figure 5.4(b) was

generated to indicate how corn RUE responds to different CO<sub>2</sub> concentrations. Generally, RUE responds to CO<sub>2</sub> increases positively, but when the CO<sub>2</sub> level is over 500 ppm, further CO<sub>2</sub> increases will not cause much further increase in RUE. For this reason, RUE impacts under both the A1B and A2 scenarios are very similar even though their CO<sub>2</sub> concentrations diverge after 2050. This divergence occurs when both scenarios are over 500 ppm CO<sub>2</sub> and SWAT is no longer sensitive to the change. Furthermore Eq. 5.3 is only suitable for CO<sub>2</sub> concentration from 330 to 660 ppm, as it starts to reverse the effect of CO<sub>2</sub> fertilization at higher concentrations. Thus the equation has been modified so that if CO<sub>2</sub> concentration is greater than 660 ppm, the equation ignores further increases. Therefore, RUE will not exceed 45.05 (RUE at 660 ppm from Eq. 5.3).

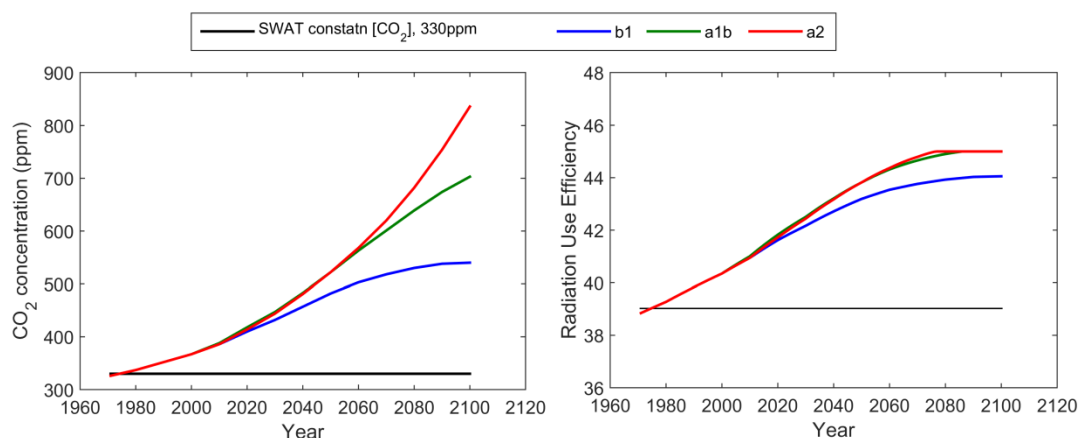


**Figure 5.4 Future changes to CO<sub>2</sub> and radiation use efficiency as estimated by the modified SWAT model.**

#### 5.4.2 Crop biophysical responses to future climate and CO<sub>2</sub> change

Section 3.1 indicates that future climate change may introduce more drought stress during the crop growing season, which may in turn impact the final yield in our study area.

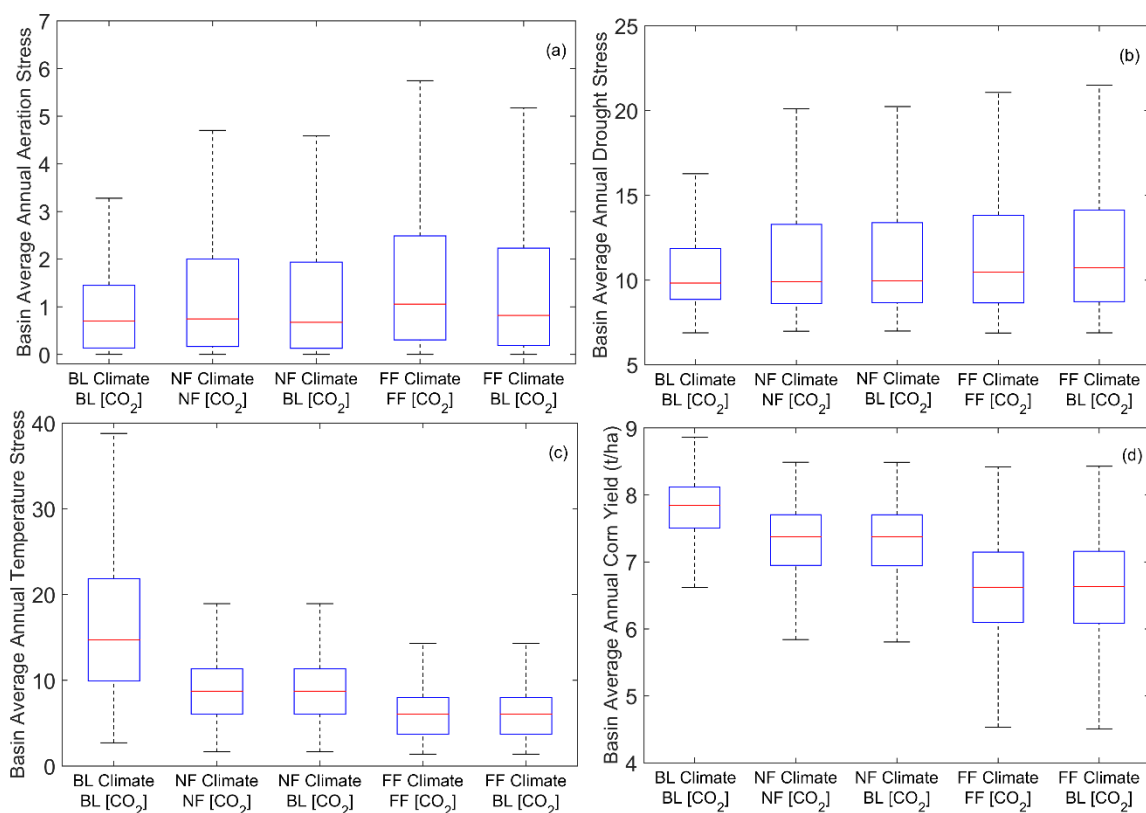
However, the enhanced CO<sub>2</sub> is also expected to increase crop yield to some extent. Their combined biophysical impacts on crop yields are unknown and might be different between the two future periods due to differences in future climate and CO<sub>2</sub> concentration. Therefore, in this section, the biophysical impacts of future climate and CO<sub>2</sub> change are explored.

Figure 5.5 exhibits the impacts of climate change and CO<sub>2</sub> enhancement on three crop stresses (aeration, drought and temperature) and final yield based on the different simulation experiments in both the baseline and two future periods. Annual stress for each corn HRU was first computed from the daily time series, and then aggregated into basin level based on HRU areas. Compared to the baseline scenario, both annual total aeration (Figure 5.5(a)) and drought stress (Figure 5.5(b)) experienced more variance in both future periods. Furthermore, the variances for both stresses were predicted to increase from the near future to the far future periods. This can be seen from the increase of Q75 (upper quartile, meaning 25% of the data lie above this threshold) and the range (Differences between upper and lower Whisker) of both stresses (Table 5.2). Limited change in the median value of aeration or drought stress was detected. The impact of CO<sub>2</sub> change on any of the stresses was not appreciable in the near future period. For the far future period, CO<sub>2</sub> enhancement slightly increases the median of annual aeration stress (1.06 vs 0.82), and slightly reduces annual drought stress (10.48 vs. 10.73).

Figure 5.5(c) indicates the temperature stress variation for different simulation experiments. In contrast to aeration and drought stress, climate change impacts to temperature stress are quite different. The median value for temperature stress for baseline, near future, and far



future periods are 14.71, 8.73, and 6.07, respectively, indicating a decreasing trend in the future periods. This decreasing trend is also accompanied by decreased variation in stress.



**Figure 5.5** Boxplots for annual basin level stress and corn yield for the different modeling experiments: a) Aeration stress, b) Drought stress, c) Temperature stress, and d) corn yield. Box plots for each experiment based on annual average results for the 30 year period as projected by three GCMs and three climate change scenarios. BL: Baseline, NF: Near future, FF: Far future.

**Table 5.1 Statistics for stresses and corn yield based on all modeling experiments.**

<b>Statistic</b>	<b>Stress/Yield</b>	<b>Baseline climate and [CO<sub>2</sub>]</b>	<b>Near future climate and [CO<sub>2</sub>]</b>	<b>Near future climate, baseline [CO<sub>2</sub>]</b>	<b>Far future climate and [CO<sub>2</sub>]</b>	<b>Far future climate, baseline [CO<sub>2</sub>]</b>
Median	Aeration Stress	0.70	0.75	0.67	1.06	0.82
	Drought Stress	9.82	9.91	9.96	10.48	10.73
	Temperature Stress	14.71	8.74	8.74	6.07	6.07
	Corn Yield (t/ha)	7.85	7.37	7.38	6.62	6.63
Q75	Aeration Stress	1.45	2.00	1.94	2.49	2.23
	Drought Stress	11.85	13.29	13.39	13.82	14.12
	Temperature Stress	21.88	11.33	11.33	8.00	8.00
	Corn Yield (t/ha)	8.12	7.71	7.70	7.15	7.16
Range	Aeration Stress	3.42	4.76	4.65	5.76	5.30
	Drought Stress	11.99	18.68	18.93	20.66	21.56
	Temperature Stress	39.81	19.22	19.22	14.46	14.46
	Corn Yield (t/ha)	2.46	3.02	3.05	4.19	4.29

The difference in yield for each experiment is caused by the effect of all three stresses. Based on Figure 5.5(d), median crop yield is projected to decrease, the reduction for the near future period is around 0.5 t/ha, while for the far future period yield loss is 1.2 t/ha. More variance in crop yield is also predicted for both future periods. Larger yield variance in the future is caused by more extremely low yield conditions rather than an increase in high yield occurrences. CO<sub>2</sub> enhancement shows a marginal effect on crop yield (around

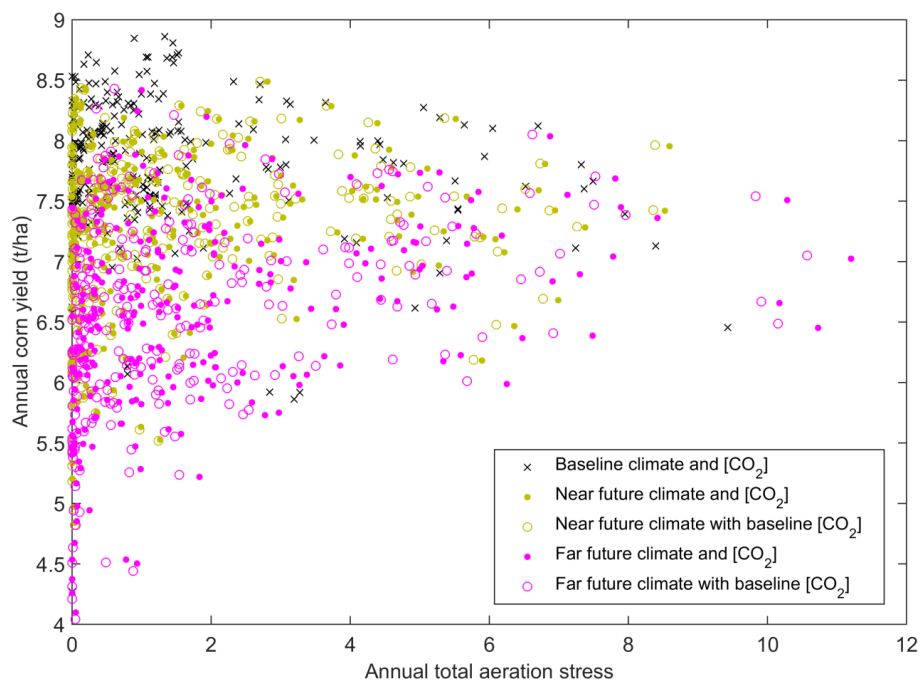
0.01 t/ha difference in median value), which is consistent with its influence on growth stresses.

The relationship between growth stresses and crop responses was further investigated by plotting annual yield versus various biophysical stresses (aeration, drought and temperature stresses) for each modeling experiment, as shown in Figure 5.6-8. Results indicate an increasing trend in aeration stresses, as seen in the increasing number of years with bigger aeration stress in contrast to the baseline period (Figure 5.6). However, there is no clear relationship between aeration stress and crop yield. This is mainly due to the low frequency of aeration stress events during the simulation period. In terms of drought stress (Figure 5.7), an inverse correlation was found between yield and annual stress. Compared to the baseline period, the two future periods experienced larger annual stresses, which is also associated with more yield loss. Another interesting point from Figure 5.7 is the effect of CO<sub>2</sub> on drought stress and yield. When the baseline period CO<sub>2</sub> was used for future periods, it resulted in larger drought stress and more yield reduction, (The gold or purple circles are always to the lower right of their counterpart dots). This indicates that CO<sub>2</sub> enhancement can reduce drought stress and reduce the risk of yield loss. We conducted t-tests between corn yields for scenarios with baseline CO<sub>2</sub> and those with near future and far future CO<sub>2</sub> concentrations. Significant differences ( $p < 0.01$ ) in mean yield were found when CO<sub>2</sub> enhancement is considered. However, the difference in mean yield is marginal (0.001 ton/ha and 0.003 ton/ha for near future and far future periods, respectively). Therefore, the positive influence of CO<sub>2</sub> enhancement on crop growth cannot compensate the negative effect of temperature and precipitation change. This finding is supported by several field

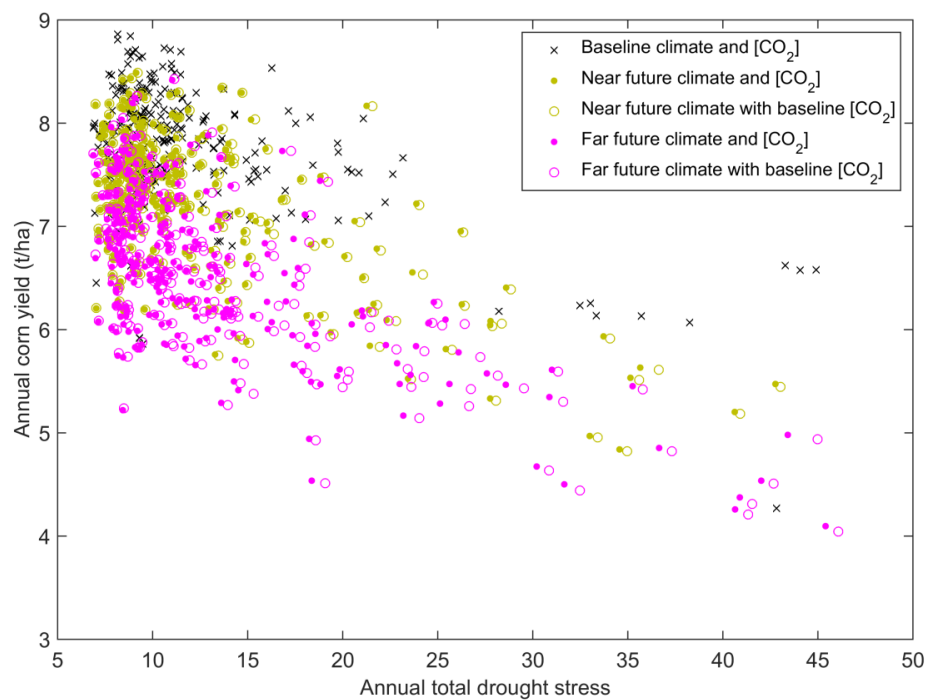
studies that also indicate that CO<sub>2</sub> enhancement effect is not significant to corn yield. For example, Leakey et al (2006) found the yield of maize is not affected by open-air elevation of CO<sub>2</sub> in the absence of drought. Ainsworth and Long (2005) also found no significant yield increase in C4 crops or C4 wild grasses in the Free-Air Concentration Enrichment (FACE) studies under different CO<sub>2</sub> treatments.

Figure 5.8 illustrates the relationship between temperature stress and crop yield for the different modeling experiments. Consistent with Figure 5.5(c), temperature stress decreased in the future period when compared to the baseline period. Decreased temperature stress is caused by the increase in mean temperature. In SWAT, temperature stress is computed based on daily mean temperature, as shown in Figure 5.9. For corn, the optimal mean growth temperature is 25 °C. When daily mean temperature is between 20 °C to 30 °C, very limited temperature stress is found. When mean temperature is below 20 °C or over 30 °C, temperature stress increases rapidly. The threshold of high temperature, beyond which heat stress may increase substantially, is consistent with other studies (e.g. Schlenker and Robert, 2009). Schlenker and Roberts (2009) found that corn yield decreases sharply, if temperature is over 29 °C. Future temperature increases may help to release stress caused by low temperature (cold condition), however, SWAT does not predict much more stress due to high temperatures, since daily mean temperature over 30 °C is still rare. Figure 5.8 also indicates that lower temperature stress is accompanied with lower yield. This can be explained by the increasing threat of drought stress. Although direct temperature stress due to warmer temperatures is not predicted by SWAT, increased temperature does exacerbate the drought stress in summer months, which is more critical

to final corn yield (Nielsen, 2008). The reduced temperature stress in the early growing season (cold condition) due to mean temperature increasing cannot compensate for the yield reduction risk due to exacerbated drought stress in summer months. This finding is consistent with other studies (Brown et al., 2000; Hawkins et al., 2013). Brown et al., (2000) applied the erosion productivity impact calculator (EPIC) crop growth model in the Missouri-Iowa-Nebraska-Kansas (MINK) region to study environmental effects of switchgrass and traditional crops under current and future greenhouse-altered climate. They found that higher temperatures would decrease cold stress, but increase heat stress with water deficit, so climate would still threaten the final corn yield. Hawkins et al. (2013) used an empirical model and GCM data to study the heat stress influence on French maize yield. They found that most large maize producing regions could experience a greater number of hot days in 2016-2035, causing an estimated 12% yield loss. However, hot days may become less damaging for yields as precipitation increases. Actually, the increase of temperature itself is not an issue if plenty of soil moisture is provided for corn. Field experiments indicate that no direct damage to photosynthetic capacity was found even when the temperature of the corn plant was raised to 37.8 °C (Nafziger 2011). It should be noted that the temperature stress computed by SWAT is the function of air temperature alone (Neitsch et al., 2009). If water is limited or the stomatal conductance is reduced due to CO<sub>2</sub> enhancement, tissue temperature should also increase, but the possible damage (Nava, 2013; Wang et al., 2008; Ristic et al., 1996) caused by this increase is not reflected by the model. Therefore, the negative effects of future temperature stress on corn growth is likely underestimated, especially when growing season rainfall is reduced and CO<sub>2</sub> is enhanced in the future.



**Figure 5.6** SWAT estimated corn yield vs. aeration stress for all model experiments



**Figure 5.7** SWAT estimated corn yield vs. drought stress for all model experiments

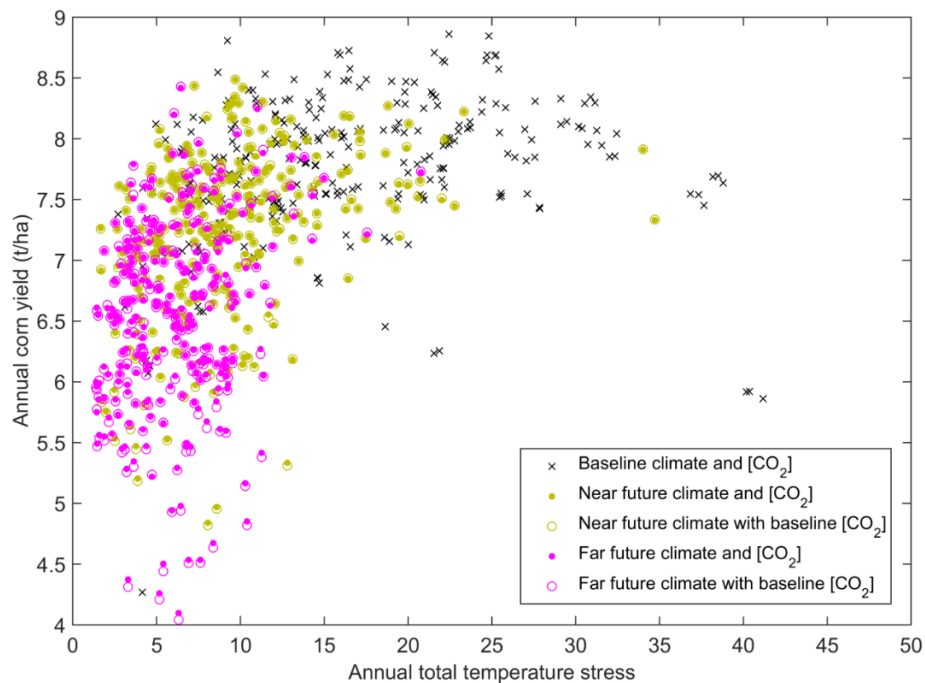


**Figure 5.8** SWAT estimated corn yield vs. temperature stress for all model experiments

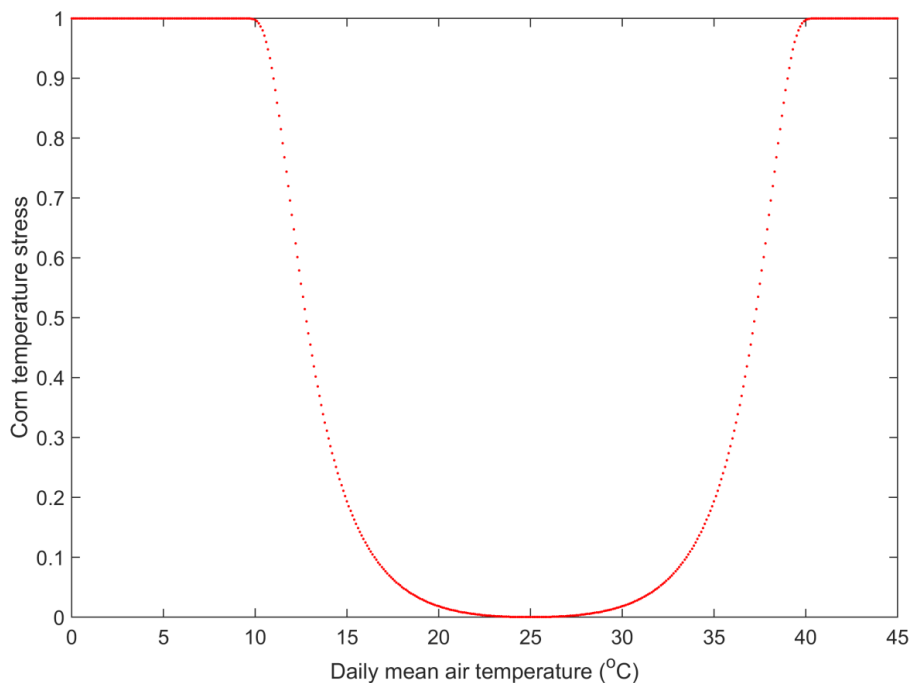


**Figure 5.9** The SWAT modeled relationship between corn temperature stress and mean daily air temperature

### 5.4.3 Streamflow response to future climate change and enhanced CO<sub>2</sub>

Flow duration curves (Figure 5.10) are used to visualize streamflow change under different modeling experiments for the whole range of annual daily flows. Figure 5.10a uses a log scale on the horizontal axis to display the streamflow change at low probability of exceedance (PE). Figure 5.10b employs log scale on the vertical axis to better visualize streamflow change at low flow conditions. Figure 5.10c uses linear scale to highlight low flow changes. For the near future period, streamflow volumes are generally predicted to increase for both small and large PE. For the far future period, streamflow is expected to decrease for large PE, while streamflow discharge for small PE will increase. This indicates that more hydrological drought and flooding events are expected to happen in the far future period (2061-2090). This is probably due to the shifted seasonal precipitation pattern in future, with wetter springs and more intense but less frequent summer storms. Warmer air temperatures coupled with unchanged summer precipitation increases ET in the study region, and in turn reduces flow volumes for low flow conditions (Cherkauer and Sinha, 2010). Table 5.3 summarizes the mean annual discharge based on different SRES scenarios. For the near future period, all three SRES scenarios predict an increasing trend in mean discharge, while for the far future period, only the B1 scenario predicts an increasing trend in mean discharge, the other two indicate a slightly decreasing trend in mean discharge.



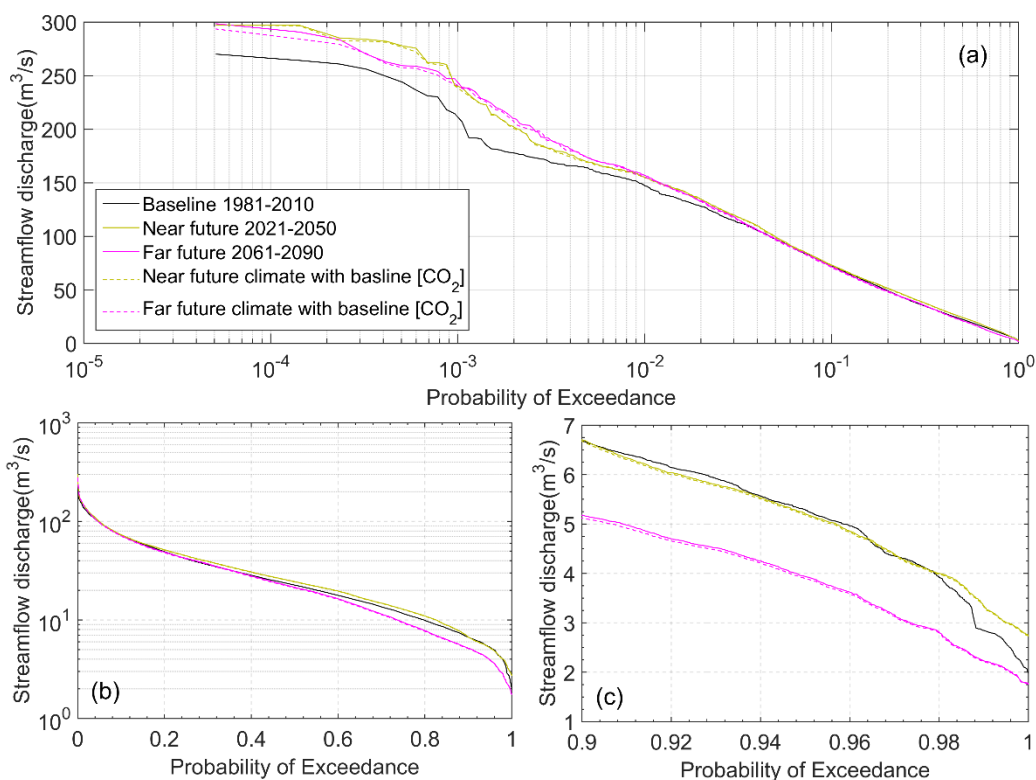


**Figure 5.10 Flow duration curves for all modeling experiments**

**Table 5.2 Mean discharge from the five modeling experiments.**

	Mean discharge (m <sup>3</sup> /s)				
	Baseline climate and [CO <sub>2</sub> ]	Near future climate and [CO <sub>2</sub> ]	Near future climate, baseline [CO <sub>2</sub> ]	Far future climate and [CO <sub>2</sub> ]	Far future climate, baseline [CO <sub>2</sub> ]
<b>b1</b>	32.63	33.20	33.01	33.66	33.26
<b>a1b</b>	32.35	34.95	34.70	29.06	28.18
<b>a2</b>	31.71	35.21	34.97	31.00	30.19

By comparing the flow duration curves with baseline and future CO<sub>2</sub> concentrations, it can be seen that CO<sub>2</sub> enhancement can increase streamflow in both low PE and high PE conditions. However, the amount of increase is quite marginal and only visible at very low

PE conditions ( $PE < 0.001$ ). For the whole flow range, the mean discharge for the near future period varies from  $34.37 \text{ m}^3/\text{s}$  to  $34.14 \text{ m}^3/\text{s}$ , so only a 0.67% increase due to  $\text{CO}_2$ -related crop impacts. The situation for the far future period is quite similar, with mean discharge increased by 1.26% due to  $\text{CO}_2$  enhancement. The increased amount of streamflow is mainly due to the improvement of plant-water relationship. Enhanced atmospheric  $\text{CO}_2$  levels result in the reduced stomatal conductance, and therefore decreases the transpiration rate for similar levels of productivity. Reduced ET leaves more water available for streamflow. This finding is consistent with many other studies (Wu et al., 2012; Niu et al., 2013; Butcher et al., 2014), which all predict annual streamflow volume increases (of 1%-4%) when  $\text{CO}_2$  enhancement effects on stomatal conductance are considered by models.

## 5.5 Conclusions

In this research, the SWAT model was used to explore future climate change and  $\text{CO}_2$  enhancement effects on corn growth and hydrology in the St. Joseph River watershed, Eastern Corn Belt. The current SWAT model was first modified to make it take dynamic  $\text{CO}_2$  concentration as a model input. Then remote sensing information was used to generate regional potential leaf area development curve for parameterization. A multi-objective calibration strategy was conducted to ensure the capturing of daily streamflow, seasonal crop growth and interannual crop yield simultaneously. After calibration, the model was driven by  $\text{CO}_2$  concentration, and downscaled, bias-corrected precipitation and temperature from three GCMs under three SRES scenarios to study potential biophysical and hydrological impacts in two future periods (2021-2050; 2061-2090).

Based on this work, we can conclude the following:

1. The St. Joseph River watershed will more likely experience significant increasing precipitation in winter and spring months. But for summer months, a slight decrease or unchanged precipitation is predicted. Air temperature is also expected to rise for all months, but especially for summer months. Increased temperature accompanied with decreased or unchanged precipitation indicates more late summer threat to corn growth due to increased drought stress in the future period.
2. Both total annual aeration and drought stresses are expected to experience more year-to-year variability in both future periods. No significant change in the median value of aeration or drought stress was detected. Temperature stress is expected to decrease in the future period when compared to the baseline period. This is mainly due to the reduction of cold stress in the early growing season; however, reduced temperature stress cannot compensate for the yield reduction risk due to exacerbated drought stress in summer months due to temperature increases and precipitation reduction.
3. Future CO<sub>2</sub> enhancement benefits the crop growth and final yield by improving radiation use efficiency (RUE) and reducing drought stresses. The improvement in RUE is not significant when the CO<sub>2</sub> level is over 500 ppm. Annual median drought stress is expected to reduce marginally (from 10.73 to 10.48) due to CO<sub>2</sub> increasing, while median aeration stress is expected to increase marginally. Therefore, the mitigation impact of CO<sub>2</sub> enhancement on crop yield reduction is not significant. Detrended crop yield is still expected to reduce by 6.1% in the near future period,

and by 15.6% in the far future period due to both climate change and CO<sub>2</sub> enhancement.

4. Climate change results in changes in streamflow frequency. Streamflow was predicted to increase for the whole flow range in the near future period, primarily due to precipitation increases. Increases in streamflow due to enhanced crop water productivity are quite low and only visible at very low PE condition ( $PE < 0.001$ ). For the far future period, high flows are expected to increase, while low flows are expected to decrease, indicating a potential for both more hydrological drought and flood events in St. Joseph River watershed.

## 5.6 References

- Ainsworth EA, Long SP. 2005. What have we learned from 15 years of free-air CO<sub>2</sub> enrichment (FACE)? A meta-analytic review of the responses of photosynthesis, canopy properties and plant production to rising CO<sub>2</sub>. *New Phytologist* **165**: 351-372.
- Andresen J, Hilberg S, Kunkel K. 2012. Historical Climate and Climate Trends in the Midwestern USA. In: U.S. National Climate Assessment Midwest Technical Input Report. J. Winkler, J. Andresen, J. Hatfield, D. Bidwell, and D. Brown, coordinators. Available from the Great Lakes Integrated Science and Assessments (GLISA) Center, [http://glisa.msu.edu/docs/NCA/MTIT\\_Historical.pdf](http://glisa.msu.edu/docs/NCA/MTIT_Historical.pdf).
- Arjal RD, Prato JD, Peterson ML. 1978. Response of corn to fertilizer, plant population, and planting date. *California Agriculture* **32(3)**: 14-15.
- Arnold JG, Srinivasan R, Muttiah RS, Williams JR. 1998. Large area hydrologic modeling and assessment part I: Model Development. *Journal of the American Water Resources Association* **34(1)**: 73-89
- Brown RA, Rosenberg NJ, Hays CJ, Easterling WE, Mearns LO. 2000. Potential production and environmental effects of switchgrass and traditional crops under current and greenhouse-altered climate in the central United States: a simulation study. *Agriculture, Ecosystems & Environment* **78**: 31-47.
- Butcher JB, Johnson TE, Nover D, Sarkar S. 2014. Incorporating the effects of increased atmospheric CO<sub>2</sub> in watershed model projections of climate change impacts. *Journal of Hydrology* **513**: 322-334.
- Cherkauer KA, Sinha T. 2010. Hydrologic impacts of projected future climate change in the Lake Michigan region. *Journal of Great Lakes Research* **36**: 33-50.
- Christensen JH, Hewitson B, Busuioc A, Chen A, Gao X, Held I, Jones R, Kolli RK, Kwon WT, Laprise R, Magana RV, Mearns L, Menendez CG, Raisanen J, Rinke A, Sarr A, Whetton P. 2007. Regional Climate Projections. In: *Climate Change 2007: The Physical Science Basis. Contribution of Working Group I to the Fourth Assessment Report of the Intergovernmental Panel on Climate Change* [Solomon S, Qin D, Manning M, Chen Z, Marquis M, Averyt KB, Tignor M, Miller HL (eds.)]. Cambridge University Press, Cambridge, United Kingdom and New York, NY, USA.
- Dohleman FG, Long SP. 2009. More productive than maize in the Midwest: how does *Miscanthus* do it? *Plant physiology* **150**: 2104-2115.

- Easterling WE, Rosenburg NJ, McKenney MS, Jones CA, Hyke PT, Williams JR. 1992. Preparing the erosion productivity impact calculator (EPIC) model to simulate crop response to climate change and the direct effects of CO<sub>2</sub>. *Agricultural and Forest Meteorology* **59**: 17-34.
- Glinski J, Stepniewski W. 1983. Soil aeration and its role for plants. Boca Raton, Florida.
- Goldblum D. 2009. Sensitivity of corn and soybean yield in Illinois to air temperature and precipitation: The potential impact of future climate change. *Physical Geography* **30**:27-42.
- Groisman, PY, Easterling DR.1994. Variability and Trends of precipitation and snowfall over the United States and Canada. *Journal of Climate* **7**:184-205.
- Grover EK, Sousounis PJ. 2002. The Influence of Large-Scale Flow on Fall Precipitation Systems in the Great Lakes Basin. *Journal of Climate* **15**: 1943-1956.
- Hawkins ED, Fricker TE, Challinor AJ, Ferro CAT, Ho CK, Osborne TM. 2013. Increasing influence of heat stress on French maize yields from the 1960s to the 2030s. *Global Change Biology* **19**: 937-947.
- Houghton JT et al., Eds., Climate Change 2001: The Scientific Basis (Cambridge University Press, Cambridge, 2001).
- Kling G, Hayhoe K, Johnson L, Magnuson J, Polasky S, Robinson S, Shuter B, Wander M, Wuebbles D, Zak D. 2003, Confronting Climate Change in Great Lakes Region, A Report of the Ecological Society of America and the Union of Concerned Scientists, Washington, D.C.
- Kunkel KE, Easterling DR, Redmond K, Hubbard K, 2003: Temporal variations of extreme precipitation events in the United States: 1895–2000, *Geophysical Research Letters* **30**, 1900, 10.1029/2003GL018052
- Leakey ADB, Uribeharrea M, Ainsworth EA, Naidu SL, Rogers A, Ort DR, Long SP. 2006. Photosynthesis, productivity, and yield of maize are not affected by open-air elevation of CO<sub>2</sub> concentration in the absence of drought. *Plant Physiology* **140**:779-790.
- Lobell DB, Asner GP. 2003. Climate and management contributions to recent trends in U.S. agricultural yields. *Science* **299** (5609).
- Long ST, Ainsworth EA, Rogers A, Ort DR. 2004. Rising atmospheric carbon dioxide: plants FACE the future. *Annual Review of Plant Biology* **55**:591-628.
- McMichael P. 2009. A food regime analysis of the 'world food crisis'. *Agriculture and Human Values* **26**:281-295.

- Meehl GA, Stocker TF, Collins WD, Friedlingstein P, Gaye AT, Gregory JM, Kitoh A, Knutti R, Murphy JM, Noda A, Raper SCB, Watterson IG, Weaver AJ, Zhao ZC (2007). Global Climate Projections. In: *Climate Change 2007: The Physical Science Basis. Contribution of Working Group I to the Fourth Assessment Report of the Intergovernmental Panel on Climate Change* [Solomon S, Qin D, Manning M, Chen Z, Marquis M, Averyt KB, Tignor M, Miller ML (eds.)]. Cambridge University Press, Cambridge, United Kingdom and New York, NY, USA.
- Mishra V, Cherkauer KA, Shukla S. 2010. Assessment of drought due to historic climate variability and projected future climate change in the Midwestern United States. *Journal of Hydrometeorology* **11**: 46-68.
- Mishra V, Cherkauer KA. 2010. Retrospective droughts in the crop growing season: Implications to corn and soybean yield in the Midwestern United States. *Agricultural and Forest Meteorology* **150**:1030-1045.
- Nafziger E. 2011. High Temperatures and Crops. University of Illinois. <http://bulletin.ipm.illinois.edu/article.php?id=1537>
- Nash JE, Sutcliffe JE. 1970. River Flow Forecasting Through Conceptual Models, Part I-A Discussion of Principles. *Journal of Hydrology* **10(3)**: 282-290.
- Nava SC. 2013. Optimum temperature and phenological stage for determining cellular membrane thermostability in corn and bean. *Phyton-international journal of experimental botany* **82**: 249-254.
- Neitsch SL, Arnold JG, Kiniry JR, Williams JR. 2009. Soil and Water Assessment Tool: Theoretical Documentation, version 2009.
- Nielsen RL, Thomison PR, Brown GA, Halter AL, Wells J, Wuethrich KL. 2002. Delayed planting effects on flowering and grain maturation of dent corn. *Agronomy Journal* **94**:549-558.
- Nielsen RL. 2008. Grain Fill Stages in Corn. Corny News Network, Purdue University. Retrieved from: <http://www.agry.purdue.edu/ext/corn/news/timeless/grainfill.html>
- Niu J, Sivakumar B, Chen J. 2013 Impacts of increased CO<sub>2</sub> on the hydrologic response over the Xijiang (West River) basin, South China. *Journal of Hydrology* **505**: 218-227.
- Oliver RJ, Finch JW, Taylor G. 2009. Second generation bioenergy crops and climate change: a review of the effects of elevated atmospheric CO<sub>2</sub> and drought on water use and the implications for yield. *GCB Bioenergy* **1**:97-114.
- Pryor, SC., ed. Climate Change in the Midwest: Impacts, Risks, Vulnerability, and Adaptation. Bloomington, IN, USA: Indiana University Press, 2012. ProQuest eLibrary.

- Rathnam CKM. 1978. Heat inactivation of leaf phosphoenolpyruvate carboxylase: protection by aspartate and malate in C4 plants. *Planta* **141**: 289-295.
- Ristic Z, Williams G, Yang G, Martin B, Fullerton S. 1996. Dehydration, damage to cellular membranes, and heat-shock proteins in maize hybrids from different climates. *Journal of Plant Physiology* **149**: 424-432.
- Rogovska NP, Richard M. 2011 Climate change consequences for agriculture in Iowa. AgMRC Renewable Energy & Climate Change Newsletter. Available from [http://www.agmrc.org/renewable\\_energy/climate\\_change\\_and\\_agriculture/climate-change-consequences-for-agriculture-in-iowa/#](http://www.agmrc.org/renewable_energy/climate_change_and_agriculture/climate-change-consequences-for-agriculture-in-iowa/#)
- Rosenzweig C, Tubiello FN, Goldberg R, Mills E, Bollmeyer J. 2002. Increased crop damage in the US from excess precipitation under climate change. *Global Environmental Change* **12**:197-202.
- Schlenker W, Roberts M. 2009. Nonlinear temperature effects indicate severe damages to U.S. crop yields under climate change. *PNAS* **106**:15594-15598
- Sinha T, Cherkauer KA. 2010. Impacts of future climate change on soil frost in the Midwestern United States, *Journal of Geophysical Research* **115**: D08105.
- Southworth, J., Randolph, J.C., Habeck, M., Doering, O.C., Pfeifer, R.A., Rao, D.G. and Johnston, J.J.: 2000, 'Consequences of future climate change and changing climate variability on maize yields in the Midwestern United States', *Agriculture, Ecosystem & Environment* **82**: 139–158.
- Stockle CL, Williams JR, Rosenberg NJ, Jones CA. 1992. A method for estimating the direct and climatic effects of rising atmospheric carbon dioxide on growth and yield of crops: Part 1- Modification of the EPIC model for climate change analysis. *Agricultural Systems* **38**:225-238.
- Thompson LM. 1988. Effects of changes in climate and weather variability on the yields of corn and soybeans. *Journal of Production Agriculture* **1**:20-29
- USEPA. 2013. Overview of Greenhouse Gases: Carbon Dioxide Emissions. Retrieved from <http://www.epa.gov/climatechange/ghgemissions/gases/co2.html>
- USGCRP 2009. *Global Climate Change Impacts in the United States*. Thomas R. Karl, Jerry M. Melillo, and Thomas C. Peterson (eds.). United States Global Change Research Program. Cambridge University Press, New York, NY, USA.
- Wall GW, Brooks TJ, Adam NR. 2001. Elevated atmospheric CO<sub>2</sub> improved sorghum plant water status by ameliorating the adverse effects of drought. *New Phytologist* **152**:231-248.



- Wang D, Heckathorn SA, Barua D, Joshi P, Hamilton EW, LaCroix JJ. 2008. Effects of elevated CO<sub>2</sub> on the tolerance of photosynthesis to acute heat stress in C3, C4 and CAM species. *American Journal of Botany* **95**(2):165-176.
- Wang R, Bowling LC, Cherkauer KA. 2016. Estimation of the effects of climate variability on crop yield in the Midwest USA. *Agricultural and Forest meteorology* **216**: 141-156.
- Wu Y, Liu S, Abdul O. 2012. Hydrological effects of the increased CO<sub>2</sub> and climate change in the Upper Mississippi River Basin using a modified SWAT. *Climatic Change* **110**: 977-1003.
- Wuebbles DJ, Hayhoe K. 2004. Climate change projections for the United States Midwest. *Mitigation and Adaptation Strategies for Global Change* **9**: 335–363.
- Wullschleger SD, Norby RJ. 2001. Sap velocity and canopy transpiration in a sweetgum stand exposed to free-air CO<sub>2</sub> enrichment (FACE). *New Phytologist* **150**: 319-331

## CHAPTER 6. CONCLUSIONS AND RECOMMENDATIONS FOR FUTURE WORK

Corn seasonal growth and yield are strongly affected by climate variability and will be affected under future climate change situation. When investigating climate impacts on corn growth via a modeling method, plant-water relationships must be seriously considered. In this dissertation, I evaluated climate impacts on crop growth by first improving representation of plant-water interactions when water is either limited or oversupplied. The modeled crop responses under various climate conditions are regulated by moisture related bio-climatic parameters, which modulate simulated crop sensitivity to climate variability. My modeling method was applied at both plot scale at several sites in the Midwest USA, where moisture data is available, and watershed scale in the St. Joseph River watershed, Eastern Corn Belt, where direct moisture evaluation is not feasible. The multi-variable calibration strategy was compared with a streamflow only calibration to evaluate the model representation in plant-water interactions based on different calibration methods. Future climate change impact on crop growth was also investigated by not only considering precipitation and temperature change, but also the increasing trend of CO<sub>2</sub>.

## 6.1 Conclusions

This study tested four main hypotheses raised in Chapter 1. The results of those hypothesis tests and main findings are concluded as follows:

***Hypothesis 1: Annual crop yield variability is regulated by moisture related (oversupplied or limited water) bioclimatic stresses. Those stresses have significant effects on crop yield at specific growing periods.***

To better quantify the effect of climate variability on crop growth via moisture related bioclimatic indices, I evaluated the SWAT model's ability to reproduce observed moisture at plot scale in four NRCS-SCAN sites across the Midwest in Chapter 2. I then calibrated biophysical parameters, including stress parameters, which are directly related to soil moisture to regulate both mean and interannual yield variability. Results indicate an improvement in both mean and interannual yield variability in all four SCAN sites after the improved simulation of soil moisture. Therefore, evaluation of soil moisture in a crop modeling study is recommended for its importance in constraining crop water availability and thus better simulates crop responses to climate variability.

Our results in Chapter 2 demonstrated that annual observed corn yield is inversely correlated with drought stress intensity in the early and middle reproductive stage, which were more critical than other growth stages. Severe drought stress in the early and middle reproductive periods is substantially correlated with low observed yields. No significant relationship between crop yield and aeration stress was found at any of the four sites, due to the fact that aeration stress is hard to detect at county scales, as well as low frequency of

events in the historical record. This finding indicates the significance of drought stresses (limited water) on seasonal crop growth, and address the importance of correct representation of moisture to evaluate drought stress.

*Hypothesis 2: Crop response to oversupplied or limited water varies with spatial scale.*

*Drought stress results in regional yield declines, while aeration stress results in higher yield decline over smaller spatial areas, but is not detectable at large special scales.*

*Drought stress explains the majority of yield reduction across all return periods.*

Leaf growth condition detected by satellite based NDVI time series is used to represent corn growth conditions at watershed scale in Chapter 3. NDVI shows larger spatial variance during the leaf development and senescence periods, but minimum variance when the canopy is fully developed. Crop responses to bioclimatic stresses are quantified via NDVI residual by comparing image NDVI with long term “normal growth curve” from remote sensing images in Chapter 3.

I found that water stresses are closely associated with NDVI residuals. Limited water stress tends to result in crop growth below normal conditions, while plenty of rainfall reduces the risk of yield loss over larger areas. The percentage of corn cells under stress are also significantly correlated with water stress. More corn pixels are under stress when water is limited at regional scale. The spatial extent of cells under stress is much lower when water is oversupplied, masking the impact of small areas of yield loss at regional scale.

Results in Chapter 2 showed that drought stress explains the majority of yield reduction across all return periods. Long term simulation of yield reduction indicates that drought stress dominates aeration stress affecting yield in the historical period both at short and long return periods (high/low probability of exceedance). For a 70-year period, the total yield reduction due to drought stress is 8.1%, 17.5%, 15.2% and 9.7% respectively for Boone, Woodbury, Madison and Mason.

*Hypothesis 3: Multi-variable calibration of streamflow, the seasonal crop growth curve (LAI development), and annual yield within an ecohydrologic model can improve simulation performance in the face of climate variability, and reduce uncertainty in moisture prediction.*

Merging satellite information into model output is helpful to improve model representation in seasonal crop growth. In Chapter 4, I found that the multi-variable calibration strategy is able to capture seasonal crop growth development, and thus reduce the equifinality in final yield estimation due to the selection of incorrect parameter sets. Interannual yield variability is also improved, which correctly reflects the climate effects on final yield. Model performance in streamflow is reduced marginally (0.820 to 0.817 in NSC), but still satisfactory. Simulated corn responses to climate variability is improved without hampering model performance in streamflow. Neither of the calibration strategies could successfully capture the bias of soil moisture, however, the uncertainty in moisture prediction is reduced when applying multi-variable calibration strategy.

*Hypothesis 4: Future climate change will have negative impacts on rainfed corn yield, and introduce more interannual variability in the Eastern Corn Belt because of increased spring wetness and decreased summer rainfall. CO<sub>2</sub> enhancement cannot compensate for yield reduction due to changes in rainfall and temperature.*

Multiple GCM outputs under different scenarios shown in Chapter 5 demonstrate that the St. Joseph River watershed will likely experience increased air temperature, especially in summer months, accompanied with decreased or unchanged precipitation. Precipitation in winter and spring months is expected to increase significantly in near future (2021-2050) and far future periods (2061-2090). These changes introduce more variability in total aeration and drought stress.

Although future CO<sub>2</sub> enhancement benefits the crop growth and yield by improving radiation use efficiency (RUE) and reducing drought stresses, the compensation to reduce yield loss risk is not sufficient. Modeling results in Chapter 5 indicate that yield is still expected to decrease by 6% in the near future period, and 16% in the far future period due to the combined effect of both climate change and CO<sub>2</sub> enhancement. More yield variability is also predicted by the model associated with the variance in total aeration and drought stress.

Streamflow frequency is also predicted to change in the future. Stream discharge is projected to increase for the whole flow range in the near future period. For the far future period, high flows are expected to increase, while low flows are expected to decrease, indicating more hydrologic drought and flood events in the St. Joseph River watershed.

## 6.2 Limitations and Future Work

In this study, crop modeling was improved via modifying and evaluating the simulation of water-plant relationships. Our understanding of climate variability and climate change impacts on crop growth is improved. However, there are still several limitations in this study, which could be addressed by future research.

1. Current yield calibration strategy does not consider the susceptibility of corn to drought stress or aeration stress. Though our study indicates yield is more related to stress in some specific periods, the same stress transformation is employed for the whole growing period. Future studies should focus on improve stress parameterization to represent susceptibility.
2. Crop death is not defined in the SWAT model, so the simulated crop can recover under any situation. This can result in unrealistic yield prediction under very extreme conditions (flooding or drought). Future study should include “crop death” in model simulation, which is more consistent with reality.
3. The difficulty in identifying aeration stress effect on crop yield is caused by scale issues, since losses are more localized within the field scale rather than county or watershed scale, and the low frequency and resolution of historical records. More future greenhouse studies are required to artificially control moisture condition, and observe how crop responds to excess water at different phenological stages.

4. The regional LAI curve was generated based on a published empirical NDVI-LAI relationship. It could be helpful to evaluate this relationship by measuring LAI directly in the study region. The seasonal LAI development method in this dissertation could also be used for other satellite images or aerial photos taken by unmanned aerial vehicles (UAVs), which do not have the same issues with clouds or spatial and temporal resolution.
5. When the model is used at watershed level, the inconsistency of soil property representation across counties introduced inconsistencies into the simulation of soil moisture and crop yield. The bias-correction approach used by this dissertation could be avoided if using more uniform soil datasets to overcome the discrepancy between soil representations across counties.
6. The current moisture evaluation method is based on in-situ sensors in the study area, which are still at point scale. Future studies will get benefits from basin level moisture evaluation by the help of the newly launched NASA-SMAP (Soil Moisture Active Passive) satellite.
7. The current SWAT algorithm to reflect CO<sub>2</sub> effect on crop growth is limited between 330 ppm to 660 ppm. For future climate studies, especially high emission scenarios, this algorithm needs to be extended to represent crop affects over 660 ppm. Generating an updated relationship will require more greenhouse studies, which could be a focus for future studies.



VITA

## VITA

### Ruoyu Wang

#### Education

**Ph.D. candidate**, Department of Agricultural and Biological Engineering, Purdue University, West Lafayette, IN, 47906. (Aug. 2011 to present, GPA 3.86). Expected graduation March 2016.

**M.S. in Forestry (Forest Hydrology)**, School of Forestry and Wildlife Sciences, Auburn University, AL, USA (Aug. 2008 to Dec. 2010, GPA 3.91)

**B.S. in Environmental Engineering**, Department of Environmental Engineering, Beijing University of Chemical Technology (BUCT), Beijing, China. (Sep. 2003 to Jun. 2007, GPA 3.33)

#### Experience

Graduate Research Assistant at Purdue University (Aug, 2011-present).

- Investigated long term historical climate variability and climate change effect on annual crop yield and seasonal growth via an integration of modeling and remote sensing technology.

Graduate Teaching Assistant at Purdue University (Aug. - Dec., 2015).

- Taught basic survey methods (Auto-levelling, RTK) and fundamental soil and water engineering tools (NRCS-GIS, ArcHydro, CROPWAT) to undergraduates for ABE 32500.

Internship at USEPA, Landscape Ecology Branch (Jan. - Jul., 2015).

- Modeled the linkage of discharge and nutrients from the Mississippi River Basin to Gulf of Mexico hypoxia using a combined system (FEST-C plus SWAT).

Graduate Research Assistant at Auburn University (Aug. 2008 – Dec. 2010).

- Investigated joint and individual impacts of land use and climate on regional hydrology and water quality in Southern, Alabama using SWAT.

#### Awards

- Student Services Contract Award from United States Environmental Protection Agency, 2014.
- Graduate School Fellowship Incentive Grant, Purdue University, 2014
- Purdue Climate Change Research Center (PCCRC) doctoral fellowship, 2011.